OBSERVATIONS OF 1-6 MeV JOVIAN ELECTRONS AT 1 AU AND A STUDY OF THEIR PROPAGATION

Thesis By

Steward Russell Hartman

In Partial Fulfillment of the Requirements

for the Degree of

Doctor of Philosophy

California Institute of Technology

Pasadena, California

1979

(Submitted May 14, 1979)

Acknowledgments

Over the years many persons have contributed to the design, construction, calibration, and data analysis of the two Caltech EIS experiments on IMP-7 and IMP-8. Dr. Edward Stone, as my thesis advisor and principal investigator of the Caltech EIS, has provided the impetus and encouragement for this study. He has given me insight into the methods and procedures of conducting scientific investigations.

I would also like to acknowledge the support and interest of Dr. Rochus Vogt who was co-investigator on the Caltech EIS experiments. I have appreciated his numerous discussions on the administration of science.

Gordon Hurford, Frank Marshall, Sol Vidor, Dick Mewaldt, and Dan Baker were involved in the testing and calibration of the EIS instruments. They also contributed to many aspects of the data analysis programs. Dick was particularly helpful in discussions on the electron response of the instruments and in assembling the basic electron data that were further analyzed in this report. The processing of the data tapes was done by Kenneth Bell and Mark Walther and was supervised by Tom Garrard.

I had many discussions on Jovian electrons with Dick Mewaldt, Rick Cook, and Neil Geherls. Neil was very helpful in commenting on the early drafts of this thesis.

This research has been supported by the National Aeronautics and Space Administration under Contract NAS 5-11066 and Grant NGR 05-002-160. The data on the solar wind and the interplanetary magnetic field were furnished by J. King of the National Space Science Data Center and his assistance is gratefully acknowledged.

I have learned much about electronics with the help of Fred Yates and Bill Althouse. Bill contributed immeasurably to the success of the EIS instruments and has quickly provided answers to all my questions on the workings of the instruments.

I have greatly enjoyed and benefited from the talks Bill and I have had on subjects ranging from the details of circuit analysis to the relationships of people. His experience, insights, and knowledge concerning technical matters and administration were very useful and interesting. I mourn the loss of the diverting and relaxing lunches we had exploring the world of board and table games.

I have appreciated the contributions of Roo Lester who provided much needed help and encouragement in finishing those last minor details on this thesis. "Eskarrik asko!"

Abstract

The 1-6 MeV electron flux at 1 AU has been measured for the time period October 1972 to December 1977 by the Caltech Electron/Isotope Spectrometers on the IMP-7 and IMP-8 satellites. The non-solar interplanetary electron flux reported here covered parts of five synodic periods. The 88 Jovian increases identified in these five synodic periods were classified by their time profiles. The fall time profiles were consistent with an exponential fall with $\tau \approx$ 4-9 days. The rise time profiles displayed a systematic variation over the synodic period. Exponential rise time profiles with $\tau \approx$ 1-3 days tended to occur in the time period before nominal connection, diffusive profiles predicted by the convection-diffusion model around nominal connection, and abrupt profiles after nominal connection.

The times of enhancements in the magnetic field, $|B|$, at 1 AU showed a better correlation than corotating interaction regions (CIR's) with Jovian increases and other changes in the electron flux at 1 AU, suggesting that $|B|$ enhancements indicate the times that barriers to electron propagation pass Earth. Time sequences of the increases and decreases in the electron flux at 1 AU were qualitatively modeled by using the times that CIR's passed Jupiter and the times that $|B|$ enhancements passed Earth.

The electron data observed at 1 AU were modeled by using a

convection-diffusion model of Jovian electron propagation[1]. The synodic envelope formed by the maxima of the Jovian increases was modeled by the envelope formed by the predicted intensities at a time less than that needed to reach equilibrium. Even though the envelope shape calculated in this way was similar to the observed envelope, the required diffusion coefficients were not consistent with a diffusive process.

Three Jovian electron increases at 1 AU for the 1974 synodic period were fit with rise time profiles calculated from the convection-diffusion model. For the fits without an ambient electron background flux, the values for the diffusion coefficients that were consistent with the data were $k_x = 1.0 - 2.5 \times 10^{21}$ cm^2/sec and $k_y = 1.6 - 2.0 \times 10^{22}$ cm^2/sec. For the fits that included the ambient electron background flux, the values for the diffusion coefficients that were consistent with the data were $k_x = 0.4 - 1.0 \times 10^{21}$ cm^2/sec and $k_y = 0.8 - 1.3 \times 10^{22}$ cm^2/sec.

---

[1] Conlon, T.F., "The Interplanetary Modulation and Transport of Jovian Electrons," J. Geophys. Res., 83, 541, 1978.

Table of Contents

List of Figures

List of Tables

I. Introduction

Observations at Earth and in the vicinity of Jupiter show that Jupiter is a source of MeV interplanetary electrons. This source of low energy electrons localized at the position of Jupiter allows investigation of particle propagation in the inner heliosphere. Study of the inward propagation of particles from a known source becomes feasible. Propagation effects over a distance of many AU can be studied by observations at 1 AU. The various models of particle propagation in the heliosphere can be compared by using Jupiter as a source of electrons not at the origin or at the boundary of a coordinate system.

This work is a study of the 1-6 MeV electron flux observed at 1 AU over the period August 1972 through December 1977. The individual Jovian increases in the electron flux observed during this period are compared to the times when corotating interaction regions and other features in the solar wind pass the positions of Earth and Jupiter. These observations will be compared with previous studies of electron increases and they will be used in the investigation of a propagation model incorporating convection and diffusion.

I-A. The Period Before the Discovery of the Jovian Source, 1964-1974

The electron flux in the 1-6 MeV energy regime has been measured by many experimenters in the fourteen years since the first observations were conducted. Observations of a few MeV interplanetary electrons began in November 1963 when a scintillator particle telescope on IMP-1 observed electrons at 1 AU in the 3-12 MeV energy range. Though the experiment lasted only until May 1964, Cline, et al. (1964) reported seeing increases of a factor $\sim$2 in intensity in the electron flux that they noted were "apparently coincident with the recurrent K_p minimum" and were not correlated with any increase in the integral flux of cosmic-rays above 15 MeV. The spectra of electrons just before an intensity increase and the spectra of the extra electrons during the increase were shown to be similar. This observation led to their suggestion that the electrons seen outside of the increases may have the same origin as those that are seen within the increases. They also noted a long-term increase in the electron flux over the $\sim$5 months of observations.

Two possible origins were suggested by Cline, et al. for these electrons. One, the electrons are galactic in origin. In this case the observed correlation of the intensity increases with the interplanetary K_p index and the long-term increases in the electron flux would be the result of variations in solar modulation

over the ~27 day solar synodic rotation period and over the 11 year solar cycle. Or two, the observed electrons originate at the sun. Possible mechanisms for generating energetic solar electrons were discussed, but no correlation with any solar radio or optical activity was observed.

The significant point is that the first observations of a few MeV interplanetary electrons clearly showed the short, ~5 to 10 day duration, increases and that these increases are correlated with recurrent quiet interplanetary conditions. Since the experiment only lasted until May 1964, Cline, et al. could not determine that the slow long-term increase that they observed was in retrospect the start of a Jovian synodic period of electron increases. For a solar wind speed of 500 km/sec, this synodic period was associated with the May 8, 1964 nominal spiral field line connection of Earth and Jupiter.

Observations of interplanetary electrons since 1964, but before 1974 when Jupiter was found to be a source of electrons, have focused on measurements of the spectra of the quiet-time electrons (Cline and Porreca, 1970; Simnett and McDonald, 1969; Beedle, et al., 1970; Lin, et al., 1972; Cline, 1973; Hurford, et al., 1974) and on the detailed study of the temporal variations of quiet-time electron intensities and spectra (Cline and McDonald, 1968; Simnett, et al., 1970; McDonald, et al., 1972; Webber, et al., 1973; Simnett, 1974).

McDonald, et al. (1972) summarized the generally observed characteristics of the temporal variations of the electron flux as:

> Quiet-time increases. These increases represent a new phenomenon and are unique to the electron population above 1 MeV. They last for periods from a few days to 2 weeks and can display a 27-day recurrence. At times the electron intensity may increase above the minimum quiescent level at 1 AU by as much as a factor of 5. Qualitatively, the energy spectra of the increases above background are similar to the spectrum determined for the galactic component ($\sim E^{-2}$). These events are strikingly anticorrelated with low-energy (<10 MeV) proton events. It appears most probable that these increases are of galactic origin.

Until the encounter of Pioneer 10 with Jupiter all the observations of the interplanetary electron flux were made at radial distances of 0.7-1.1 AU and displayed increases in intensity with characteristics similar to those quoted above.

With these observations the discussion of the origin and propagation of the interplanetary electron flux and its intensity increases centered around a galactic origin and the effects of solar modulation or of variations in the properties of the heliosphere on the sunward movement of the electrons. For this period the review by Simnett (1974) summarizes both the observations of the intensity increases and the ideas on the source and propagation of these interplanetary electrons.

I-B. Jovian Source Discovery, 1974

When Pioneer 10 approached Jupiter large variations in the intensity of electrons were observed. Chenette, et al. (1974) reported seeing bursts of 3-30 MeV electrons lasting 2-3 days up to 1 AU from the planet. These bursts were not correlated with known solar activity, their maximum intensity grew with increasing distance from the Sun, and similar increases did not appear in the data from Pioneer 11 which was closer to the sun. They also demonstrated that the spectral index for the electron increases had a ten hour periodicity whose maxima were synchronous with the occurrence of maxima in the spectral index for energetic electrons inside the Jovian magnetosphere. Chenette, et al. concluded that the source of these electron increases was centered at Jupiter.

Teegarden, et al. (1974) also reported Pioneer 10 observations of 0.2-8 MeV electron increases that occurred more frequently and were larger as Pioneer 10 approached the vicinity of Jupiter. They eliminated a solar origin for these electron increases by noting that Pioneer 11, which was less than 3 AU from the sun during this period, did not show similar electron increases. For one large increase they computed a spectrum which was similar to the spectrum observed inside the Jovian magnetosphere.

After concluding that Jupiter was the source of the electron

increases seen near Jupiter by Pioneer 10, they reexamined the quiet-time increases observed at 1 AU from 1964 through 1972 to see if these increases were also of Jovian origin. Teegarden, et al. plotted the 1 AU electron observations for 13 month epochs to show that the increases have a periodicity of 13 months which is the synodic period of Earth and Jupiter. They noted that the time periods over which the electron increases occurred were consistent with the times when Earth and Jupiter were connected by an ideal spiral field line for a solar wind speed of 350 km/sec. The spectra of the electron increases that they observed on Pioneer 10 and the spectra of electron increases previously measured near Earth were similar. From this evidence Teegarden, et al. concluded that Jupiter is a source of interplanetary electrons which propagate to Earth and that the 13 month periodicity of the quiet-time increases observed at 1 AU imply that most of these increases are Jovian in origin. They also suggested that all of the 0.2-40 MeV electron flux observed at 1 AU could be Jovian in origin.

I-C. Observations from 3 AU to 12 AU

The Pioneer 10 pre-encounter observations of Jovian electrons showed increases in the intensity of MeV electrons that lasted from 2-4 days (Chenette, et al., 1974; Teegarden, et al., 1974),

had rise times of the order of 1-2 days, and roughly equal fall times (Teegarden, et al., 1974). Post-encounter Pioneer 10 data showed that Jovian electron increases persisted out to ~11 AU and had a ~25 day recurrence (Chenette, et al., 1977b; Pyle and Simpson, 1977). Data obtained with the Pioneer 11 spacecraft displayed similar properties (Chenette, et al., 1977b; Gold, et al., 1977; Conlon, 1978).

The spectral index of the 6-30 MeV increases seen by Chenette, et al. (1974) had a 10 hour periodicity that was synchronous with the spectral index of electrons observed within the Jovian magnetosphere. Conlon (1978) reported that the 3-6 MeV electron flux observed by Pioneer 11 did not show this periodicity, but that the higher 6-30 MeV flux did have the 10 hour periodicity.

From the pre-encounter observation of Jovian electron increases by Pioneer 10, Chenette, et al. (1974) stated that the particles had to propagate across the average spiral structure of the interplanetary magnetic field. Smith, et al. (1976) reported that within ~0.2 AU of Jupiter some of the electron bursts seen by Pioneer 10 were correlated with the direction of the magnetic field aligned along the line connecting Jupiter and Pioneer 10. However, Conlon (1978) pointed out that no such alignment has been observed more than ~0.2 AU from Jupiter.

Corotating interactive regions (CIR's) which are formed at

~3-4 AU when a high speed solar wind stream overtakes a slower speed solar wind stream, were also discovered by the Pioneer 10 spacecraft (Smith and Wolfe, 1976). Conlon and Simpson (1977) found that the occurrence of the electron increases seen by Pioneer 10 were correlated with the positions of Pioneer 10 and Jupiter relative to the position of a CIR. Electron increases observed by Pioneer 11 were also correlated with CIR's in a similar fashion (Chenette, et al., 1977b; Conlon, 1978). Conlon and Simpson stated that CIR's form impenetrable barriers to the propagation of MeV electrons and that the observed ~25 day recurrence of the electron increases was probably due to modulation by CIR's. Besides the effects of CIR's Conlon (1978) also found that some increases seen by Pioneer 11 were correlated with corotating quiet regions (CQR's) but that CQR's were not as effective barriers to electron propagation as CIR's were.

The electron increases observed by Pioneer 10 and Pioneer 11 were at maximum intensity closest to Jupiter and the maximum intensity decreased with increasing distance out to ~11 AU where the electron flux level was comparable to the quiet-time intensities seen at 2-3 AU with no observable recurrent increases (Chenette, et al., 1977b; Pyle and Simpson, 1977; Conlon, 1978). The increases showed an asymmetry with more and larger increases occurring at larger distances from Jupiter after encounter than occurred at equal distances before encounter.

The trajectory of Pioneer 10 was such that in early 1976 the spacecraft passed behind and 0.6 AU above the Jovian magnetotail at an heliocentric distance of 9.6 AU. Even though recurrent electron increases were observed out to ~11 AU, Pyle and Simpson (1977) observed that there were no identifiable magnetospheric electrons during the period of closest approach to the magnetotail.

For the pre-encounter period of Pioneer 11, no decrease in the Jovian electron intensity occurred when a magnetic sector boundary passed the position of Pioneer 11 (Conlon, 1978). Conlon stated that this implies that at Pioneer 11 the sector boundaries did not form effective barriers to the propagation of Jovian electrons.

I-D. Observations Near 1 AU

The properties of MeV interplanetary electrons at 1 AU have been extensively measured since the first measurements in 1964. The flux at 1 AU of a few MeV interplanetary electrons has increases of factors of 2-10 above the lowest flux levels with the largest increases occurring at and just after the time for the best connection of an ideal interplanetary spiral magnetic field line for a solar wind speed of 400-600 km/sec (Teegarden, et al., 1974; L'Heureux and Meyer, 1975, 1976; Mewaldt, et al., 1975, 1976;

Krimigis, et al., 1975; Chenette, et al., 1977a,c; Hartman, et al., 1977). The maxima of the Jovian electron increases have a 13 month periodicity (Teegarden, et al., 1974; L'Heureux and Meyer, 1975, 1976; Mewaldt, et al., 1975, 1976; Gold, et al., 1977) and the increases occur throughout this 13 month synodic period of Earth and Jupiter (Chenette, et al., 1977a,c; Hartman, et al., 1977). The synodic envelope of the Jovian increases over the~13 month synodic period is asymmetric about the nominal connection time when Earth and Jupiter are connected by a spiral magnetic field line for a given solar wind speed, with more increases occurring after the nominal connection time than before. In general the shape of the synodic envelope is similar from synodic period to synodic period (Hartman, et al., 1977) except that there are fewer Jovian electron increases at the beginning of the 1973, 1976 and 1977 synodic periods (Mewaldt, et al., 1976; Hartman, et al., 1977).

The Jovian electron increases at 1 AU have a slow rise of 1-5 days and last from 5-20 days. The increases often display a 27 day recurrence and are anticorrelated with increases in the flux of a few MeV protons. Cline, et al. (1964) reported that the quiet-time increases were not attenuated by passage into Earth's magnetosphere. Gold, et al. (1976, 1977) reported a correlation of the Jovian increases with high speed solar wind streams.

McDonald, et al. (1972) reported that the increases tend to occur wholly within an interplanetary magnetic field sector, but L'Heureux and Meyer (1976) did not observe a striking correlation of increases and sector structure. Electron increases were reported to be larger and more numerous during periods in which there were only 2-4 stable sectors per solar rotation (Cline and McDonald, 1968; Teegarden, et al., 1974; L'Heureux and Meyer, 1976).

I-E. Models of Jovian Electron Propagation

I-E-1. Corotation and Solar Wind Speed Variations

Two simple models used to explain the longitudinal extent of Jovian electron increases observed at 1 AU were corotation and solar wind speed variations. Teegarden, et al. (1974) first pointed out that since electron increases last for over 5-12 days at 1 AU, a model using corotation to Earth of a flux tube that was loaded with electrons when it passed by Jupiter requires containment times ~15 days which is much longer than the decay times $\lesssim$ 1 day observed for solar flares. Teegarden, et al. also mentioned the possibility that since different solar wind speeds would generate different Archimedean spirals of the average interplanetary magnetic field lines, nominal connection

of Earth and Jupiter would occur over a wide range in longitude. However, they also noted that the observed range of solar wind speeds could only account for about 90° of the up to 180° longitudinal spread at 1 AU. Chenette, et al. (1977c) noted that observations of the solar wind speed (Gosling, et al., 1976) during the flight of Pioneer 10 were inconsistent with the extent of Jovian electron increases observed at the same time.

I-E-2. Jovian Magnetotail

During the years 1974 to 1977 the observations showed a tendency for Jovian increases at 1 AU to occur for a period of up to 5 months following the nominal connection time. The Jovian magnetotail was suggested (Mewaldt, et al., 1976; Pesses and Goertz, 1976) as a possible explanation of this tendency.

The model has energetic electrons populating the Jovian magnetotail and propagating to 1 AU on interplanetary magnetic field lines that are merged with the tail magnetic field lines. Figure I-1, from Mewaldt, et al., (1976), illustrates the geometry. Electrons would only be observed at 1 AU over the region of Earth's orbit that can be nominally connected to the Jovian magnetosphere. The length of the magnetosphere would determine the duration of the occurrence of electron increases

Figure I-1

Geometry of the magnetotail model. A heliocentric plot showing the shaded region in which the interplanetary magnetic field might be interconnected with an extended Jovian magnetotail of $\sim$ 2 AU in length. A solar wind velocity of 400 km/sec has been assumed. Earth and Jupiter positions are for April 1974. The tick marks on the Pioneer 10 trajectory mark 6-month intervals from the Jovian encounter on December 4, 1973. From Mewaldt, et al. (1976).

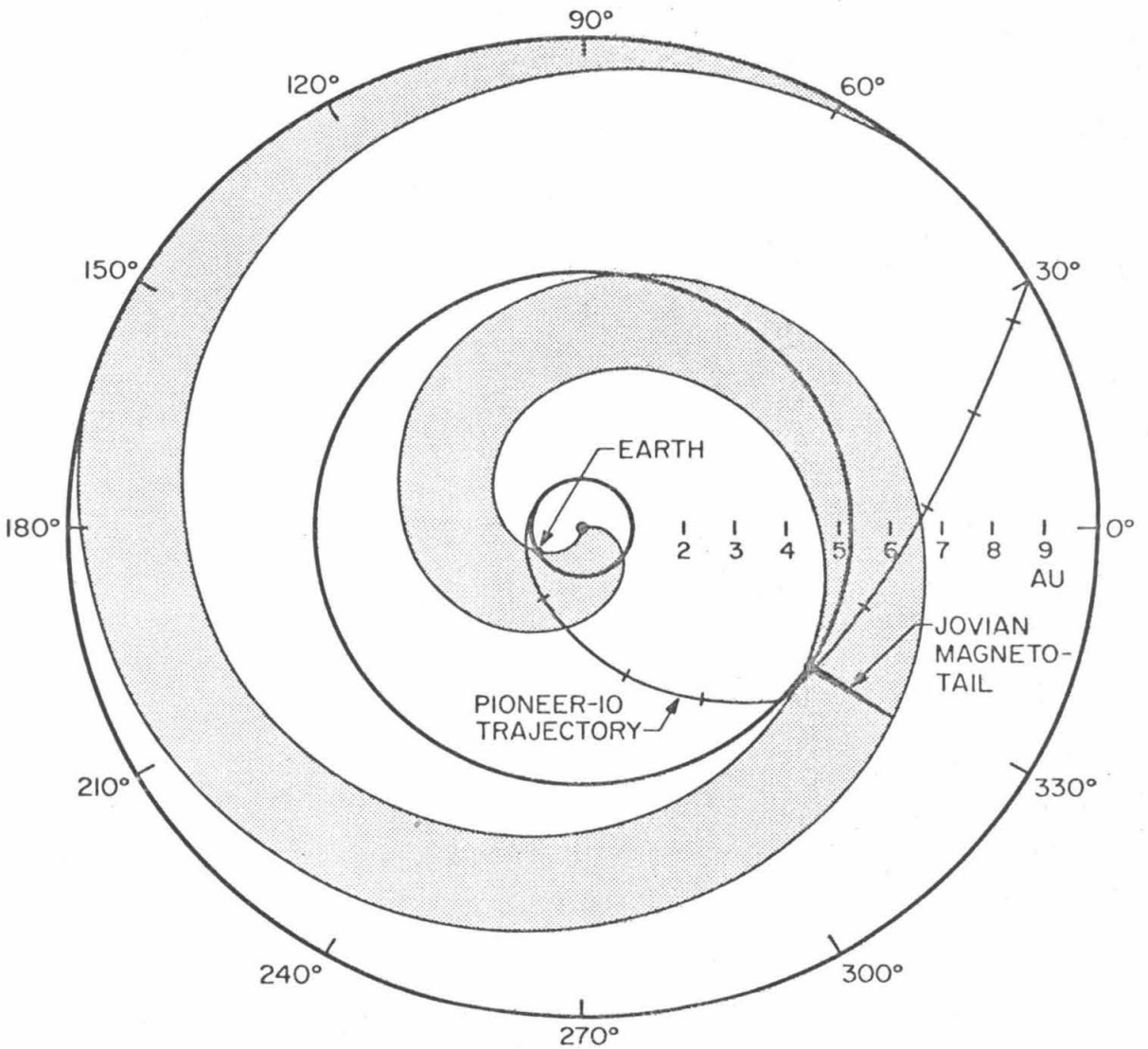
90°
120°
60°
150°
30°
180°
0°
210°
330°
240°
300°
270°
EARTH
1
2
3
4
5
6
7
8
9
AU
JOVIAN
MAGNETO-
TAIL
PIONEER-10
TRAJECTORY

in any synodic period with minor variations produced by different solar wind speeds. Given that Jovian electron increases at 1 AU occur over an interval of 4 months and assuming a solar wind speed of 400 km/sec, the length of the magnetotail was calculated as ~2 AU (Mewaldt, et al., 1976; Pesses and Goertz, 1976).

This model does not explain the pre-encounter electron increases observed by Pioneer 10 and Pioneer 11. However, Pesses and Goertz do not believe that the pre-encounter Pioneer 10 increases were associated with the electron increases seen at Earth. The Jovian increases seen at 1 AU at times before the nominal connection time could be explained by high speed solar wind streams making connection of magnetic field lines at Earth with the Jovian magnetotail possible during this period.

The magnetotail model also has difficulty explaining the observations of Pioneer 10 after encounter. As stated earlier, Conlon and Simpson (1977) concluded that CIR's act as barriers to the passage of Jovian electrons. From this barrier effect of the CIR's and from the time when the maxima of Jovian electron increases in the post-encounter time period begin to show a $1/R$ dependence, Pyle and Simpson (1977) find that the time behavior of the Jovian increases is consistent with a source region that extends at most 1 AU behind the planet and that is continuously emitting electrons.

Pyle and Simpson also note that no large electron fluxes

were observed within a CIR as might be expected if the magnetic field lines within a CIR were merged with a magnetotail that is populated with electrons and that directional anisotropies observed at the times of electron increases near CIR's were less than ~10 percent for the post-encounter time period.

Krimigis, et al. (1975) used the Jovian magnetotail as a possible explanation of the duration, up to 20 days, of the individual electron increases that are seen at Earth. They proposed that the flux tube containing Earth is merged to the Jovian magnetotail as the tube is convected down the length of the Jovian magnetotail. They suggest that an increase lasting 20 days implies a magnetotail length of 4.6 AU if the solar wind speed is 400 km/sec. However, as Pesses and Goertz (1976) and Jokipii (1976) point out, the flux tube does not stay connected to Earth for 20 days so the electrons would have to propagate from the region of the flux tube to Earth.

Later observations of the electron flux at 1 AU (Hartman, et al., 1977; Chenette, et al., 1977a,c) indicate that Jovian electron increases are seen throughout the synodic period and that the previous "2-4 month" tendency of Jovian increases to appear after the nominal connection time was because only the largest Jovian electron increases were observed. Any model incorporating the Jovian magnetotail must now explain the synodic envelope of the Jovian electron increases, not just

the occurrence of Jovian increases around the nominal connection time.

I-E-3. Scatter Free Diffusion

The correlation of high speed solar wind streams found by Gold, et al. (1976, 1977) led to the suggestion (Gold and Roelof, 1976; Gold, et al., 1976, 1977) that electrons diffuse with a long mean free path or undergo scatter free diffusion down interplanetary magnetic field lines that are associated with solar wind streams. The model proposes electron propagation from a magnetotail or an extended region behind Jupiter onto interplanetary magnetic field lines and then inward to Earth or outward to a stream-stream interaction region or CIR. Figure I-2, from Gold and Roelof (1976), shows the geometry. The electrons move freely along a stream-stream interaction region and then propagate along magnetic field lines that merge into the magnetic field lines in the interaction region on the side toward Jupiter. This means that electrons would propagate to the pre-encounter positions of Pioneer 10 and Pioneer 11 and also that electrons would propagate to 1 AU at times before the nominal connection time.

A difficulty in this model is the length of the Jovian

Figure I-2

Geometry of the scatter free diffusion model. Suggested route (arrows) of electron transport from the Jovian magnetotail via slow stream field lines to an advancing stream-stream interaction region at r_2 and then again via slow stream field lines from r_1 to the Pioneer spacecraft. From Gold and Roelof (1976).

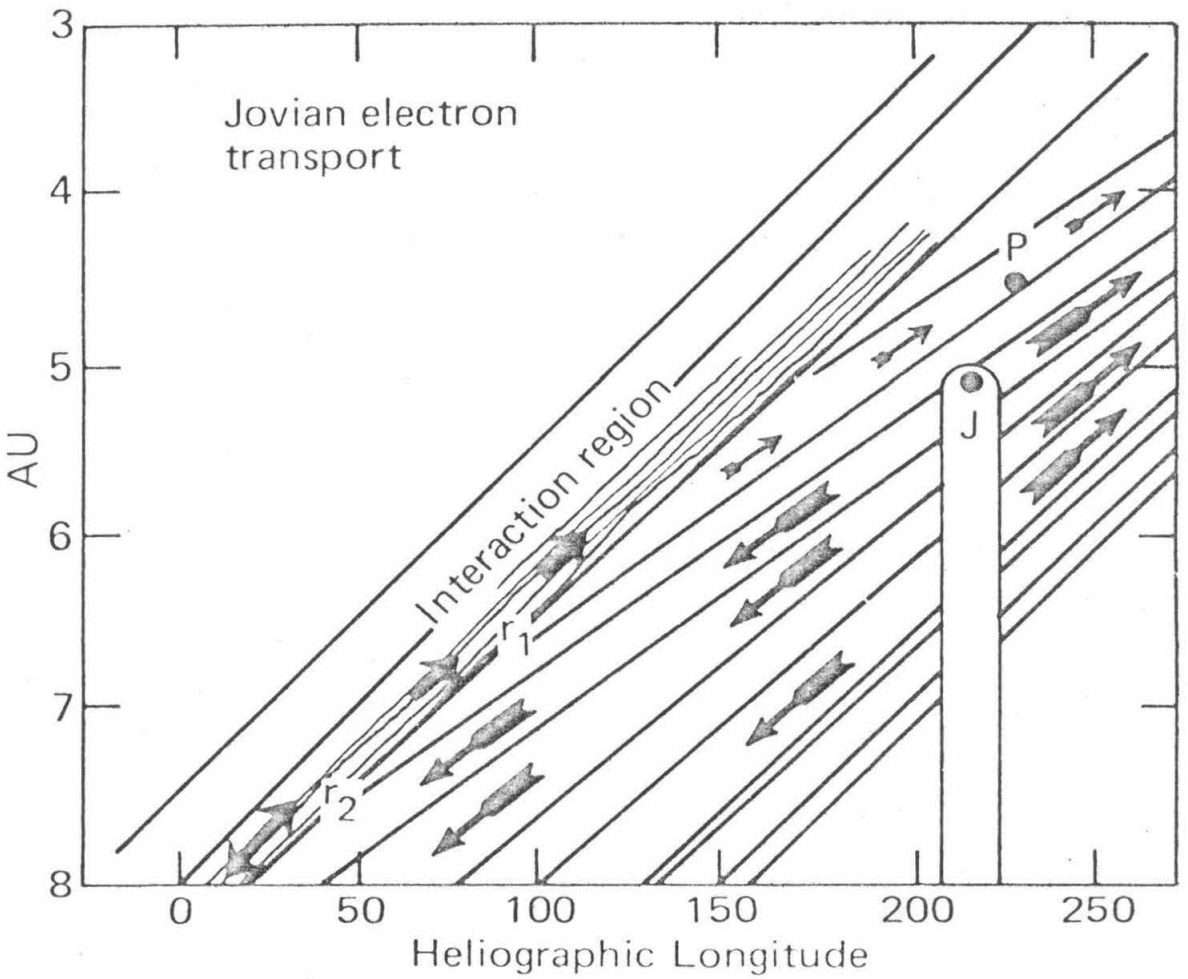
Jovian electron
transport
Interaction region
P
J
r_1
r_2
AU
3
4
5
6
7
8
0
50
100
150
200
250
Heliographic Longitude

magnetotail or emitting region needed to explain the synodic envelope of Jovian electron increases seen at Earth. In this respect this model has the same difficulty as the magnetotail model. Further, even though the model does have a mechanism to propagate electrons to the pre-encounter region, the detailed properties of the stream-stream interaction region are not discussed.

This scatter free diffusion model would also predict high fluxes within CIR's and flows or anisotropies along magnetic field lines. As with the magnetotail model, this model is inconsistent with the observations of Pyle and Simpson (1977).

I-E-4. Field Line Random Walk

Jokipii (1976) proposed that the random walk of magnetic field lines could distribute Jovian electrons around Earth's orbit. The idea was that magnetic field lines near Jupiter are populated with electrons, that these magnetic field lines then separate by random walking in space, and that the electrons on the separating magnetic field lines are spread out in longitude producing the 3-4 month time interval during which Jovian increases are seen at Earth.

Jokipii calculated that the spread produced by this model is about 4 months in extent. However, as stated earlier Jovian

increases are observed throughout the whole Jovian synodic period. A larger random walk than Jokipii derived would be needed to spread the electrons around all of Earth's orbit.

I-E-5. Convection-Diffusion

The fact that Jovian electrons had to propagate across the average spiral structure of the interplanetary magnetic field to the pre-encounter positions of Pioneer 10 (Chenette, et al., 1974) and Pioneer 11 (Conlon, 1978) led to a model of electron propagation incorporating convection and diffusion. Conlon (1978) found that the Pioneer 11 pre-encounter time behavior of Jovian increases could be modeled by assuming that if CIR's are impenetrable barriers to Jovian electrons (Conlon and Simpson, 1977) then the time that an increase occurred at Pioneer 11 was only a function of when CIR's passed either Pioneer 11 or Jupiter. The region between two CIR's was assumed to be empty of electrons until the front CIR passed Jupiter. After the front CIR passed Jupiter, the region of space between the CIR's started filling up with electrons. This filling was modeled by a two dimensional convection-diffusion equation. In this model Jupiter was assumed to be a point source (Pyle and Simpson, 1977; Chenette, et al., 1977b,c).

The coordinate system used in this convection-diffusion

model is shown in Figure I-3, from Chenette, et al. (1977c). This Cartesian coordinate system ignores the spiral structure of the interplanetary magnetic field, but it is a reasonable approximation to the average structure of the interplanetary magnetic field within a few AU of Jupiter. This model and the geometry are discussed in more detail in Appendix C. Using a value for the perpendicular diffusion coefficient of $k_x = 5 \times 10^{20}$ cm^2/sec, Conlon (1978) was able to fit the rise time profiles of three Pioneer 11 pre-encounter Jovian increases. The expected synodic envelope of Jovian increases at Earth was calculated from the equilibrium solution of this convection-diffusion model (Chenette, et al., 1977a,b,c; Conlon, 1978). Even though the spiral structure of the interplanetary magnetic field was ignored, the asymmetry of the synodic envelope was reproduced.

Figure I-3

Schematic drawing of the coordinate system used in the convection-diffusion model. Though the model is formulated in Cartesian coordinates, the values of the coordinates are measured parallel and perpendicular to the average interplanetary spiral magnetic field lines. The heavy spiral lines are the average field lines passing through Earth for the time period before the nominal connection time, $Earth_1$, and the time period after the nominal connection time, $Earth_2$. In this plot Θ is the spiral field angle at Jupiter given by $\Theta = TAN^{-1}\left(V_{SW}/\Omega_{\odot} \cdot R_J\right)$ where V_{SW} is the solar wind speed, $\Omega_{\odot}$ is the solar rotation rate, and R_J is the orbital radius of Jupiter. From Figure 2 of Chenette, et al. (1977c).

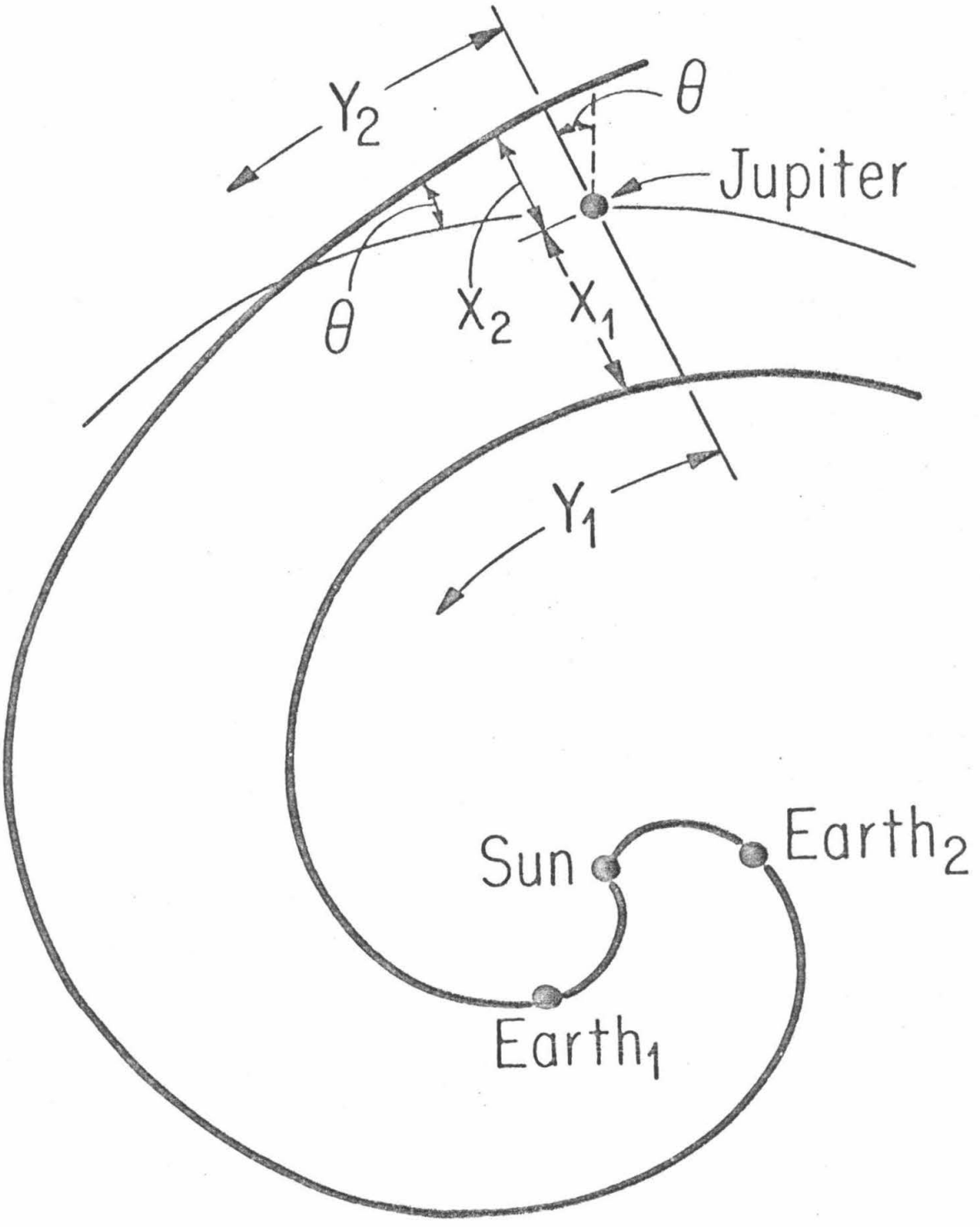
Y2
θ
Jupiter
θ
X2
X1
Y1
Sun
Earth2
Earth1

II. Data Analysis and Selection

II-A. Spacecraft

The data reported in this study were acquired by the two similar Caltech Electron/Isotope Spectrometer (EIS) instruments flown on the IMP-7 and IMP-8 satellites. This section is a review of the properties of the spacecraft and the EIS instruments germane to this study. More detailed information on the experiments is availible elsewhere (Hurford, et al., 1974; Mewaldt, et al., 1975; Hartman, 1976).

The IMP-7 and IMP-8 satellites are both in Earth orbits that are perturbed by the sun and moon. IMP-7 was launched on 72.270[†] and has osculating orbital elements for the date 76.060 of a semi-major axis of 35.0 Earth-radii, an eccentricity of 0.116, and an inclination of 26.0 degrees. IMP-8 was launched on 73.303 and has osculating orbital elements for 76.061 of a semi-major axis of 34.5 Earth-radii, an eccentricity of 0.097, and an inclination of 22.7 degrees. The actual orbits, projected onto the ecliptic plane, are plotted in Figure II-1 for the time period

---

† Within this study the IMP data will be referred to by the last two digits of the year and by the day-of-year number, e.g. Jan 1, 1974 is 74.001.

Figure II-1

Orbits of IMP-7 and IMP-8 for the time period 76.059 to 76.072 projected onto the ecliptic plane. The coordinates are Geocentric Solar Ecliptic (GSE) with distances given in Earth-radii. Also shown are the average positions of Earth's bow shock and magnetopause as determined by Behannon (1968).

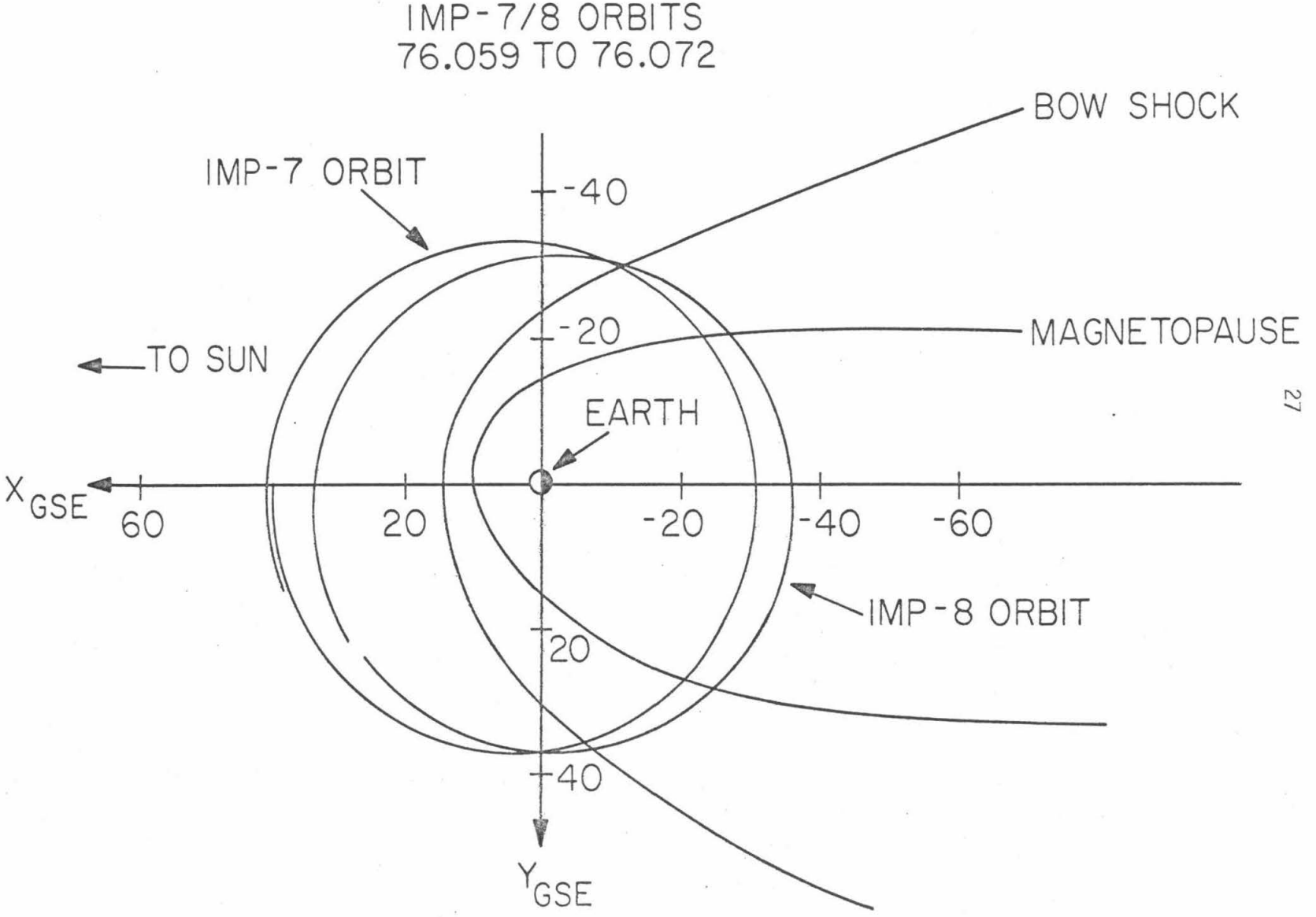
IMP-7/8 ORBITS
76.059 TO 76.072
BOW SHOCK
IMP-7 ORBIT
-40
-20
MAGNETOPAUSE
TO SUN
EARTH
X_{GSE}
60
20
-20
-40
-60
IMP-8 ORBIT
20
-40
Y_{GSE}

76.059 through 76.072. Also plotted in Figure II-1 is the average position of Earth's magnetosphere from Behannon (1968). Both satellites pass through part of Earth's magnetosphere during each orbit, but they spend a goodly portion of each orbit outside the bow shock in interplanetary space. During much of the time at least one spacecraft is in interplanetary space. Figure II-2 shows the azimuthal separation of the IMP-7 and IMP-8 satellites from the launch of IMP-8 in 73.303 until 77.329. The fraction of interplanetary coverage is low only from about the middle of 1975 until the middle of 1976 during which time the spacecraft are separated in azimuth by less than 80 degrees.

Bursts of magnetospheric electrons can contaminate observations of interplanetary electrons. The time periods of each spacecraft that contain such identified bursts will be eliminated from the data as outlined later. Figure II-2 also shows that for only a small fraction of the total observation period, near the beginning of 1976, are the spacecraft close enough together for both to see the same magnetospheric burst.

Both satellites have an orbital period of approximately 12-13 days. Twice this period is near the solar synodic rotation period of 27 days as seen at Earth. This coincidence requires careful analysis when attempting possible time correlations of the IMP data with recurrent interplanetary electrons.

Figure II-2

Plot of the difference in orbital azimuth of the IMP-7 and IMP-8 satellites from the launch of IMP-8 on 73.303 until 77.329. The vertical scale is the IMP-7 azimuth, ϕ_{IMP-7}, minus the IMP-8 azimuth, ϕ_{IMP-8}, both in degrees and in the Geocentric Solar Ecliptic coordinate system. Until 1976 IMP-7 is ahead of IMP-8, the positive differences, and then IMP-7 starts to follow IMP-8, the negative differences.

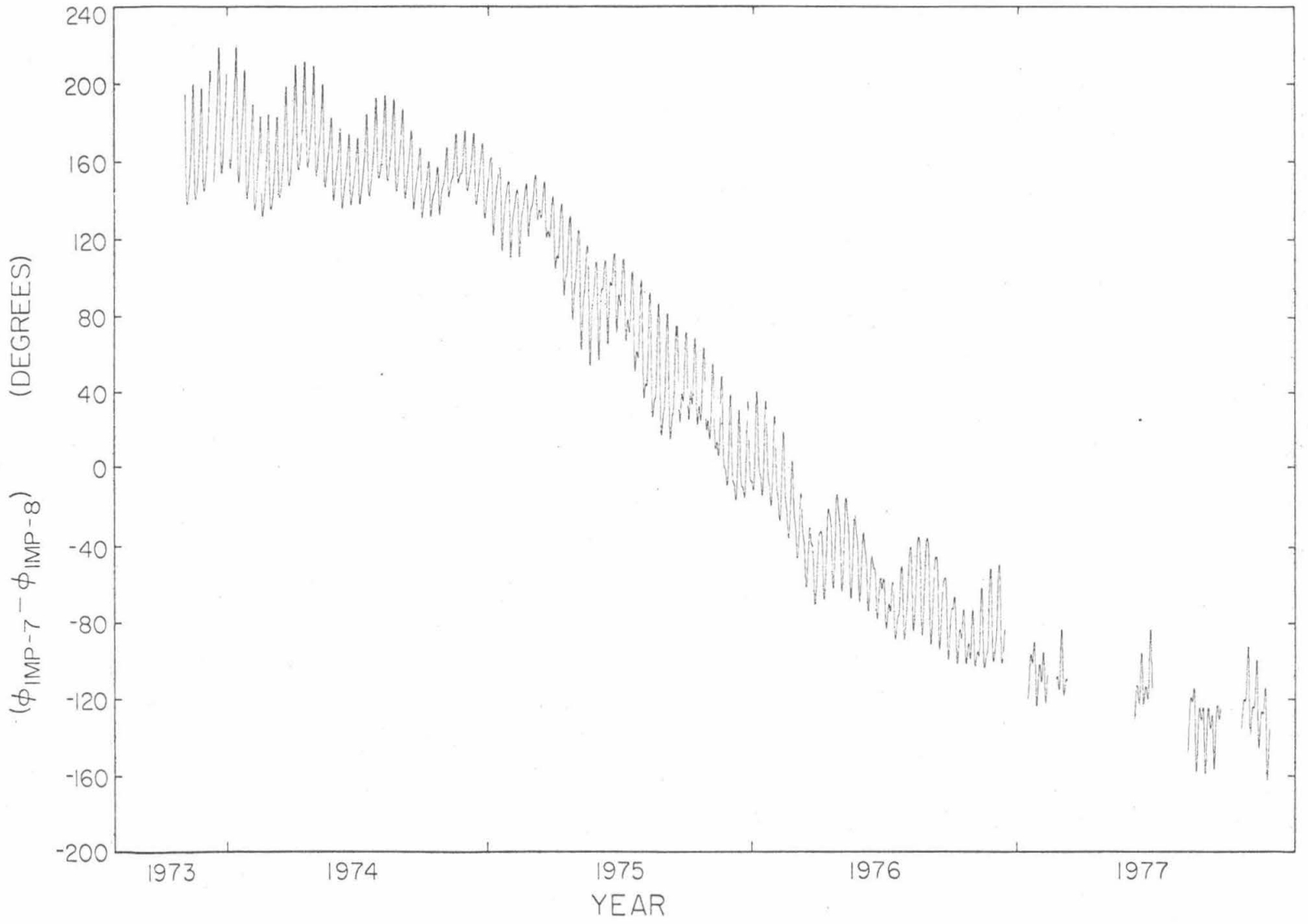
240
200
160
120
80
40
0
-40
-80
-120
-160
-200
(DEGREES)
$(\phi_{IMP-7} - \phi_{IMP-8})$
1973
1974
1975
1976
1977
YEAR

II-B. Electron/Isotope Spectrometers

The EIS experiments are each composed of a particle telescope and electronic instrumentation. The telescopes consist of a stack of silicon detectors surrounded by a plastic scintillator anti-coincidence detector as shown in Figure II-3. The telescope stack for IMP-8 differs from that of IMP-7 in that the annular detectors D3 and D4 are replaced with solid detectors and placed between D8 and D9. This change increases the Narrow Geometry geometrical factor for IMP-8. In all other respects IMP-8 responds so closely to the response of IMP-7 that the following description, though stated explicitly for IMP-7, also applies to IMP-8.

All of the solid state detectors are fully depleted silicon surface barrier detectors with negligible dead layers. The nominal detector thickness is 1000μm except for D2 which is 50μm thick. Detectors D0, D1, D3, and D4 (only D0 and D1 on IMP-8) are annular detectors that define the Narrow Geometry opening angle. D11 is an anti-coincidence shield viewed by a photomultiplier tube. An aluminized mylar window, ~2.4 mg/cm^2 thick on IMP-7 and ~3.2 mg/cm^2 thick on IMP-8, protects the detectors from sunlight.

The instrument has three basic modes of operation labeled Narrow Geometry, Wide Geometry, and Neutral. In each mode the

Figure II-3

Cross sections of the Caltech Electron/Isotope Spectrometers on IMP-7 and IMP-8. The detectors D0 through D10 are fully depleted silicon surface barrier detectors 1000μm thick except for D2 which is 50μm thick. D11 is a plastic scintillator anticoincidence shield. The detectors D0, D1, D3, and D4 on IMP-7 are annular detectors which define the Narrow Geometry of the detector telescope. The IMP-8 telescope has D3 and D4 as solid detectors moved deeper into the stack in order to increase the Narrow Geometry geometrical factor for IMP-8.

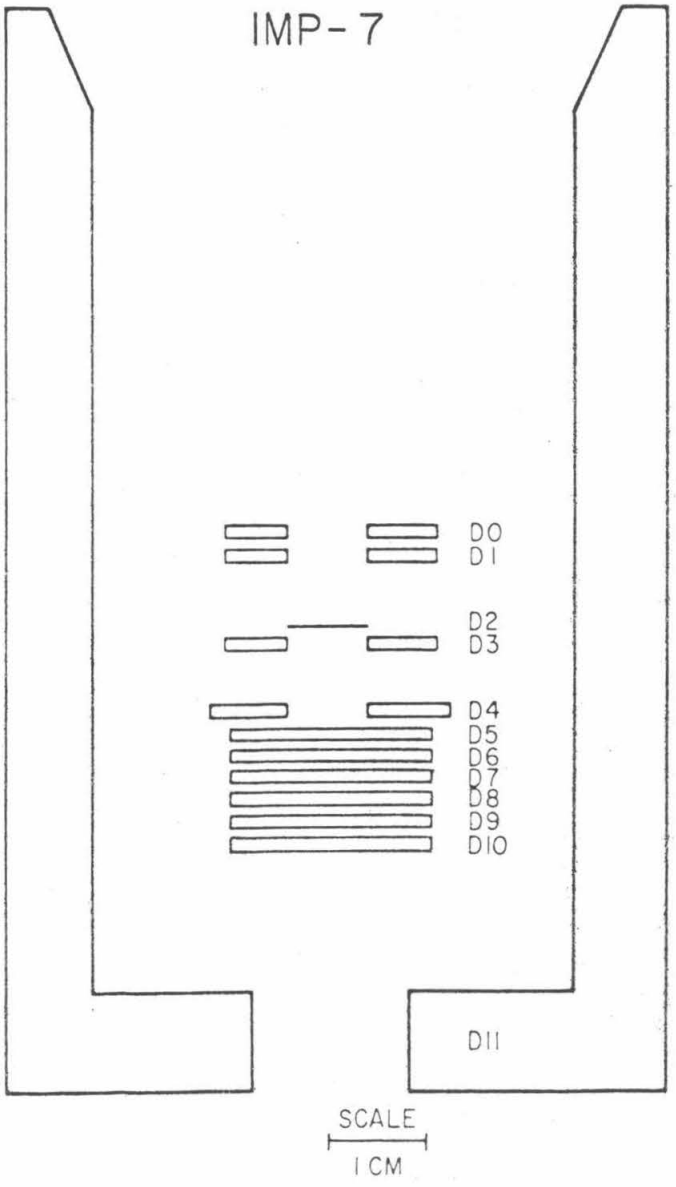
IMP-7
D0
D1
D2
D3
D4
D5
D6
D7
D8
D9
D10
D11
SCALE
1 CM

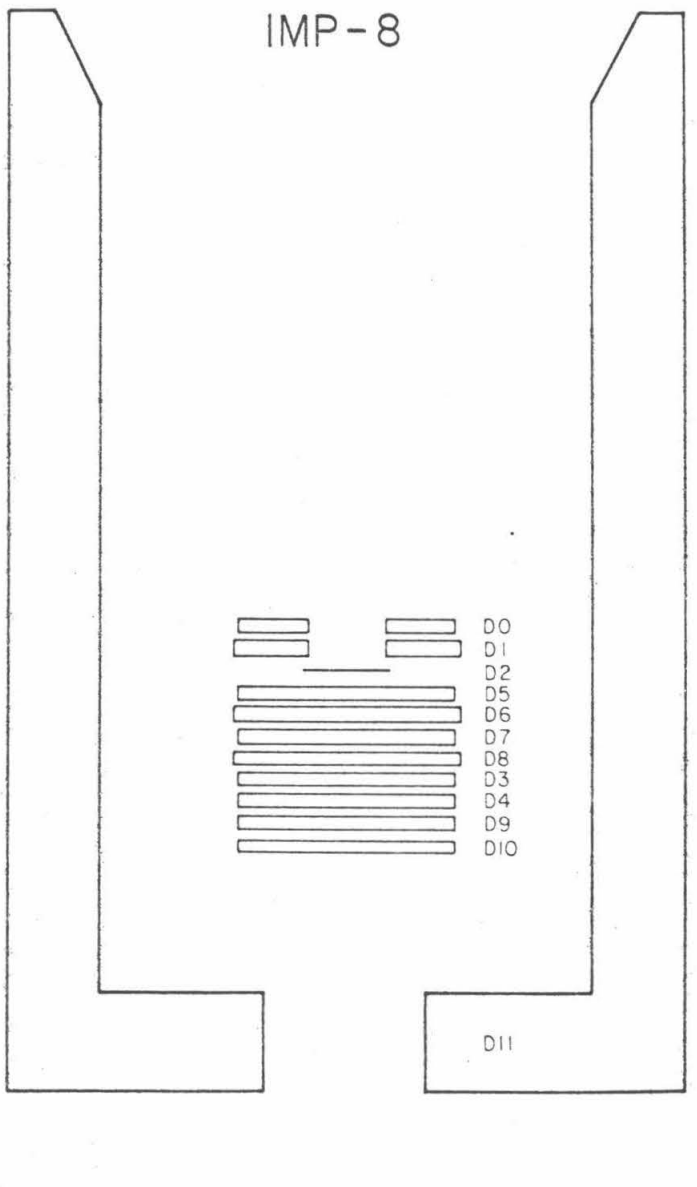
IMP-8
D0
D1
D2
D5
D6
D7
D8
D3
D4
D9
D10
D11

detector outputs are pulse height analyzed and the range information, together with the energy loss and total energy, are used to identify the analyzed particle. Only the Wide Geometry and Neutral event modes are used in this study.

A Wide Geometry event is a particle that triggers D0 and possibly any other detectors except D10 or D11. The geometrical factor for these events is defined by D0, D11 and the last detector triggered. Calculated values of the geometrical factor vary from 1.57 cm^2-sr to 0.25 cm^2-sr (Hartman, 1973) for IMP-7 and from 1.12 cm^2-sr to 0.41 cm^2-sr (Vidor, 1974) for IMP-8. The Neutral analysis mode includes events that trigger D7 without triggering D0 through D4, D5, D10, or D11. This mode is used to monitor the background of neutral particles such as gamma-rays which interact within the detector stack and contribute to the total number of counted events.

Besides analyzing individual events, the instrument also measures the rates of selected event types. Table II-1 lists some of these rates and their logic equations or detector signatures. Also listed are the physical significance of these rates and their approximate energy ranges for electrons and protons. The rates are used to conveniently monitor the flux of selected particle types and to calculate the live-times for the Narrow and Wide Geometry modes. The rates do not all have 100 percent live-time. In particular the ELO and PLO rates must be corrected

Table II-1

Rate	Logic equation	Particle and energy range for electrons and protons
ELO	$N \cdot S \cdot \overline{d2h} \cdot D5 \cdot \overline{d5h} \cdot \overline{d6} \cdot \overline{d7} \cdot \overline{aip}$	Electrons, 0.16 to 1 MeV
EHI	$N \cdot S \cdot \overline{d2} \cdot D5 \cdot \overline{d5h} \cdot D6$	Electrons, 1 to 6 MeV
PLO	$N \cdot S \cdot D2H \cdot \overline{d5} \cdot \overline{d5h} \cdot \overline{d6} \cdot \overline{d7} \cdot \overline{aip}$	Nuclei, 1.2 to 2.4 MeV
PHI	$N \cdot S \cdot D2 \cdot D5H \cdot \overline{d6}$	Nuclei, 4 to 10 MeV
DOS	$D0 \cdot S$	Electrons, 0.16 to 6 MeV and nuclei, 1 to 43 MeV
DO1S	$D0 \cdot D1 \cdot S$	Electrons, 1 to 6 MeV and nuclei, 12.5 to 43 MeV
PEN	$N \cdot D5 \cdot D6 \cdot D10 \cdot \overline{d11}$	Electrons, >3 MeV and nuclei, $\gtrsim 30$ MeV
NEUT	$N \cdot \overline{d5} \cdot D7 \cdot S$	Gamma-rays and neutrons

Di signifies a triggered detector and $\overline{di}$ signifies a not-triggered detector.

$N = \overline{d0} \cdot \overline{d1} \cdot \overline{d3} \cdot \overline{d4}$

$S = \overline{d10} \cdot \overline{d11}$

AIP = Arithmetic In Progress

D2H and D5H are the high level thresholds of D2 and D5 respectively.

The IMP-8 PEN rate is not a useful quantity.

for the dead-time produced by the Arithmetic In Progress (AIP) term. The AIP term reflects the fact that the D2H threshold is determined by the D2 pulse height and therefore no new rate events for ELO and PLO can be seen while the D2H pulse height is being calculated.

The spacecraft is spin stablized with the spin axis close to the normal to the ecliptic plane. Since the telescope axis is perpendicular to the spin axis, as the spacecraft spins the telescope opening angle scans particle fluxes within the ecliptic plane. Each revolution of the spacecraft is divided into eight equal sectors and each event is tagged according to its sector of incidence. Selected rates are also accumulated by sectors. This labeling of events and rates by sector enables the calculation of anisotropies within the ecliptic plane.

II-C. Electron Measurements

Electrons are separated from nuclei by energy loss, total energy, and range information. The two parameter dE/dx versus total E event analysis technique means that only those electrons with sufficient energy to trigger at least DO and D1 can be uniquely identified as electrons. The energy range of incident electrons that have ranges from DO1 events to DO through

D9 (DO-9) events is ~1 to ~10 MeV. The event types used in this study are defined by their range signatures and pulse heights and are listed in Hartman (1978).

Jovian electron increases observed at Earth are typically small having an increase of a factor <10 as compared to solar flares which have an increase of many orders of magnitude. These low fluxes require the use of the Wide Geometry analysis mode which has a geometrical factor for electrons larger than the geometrical factor for Narrow Geometry electrons.

The flux of ~1-6 MeV electrons is calculated by first subtracting from the observed event counts an estimate of the contribution due to the neutral background and then dividing by the Wide Geometry live-time and by the effective geometrical factor for electrons. The electron flux plotted in the figures in this study will be expressed usually as a count rate, COUNTS/SEC.

II-C-1. Electron Response

Electron measurements in the energy range of 1-6 MeV are complicated by the large amount of scattering occurring at these energies (Lupton and Stone, 1972a,b). This scattering necessitates electron particle calibration of the telescope to determine its response to incident electrons.

The calibration of the IMP-7 flight telescope was done

with monoenergetic electron beams of 0.2 to ~3 MeV from a beta spectrometer. The detailed results of this calibration are compiled and discussed in Mewaldt (1975). Important to the measurement of 1-6 MeV Wide Geometry electrons is the energy dependence of the geometrical factors for the different ranges.

The geometrical factors for the Wide Geometry ranges D01 through D0-7 are plotted in Figure II-4a (Mewaldt, 1975) as a function of the incident electron energy. These geometrical factors have been integrated over the incident angle of the calibration beams and they correspond to an incident isotropic flux of particles.

An effective geometrical factor, G_{eff}, and an effective energy threshold, $E_{T(eff)}$, are defined by the equation

$$G_{eff} \int_{E_{T(eff)}}^{6\,MeV} \left(\frac{dJ}{dE}\right) dE = \sum_{\substack{ALL \\ RANGES}} \int_{0}^{\infty} G_i(E) \left(\frac{dJ}{dE}\right) dE$$

where $\frac{dJ}{dE}$ is the incident electron spectrum and the $G_i(E)$ are the response functions for the various ranges. The differential electron spectrum is assumed to be a power law of the form $\frac{dJ}{dE} \propto E^{-\gamma}$ The effective threshold energy is chosen as the energy that produces an effective geometrical factor approximately independent of the power law index, γ, over the range $0.5 \leq \gamma \leq 4$.

Figure II-4

Electron response functions of the IMP-7 EIS. Figure II-4a is the calibrated response functions for various ranges of the IMP-7 telescope (Mewaldt, 1975). Figure II-4b is, for the incident energy interval 0.0 to 2.9 MeV, the IMP-7 calibrated response functions in Figure II-4a summed over the ranges and, for the energy interval 2.9 to 10 MeV, the estimated IMP-7 response derived from the calibration data for a telescope similar to the IMP-8 flight telescope. The detector range in Figure II-4a refers to the last detector triggered. The curve for detector range 1, corresponding to electrons that triggered detectors DO and D1, DO1 events, has been multiplied by one-half.

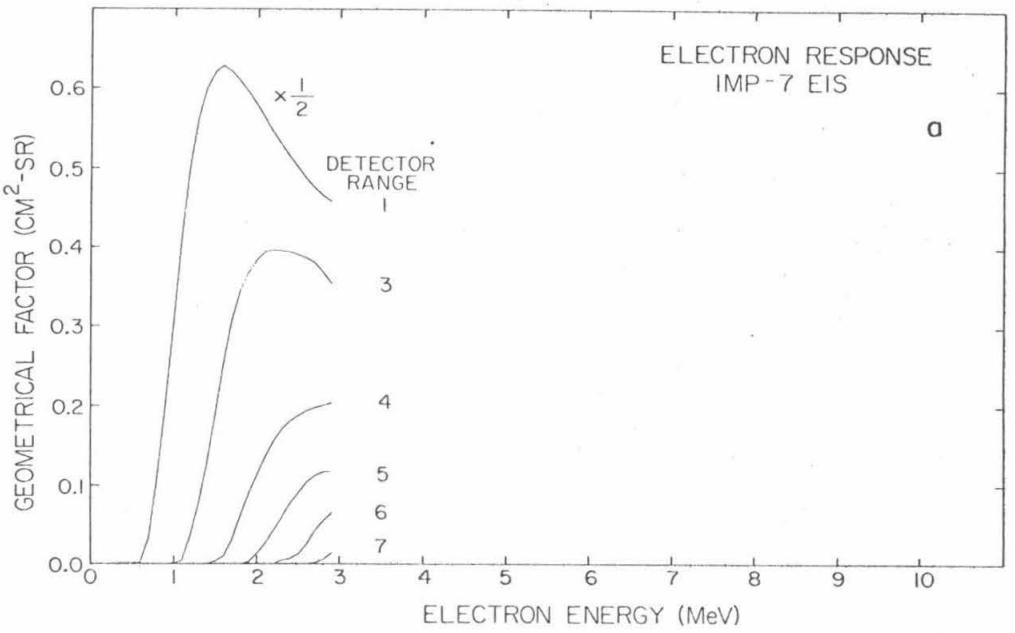
ELECTRON RESPONSE
IMP-7 EIS
a
×1/2
DETECTOR RANGE
1
3
4
5
6
7
GEOMETRICAL FACTOR (CM²-SR)
ELECTRON ENERGY (MeV)

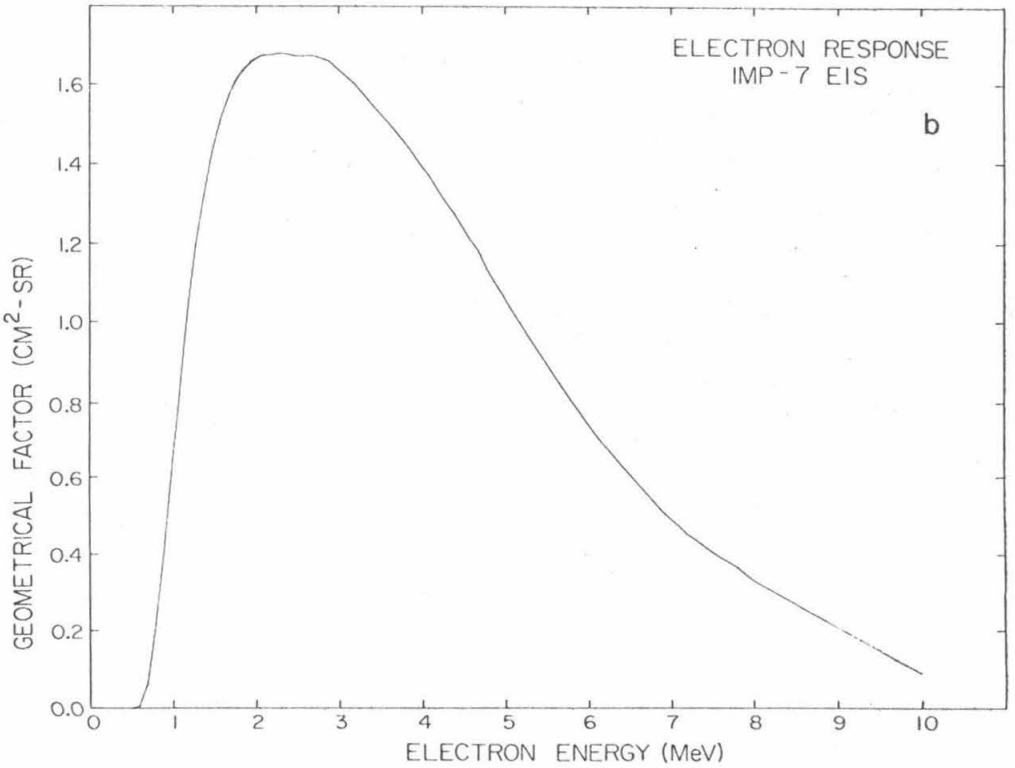
ELECTRON RESPONSE
IMP-7 EIS
b
GEOMETRICAL FACTOR (CM²-SR)
ELECTRON ENERGY (MeV)

This range of γ covers the observed Jovian electron spectra of γ = 1.3-2.0 (Teegarden, et al., 1974; Mewaldt, et al., 1975, 1976).

As shown in Figure II-4a, IMP-7 was only calibrated with electrons of up to 2.9 MeV. The IMP-7 electron response below 3 MeV is the sum of the response functions in Figure II-4a. The electron response from 2.9 MeV to 10 MeV is estimated from the response of a telescope similar to the IMP-8 flight telescope that was calibrated for electrons of energies up to 10 MeV. This calibration curve was normalized to the IMP-7 calibrated response at 2.9 MeV. The electron response function used to calculate an effective geometrical factor is plotted in Figure II-4b.

The effective geometrical factor is plotted in Figure II-5 against the power law index with the threshold energy as a parameter. The curve with an effective threshold of 1 MeV is essentially flat in the range γ = 0.5-4. The effective geometrical factor is taken as 1.50 cm^2-sr. These numbers are representative of an ideal telescope with a constant electron response function for incident electrons from 1-6 MeV that has the same total counting rate as the IMP telescope.

Figure II-5

Plot of the effective geometrical factor versus the spectral index of incident particles with the power law $\frac{dJ}{dE} \propto E^{-\gamma}$. The set of curves are for threshold energies, $E_{T_{(eff)}}$, from 0.5 to 1.4 MeV.

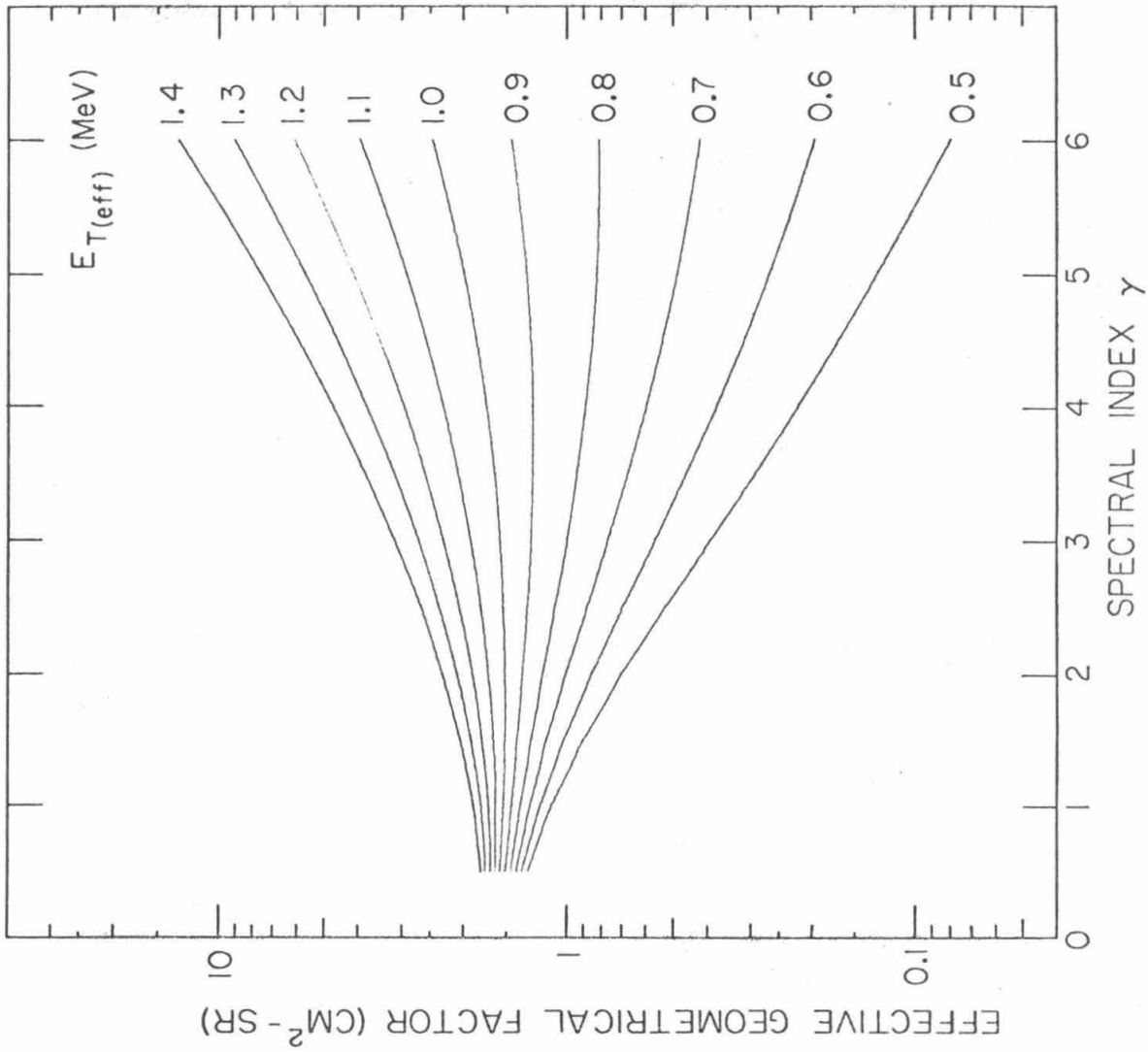
$E_{T(eff)}$ (MeV)
1.4
1.3
1.2
1.1
1.0
0.9
0.8
0.7
0.6
0.5
10
1
0.1
0
1
2
3
4
5
6
SPECTRAL INDEX γ
EFFECTIVE GEOMETRICAL FACTOR (CM^2 - SR)

II-C-2. Background

The background for electron events is mainly due to gamma-rays that are generated within the spacecraft material and that scatter in the detectors or in nearby material and produce recoil electrons that are then detected simulating incident electrons. This background is extensively discussed in Mewaldt, et al. (1977). The Neutral analysis mode monitors the background of gamma-rays and neutrons. The background correction is calculated by the equation

$$CEC = EC - CF \cdot NEC$$

where CEC is the corrected event count, EC is the raw event count, CF is the correction factor for this event type, and NEC is the neutral event count. The corrected event count is set equal to zero if the background correction is greater than the raw event count. The correction factors used in the background subtraction when calculating the 1-6 MeV electron flux are

$$CF = 0.20 \pm 0.01 \text{ for IMP-7 and}$$

$$CF = 0.235 \pm 0.010 \text{ for IMP-8.}$$

These correction factors are derived from the gamma-ray calibrations performed on the instruments before their launches.

Histograms for six-hour averages of the actual raw flux, the estimated background flux, and the corrected flux are shown in Figure II-6 for IMP-7 and in Figure II-7 for IMP-8. These

Figure II-6

IMP-7 histograms of flux and background. The top panel contains the histograms of the raw flux and the estimated background flux. The background flux histogram has been divided by 5. The middle panel is the histogram of the ratio of the estimated background flux to the raw flux. The bottom panel contains the histograms of the raw flux and the background corrected flux. Each histogram contains 6563 six-hour averages.

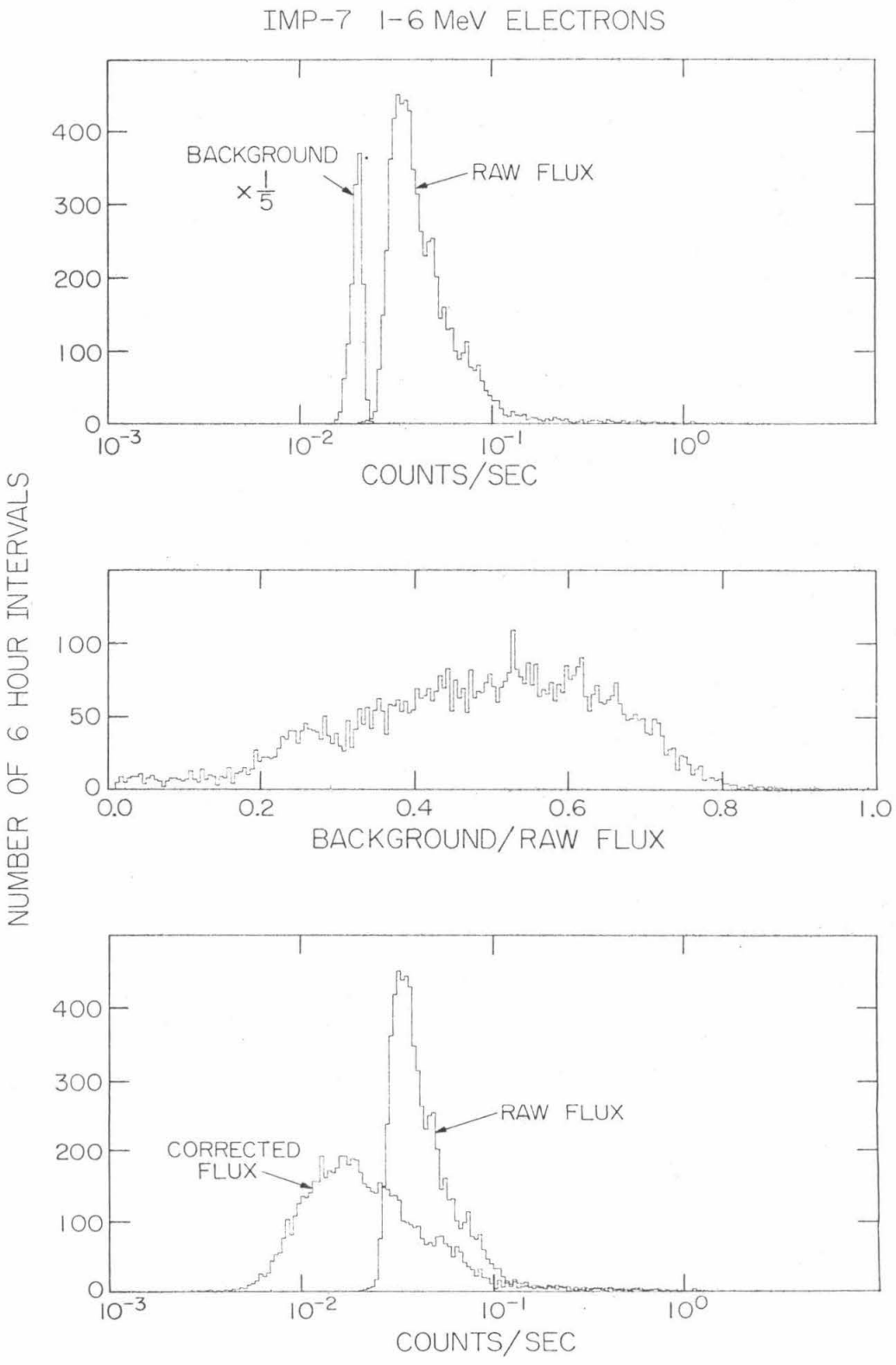
IMP-7 1-6 MeV ELECTRONS
NUMBER OF 6 HOUR INTERVALS
BACKGROUND
× 1/5
RAW FLUX
400
300
200
100
0
10^-3
10^-2
10^-1
10^0
COUNTS/SEC
100
50
0
0.0
0.2
0.4
0.6
0.8
1.0
BACKGROUND/RAW FLUX
RAW FLUX
CORRECTED
FLUX
400
300
200
100
0
10^-3
10^-2
10^-1
10^0
COUNTS/SEC

Figure II-7

IMP-8 histograms of flux and background. The top panel contains the histograms of the raw flux and the estimated background flux. The background flux histogram has been divided by 5. The middle panel is the histogram of the ratio of the estimated background flux to the raw flux. The bottom panel contains the histograms of the raw flux and the background corrected flux. Each histogram contains 5376 six-hour averages.

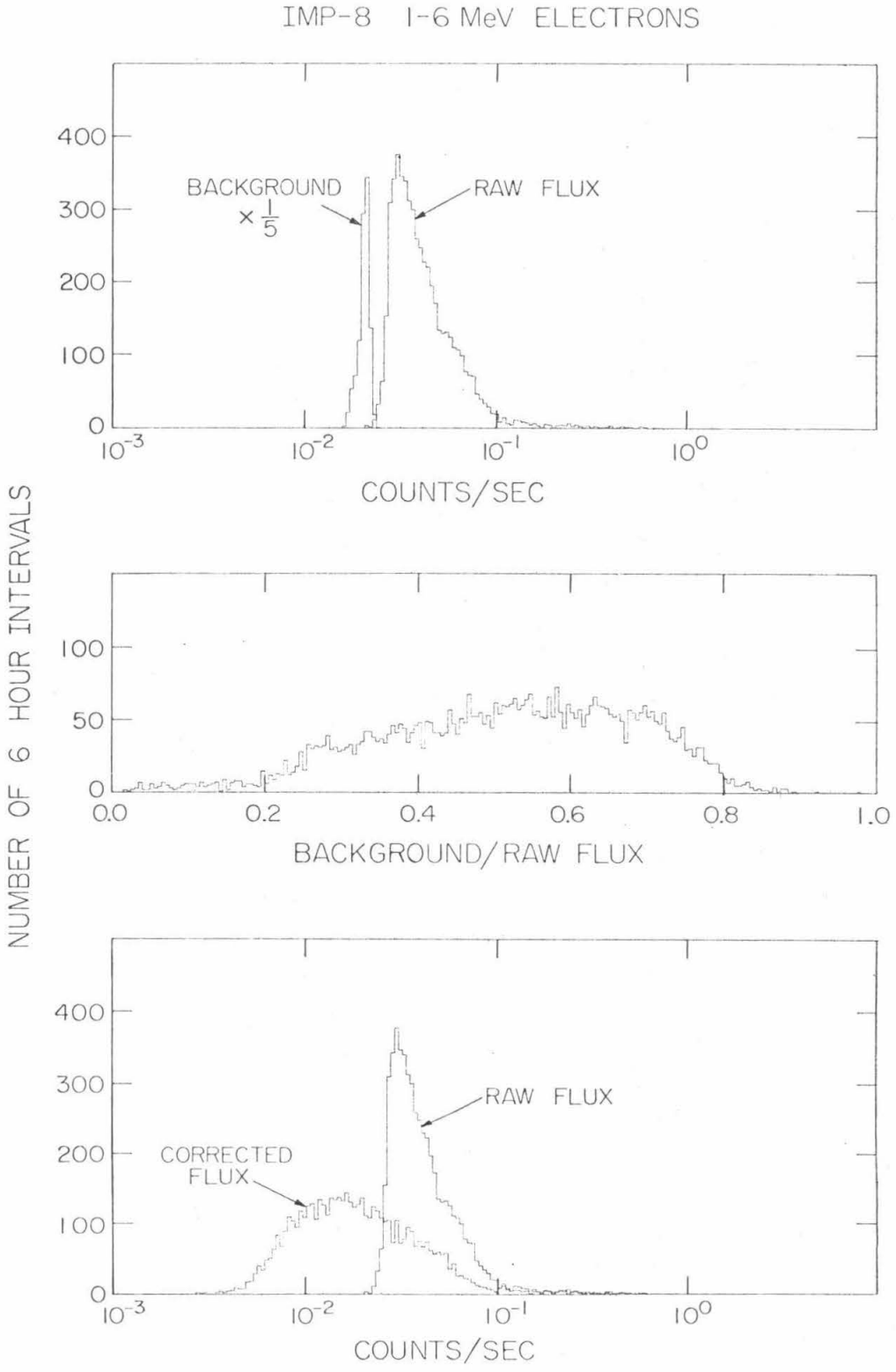
IMP-8 1-6 MeV ELECTRONS
NUMBER OF 6 HOUR INTERVALS
400
300
200
100
0
BACKGROUND
× 1/5
RAW FLUX
10^-3
10^-2
10^-1
10^0
COUNTS/SEC
100
50
0
0.0
0.2
0.4
0.6
0.8
1.0
BACKGROUND/RAW FLUX
400
300
200
100
0
RAW FLUX
CORRECTED
FLUX
10^-3
10^-2
10^-1
10^0
COUNTS/SEC

plots show that the estimated background flux is always less than the raw flux and is rarely more than 80 percent of the raw flux and that the background flux is essentially constant.

II-C-3. Data Processing

The raw experimental data are stored on magnetic tapes and go through intermediate processing steps before the data are in a form convenient for use. The initial IMP data processing and generation of the abstract tapes containing the data are described in Garrard (1974) and references therein.

The IMP data used in this study were stripped from the abstract tapes and accumulated for one hour intervals. The tapes containing the stripped data are described in Hartman (1978) and were the input data for generating flux, rate, and orbit information for any time interval that was a multiple of one hour.

The data for one hour intervals were checked for "bad" data periods and then were summed into intervals six hours long. The data for one hour intervals were defined to be "bad" if any of the rates NEUT, DOS, DOlS, ELO, PLO, D8, PHI, or PEN had a rate accumulation time of zero seconds. When the one hour interval was "bad" it was not added into the sum for the six hour interval. Also the neutral rate was checked for each one hour interval. If the neutral rate on IMP-7 was less than

0.06/sec or greater than 0.14/sec, then the neutral rate was ignored and a new neutral rate derived from the D8 rate by the procedure outlined in Appendix A. The procedure for checking the one hour intervals for the IMP-8 data was the same except that the neutral rate was "bad" when the rate was less than 0.05/sec or greater than 0.13/sec. The neutral rate was rarely "bad" except for a period of a few months in 1973 on IMP-7.

II-C-4. Flux Calculation

The live-time for a particular event type was calculated from the rate and event counts of an event type that has a priority equal to the desired event type. For Wide Geometry events the estimate of the live-time was calculated from the Neutral event count and the neutral rate by the equation

$$(\text{live-time}) = (\text{NEC} / \text{NEUT}) .$$

When the neutral rate was "bad" as discussed in the previous section, the live-time contribution from those "bad" one hour intervals was derived from the D01S event count and the D01S rate. This was a result of the procedure described earlier that was used to calculate a neutral rate and event count when the neutral rate was "bad".

Since Wide Geometry events have a lower analysis priority than Narrow Geometry events, the live-time for Wide Geometry events can approach zero during solar flares when the rate of Narrow Geometry events is high.

The flux of electrons in the energy range of 1-6 MeV was then calculated using the following equation

$$FLUX = \frac{(EC - CF \cdot NEC)}{\left(\frac{NEC}{NRC} \cdot NAT\right)} \cdot \left(\frac{F}{GF}\right) \qquad \text{II-1}$$

where FLUX is the flux of 1-6 MeV electrons, EC is the raw event count of electron events, GF is the effective geometrical factor, and F is the normalization factor. The values of CF for 1-6 MeV electrons are 0.20 for IMP-7 and 0.235 for IMP-8 and the value of GF is $\sim$1.5 cm^2-sr. For IMP-7 the normalization factor is unity and for IMP-8 the normalization factor is 1.095.

II-C-5. Error Analysis of the Flux Calculation

The sources of error in determining the flux are of three types: one, the statistical fluctuations in the number of counts measured for both the events and the rates; two, errors in determining the calibrated values of the geometrical factor and of the neutral correction factor; and three, systematic errors in the estimation of the rates or the live-time due to various instrumental properties that are not well understood or are not included in those estimates.

The statistical errors and errors in the calibrated values F, CF, and GF used in the calculation of the 1-6 MeV electron flux are discussed in detail in Appendix A. The histograms

plotted in Figure A-1 of Appendix A show that the range of the relative statistical error is ~5 to ~20 percent and that for the six-hour averages the statistical error is usually greater than the constant contribution to the relative error from the error in determining F, CF, and GF which together contribute ~7-8 percent to the relative error. Figure A-2 of Appendix A shows that most six-hour averages of the electron flux are measured to a significance greater than 2σ from a zero flux level.

An example of a possible source of systematic error is the rate dead-time which was ignored when calculating the live-time. At high rates the rejected event time of ~15μsec can become important. The high rates usually occur during solar flares but since the time periods containing solar flares have been eliminated from the data, ignoring this dead-time should not affect the fluxes during the other lower rate periods.

II-C-6. Relative Calibration of IMP-8 to IMP-7

In order to combine the fluxes measured by the two satellites, the normalization factor, F, in Equation II-1 must be known. Since the IMP-7 flight telescope was calibrated, while the IMP-8 flight telescope was not, the normalization factor is assumed unity for IMP-7 and is found for IMP-8 by examining the ratio of the background corrected counting rates observed by both

satellites.

The background corrected counting rate is Equation II-1 without the term (F / GF). The background correction is assumed accurate so that the ratio reflects the normalization at all flux levels. Taking the ratio of the counting rates as the normalization factor assumes that both satellites observe the same fluxes. In fact one or the other telescope sometimes sees a higher counting rate, mostly due to electron bursts from Earth's magnetosphere. Because of the ~5 years of observations, the distribution of the counting rate ratio can be used to find out how reasonable the above assumption is and to determine a value of F for IMP-8.

Plotted in Figure II-8 is the distribution of the counting rate ratio (FLUX IMP-7)/(FLUX IMP-8) for the background corrected counting rates of the IMP-7 and IMP-8 satellites. The data are for one day averages with 1337 data points in the distribution. The solid curve is a Gaussian fitted to the peak or center of the distribution by measuring the full width at half maximum, FWHM, calculating the sigma from its relation to the FWHM for a Gaussian, σ = FWHM / 2.354, and taking the mean as the midpoint between the end-points for the FWHM. This procedure yields μ = 1.095, σ = 0.132 with χ^2_{FWHM} = 16.2 /(29 - 2) or 0.6 for the data points within the FWHM.

The excess counts outside the peak are due to the satellites

Figure II-8

Histogram of the ratio of the background corrected counting rates, (FLUX IMP-7)/(FLUX IMP-8), observed by the IMP-7 and IMP-8 satellites for one day averages. The solid curve is a Gaussian fit to the peak between the end-points of the full width at half maximum. The parameters of the Gaussian are μ = 1.095, σ = 0.123, and χ^2_{FWHM} = 0.6.

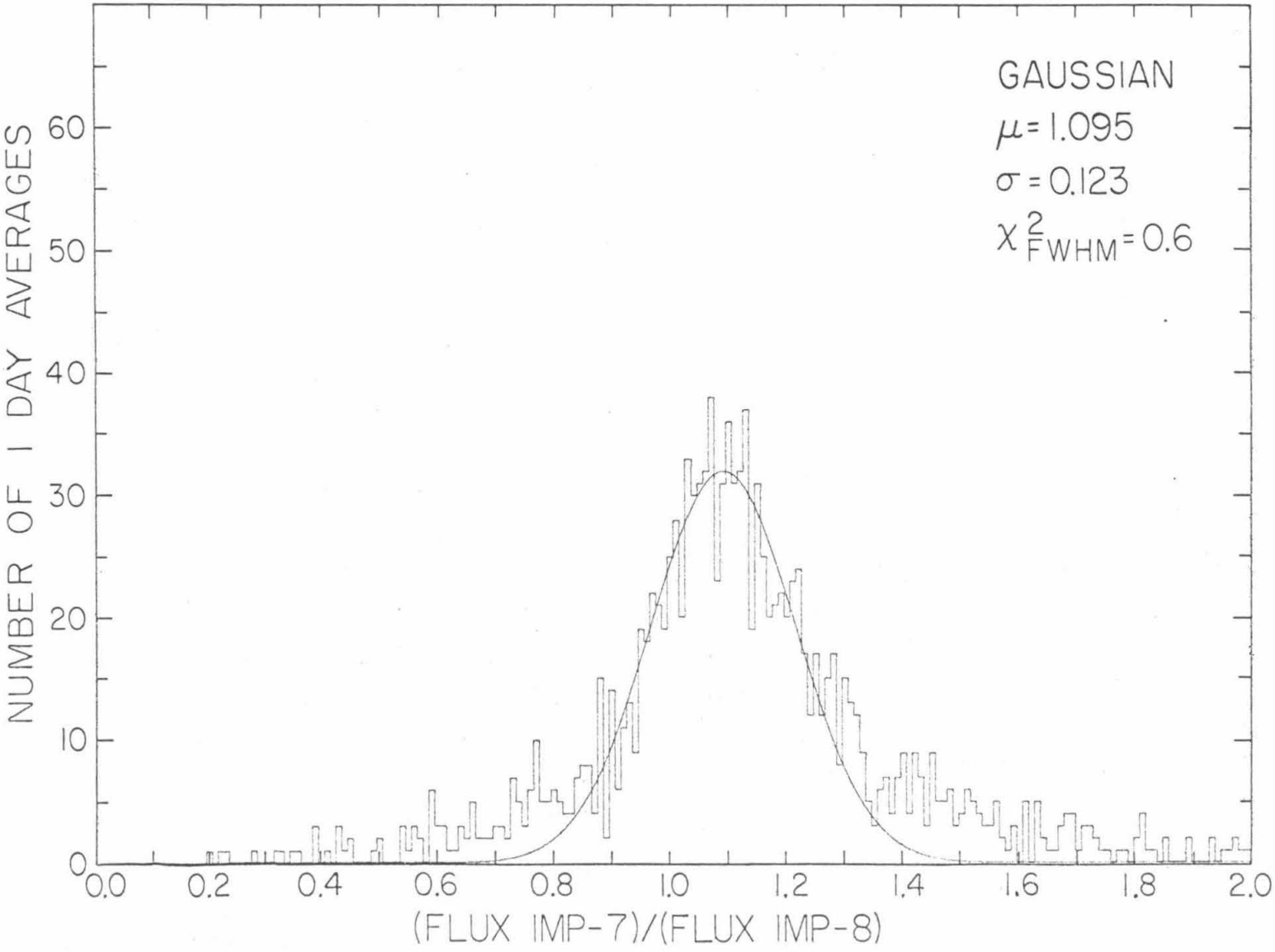
GAUSSIAN
μ = 1.095
σ = 0.123
χ²FWHM = 0.6
NUMBER OF 1 DAY AVERAGES
0
10
20
30
40
50
60
0.0
0.2
0.4
0.6
0.8
1.0
1.2
1.4
1.6
1.8
2.0
(FLUX IMP-7)/(FLUX IMP-8)

not observing the same flux. These counts are a small fraction of the total number of observations so the assumption that the satellites do see the same flux is reasonable. In subsequent sections the value F = 1.095 will be used to normalize the IMP-8 fluxes to the IMP-7 fluxes.

II-D. Identification and Elimination of Periods of Solar Flares and Magnetospheric Electron Bursts

As previously noted, the 1-6 MeV electron flux observed by the IMP satellites contain time periods during which solar flares and magnetospheric bursts occur. In order to study only the interplanetary non-solar electron flux, these solar flares and magnetospheric electron bursts must be identified and the time periods of their occurrence deleted from the data.

A sample of the information used to identify solar flares and magnetospheric electron bursts is plotted in Figure II-9. The time period covered is from 75.134 to 75.294 and each plot is for six-hour averages from the IMP-7 satellite. The plots are, from top to bottom, the ratio of the two electron rates EOlS and EOS, the CELO rate, the PLO rate, and the counting rate of 1-6 MeV electrons.

The quantity EOlS / EOS is the ratio of the corrected rate, EOlS, of 1-6 MeV electrons to the corrected rate, EOS, of

Figure II-9

A sample of the data used in the identification of solar electron flares and magnetospheric electron bursts. The data are six-hour averages for IMP-7 and cover the time period 75.134 to 75.294. From top to bottom the plots are: the ratio, EO1S/EOS, of the corrected electron count rates; the corrected ELO rate, CELO; the PLO rate; and the count rate of 1-6 MeV electrons. The bars indicate the time periods eliminated from the data with bars labeled "F" being solar flares and unlabeled bars being mangetospheric electron bursts.

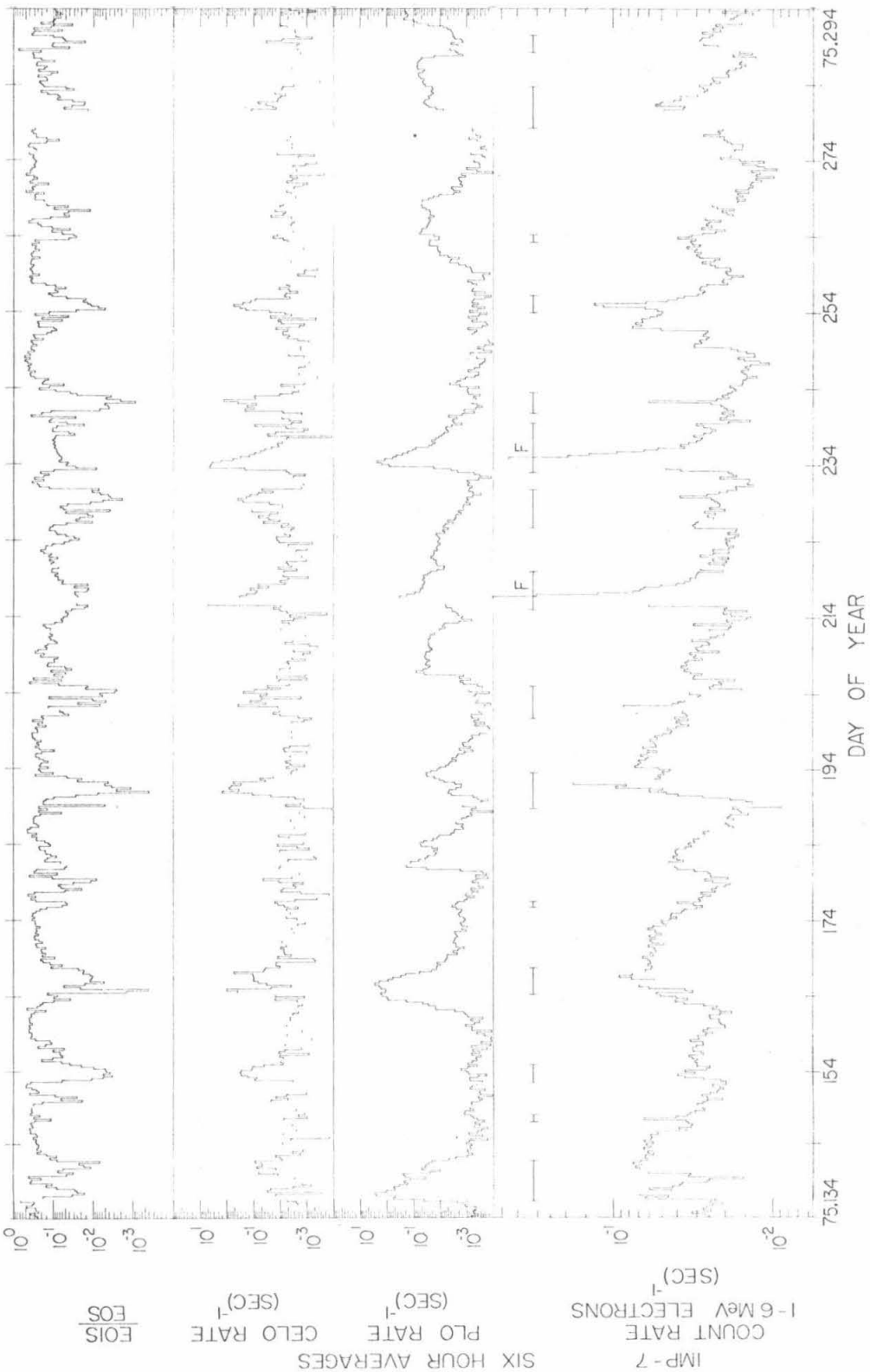
IMP - 7
SIX HOUR AVERAGES
COUNT RATE
1 - 6 MeV ELECTRONS
(SEC)$^{-1}$
PLO RATE
(SEC)$^{-1}$
CELO RATE
(SEC)$^{-1}$
EOIS / EOS
DAY OF YEAR
75.134
154
174
194
214
234
254
274
75.294
F
F

0.16 to 6 MeV electrons. The rates have been corrected for neutral background and for an estimated nuclei contribution by the method described in Garrard, et al. (1977). These corrections are good only at relatively high count rates, $\gtrsim$ 10-100/sec. At the low count rates, $\sim$ 0.01-0.1/sec, observed outside of the magnetosphere these rates also include nuclei, mainly protons and helium, that satisfy the rate logic equations listed in Table II-1.

During energetic electron events in Earth's magnetotail the electron spectra are typically steep with $\gamma \gtrsim 4$ (Baker and Stone, 1977). For these steep spectra the ratio, E01S / E0S, is small, $\lesssim$ 0.05, and is used as an indicator for the times that magnetospheric electrons dominate the electron flux. These time periods are seen as abrupt changes in the ratio to values $\lesssim$ 0.05. These periods last for $\sim$3-5 days, which is about equal to the time for the satellite to pass through much of Earth's magnetosphere, and have a periodicity of $\sim$12 days due to the satellite passing through part of the magnetosphere during each orbital period.

The CELO rate is the rate of low energy Narrow Geometry electrons from 0.16 to 1 MeV and is an indicator of the actual flux of these low energy electrons. The CELO rate is the ELO described in Table II-1 corrected for gamma-ray background for IMP-7 and IMP-8 respectively by the equations

$$CELO = ELO - 0.55 \cdot NEUT \ ,$$

$$CELO = ELO - 0.60 \cdot NEUT$$

where ELO is the uncorrected count rate and NEUT is the neutral rate (Garrard, et al., 1977).

A typical neutral rate of 0.1/sec has an estimated statistical error for a six-hour average of 0.002/sec. The background correction for the raw ELO rate is then (0.055 ± 0.0011)/sec. For a corrected ELO rate of 0.02/sec the raw ELO rate is ~ 0.075/sec. Using this raw ELO rate and the above background correction we would calculate for a six-hour average a corrected ELO rate of CELO = (0.02 ± 0.0022)/sec. The ratio of the estimated error to the CELO rate at the 10^{-2}/sec level is $\sim$10 percent. Thus the many increases in the CELO rate seen in Figure II-9, e.g. at 74.154 or 74.191, are significant. Most of these increases are coincident with the changes in the EO1S / EOS ratio. The CELO rate is used to confirm the existence of magnetospheric electrons.

Time periods were eliminated due to magnetospheric electron contamination if the 1-6 MeV electron increase had an abrupt rise and fall both $\lesssim$ 18 hours and had lasted $\lesssim$ 5 days, if there was no associated PLO increase, if the ratio EO1S / EOS changed to a value $\lesssim$ 0.05 within 18 hours and if the CELO rate had a coincident increase. The last criterion tests for the presence

of a large flux of magnetospheric electrons which may, even with $\gamma \gtrsim 4$, significantly contaminate the 1-6 MeV electron count rate. The deletions at 75.154, 75.192, and 75.254 are good examples of times identified as magnetospheric electron bursts. The periods 75.145, 75.165, and 75.264 also satisfy the criteria but the 1-6 MeV electron increases are much smaller.

It is important to understand that the elimination was performed on data averaged for six-hour periods. Short duration phenomena, such as a single magnetospheric burst lasting < 5 minutes, are averaged over the entire six-hour period and may not appear as an increase in these plots. To check that the contamination to the 1-6 MeV electron count rate is small for those periods not containing identified magnetospheric electron bursts, e.g. at 75.160, the contribution from a flux of electrons with a spectrum of $\gamma \geq 4$ is calculated with the assumption that the CELO rate $\sim 5 \times 10^{-3}$/sec is entirely due to magnetospheric electrons. For these choices of γ and CELO Figure 4 of Garrard, et al. (1977) gives

$$\frac{dJ}{dE} \leq 10^{-3} \cdot E^{-\gamma} \quad (\text{cm}^2\text{-sr-sec-MeV})^{-1}.$$

The contribution to the 1-6 MeV electron count rate is given by

$$R \leq 10^{-3} \cdot \left(\int_0^{10} E^{-\gamma} G(E)\, dE \right) \qquad \text{sec}^{-1}$$

where G(E) is the electron response function shown in Figure II-4b. For $\gamma \geq 4$ the integral is ≤ 0.56 so $R \lesssim 5.6 \times 10^{-4}$/sec. The lowest observed 1-6 MeV electron count rates are $\sim 10^{-2}$/sec, so the contribution of magnetospheric electrons during periods without identified magnetospheric bursts is $\lesssim 5$ percent.

The PLO rate is the rate of nuclei, mainly protons, of energy 1.2-2.4 MeV. The PLO rate has many increases of factors $>$ 2 orders of magnitude. An electron increase was identified as a solar flare if the 1-6 MeV electron count rate increased by a factor >10 in $\lesssim 18$ hours and had an exponential decay, if the PLO rate had a coincident rise within 18 hours of the electron increase and also had an exponential decay, and if, for the time period after 73.303, the electron increase was observed by both IMP satellites. The time periods beginning at 75.215 and 75.234 in Figure II-9 are two examples of solar flares.

III. Observations

III-A. The Five Synodic Periods, 1973-1977

After elimination from the data base of the time periods containing solar flares and magnetospheric bursts, the fluxes observed by the two spacecraft have been averaged together to form the data base used in this study. Figure III-1 is a plot of the 1-6 MeV electron count rate for the five years and three months covered by the IMP spacecraft from their launch until the latter part of 1977. The data are averaged over six-hour intervals. The scale at the left is the count rate of 1-6 MeV electrons and the scale at the right is the flux of 1-6 MeV electrons in $(cm^2\text{-sr-sec})^{-1}$. The two error bars near the scale at the right are typical statistical errors in the data points as calculated in Appendix A.

The ~13 month periodicity noted by Teegarden, et al. (1974) is apparent in this plot. This ~13 month period is the synodic period of Earth and Jupiter and was a major reason that Teegarden, et al. concluded that Jupiter was the source of the electrons seen in the intensity increases at 1 AU.

Four complete ~13 month synodic periods and part of a fifth period occurred from late 1972 through 1977. The arrows at the bottom of Figure III-1 point to the nominal connection times of

Figure III-1

Plot of the 1-6 MeV electron flux for the period 72.273 to 77.365 with solar flares and magnetospheric bursts eliminated. The data are averaged over six-hour intervals and are also an average of the IMP-7 and IMP-8 fluxes. The scale at the left margin is the count rate and the scale at the right margin is the flux in $(cm^2\text{-sr-sec})^{-1}$. The two vertical bars near the right margin indicate the typical statistical error in the flux measurements (see Appendix A). The arrows at the bottom mark the nominal connection times of Earth and Jupiter for a solar wind speed of V_{SW} = 500 km/sec.

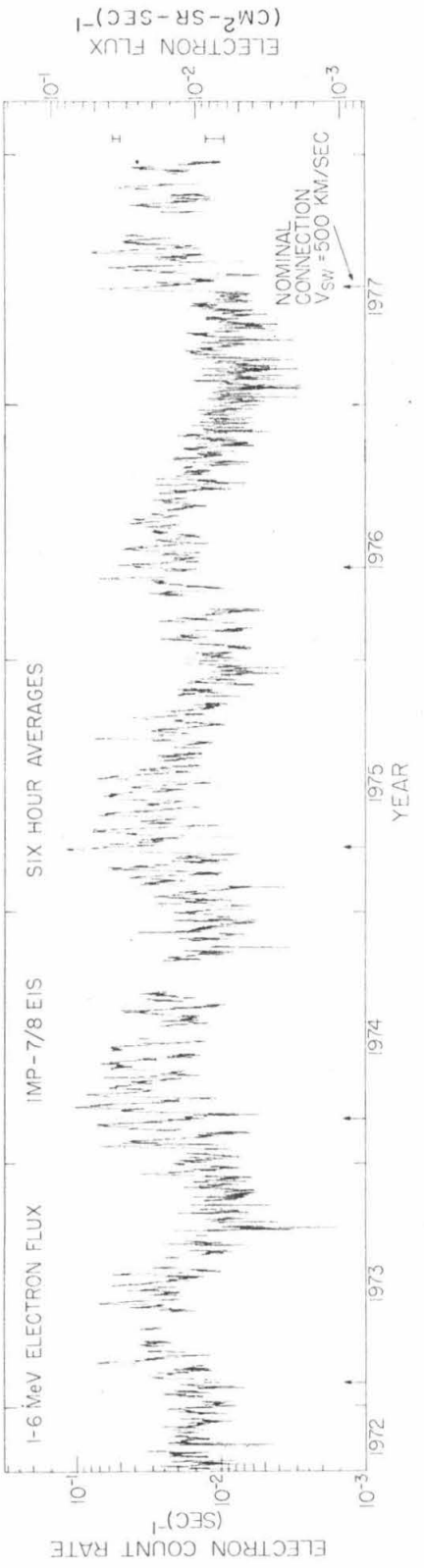
1-6 MeV ELECTRON FLUX
IMP-7/8 EIS
SIX HOUR AVERAGES
NOMINAL CONNECTION V_{SW} =500 KM/SEC
ELECTRON COUNT RATE (SEC)$^{-1}$
ELECTRON FLUX (CM^2-SR-SEC)$^{-1}$
YEAR
1972
1973
1974
1975
1976
1977

Earth and Jupiter for a solar wind speed of 500 km/sec. Each of the five synodic periods is labeled by the year within which the Earth and Jupiter nominal connection for a solar wind speed of 500 km/sec occurred.

The five synodic periods are plotted separately in Figure III-2 from 1973 in the top panel to 1977 in the bottom panel. The data are again averaged over six-hour intervals and the scale is the 1-6 MeV count rate. The synodic periods are aligned on their nominal connection times for a solar wind speed of V_{SW} = 500 km/sec with the date of the nominal connection time given in each plot above the nominal connection time which is the zero point on the abscissa. The nominal connection times for solar wind speeds of V_{SW} = 400 km/sec and 600 km/sec are listed for each of these synodic periods in Table B-1 of Appendix B. For these five synodic periods the nominal connection time for V_{SW} = 400 km/sec is from +53 days to +59 days after the nominal connection time for V_{SW} = 500 km/sec and the nominal connection time for V_{SW} = 600 km/sec is from -34 days to -38 days before the nominal connection time for V_{SW} = 500 km/sec. The flux is plotted from 200 days before to 300 days after the nominal connection time for V_{SW} = 500 km/sec. Since the actual synodic period from 1973 to 1977 was 393-404 days (see Appendix B), this 500 day plotting interval includes each full synodic period and parts of the previous synodic period and the following synodic period.

Figure III-2

Plots covering the five synodic periods from 1973 to 1977. The data are identical to those plotted in Figure III-1 but have been plotted for each synodic period by taking data from 200 days before the nominal connection time for V_{SW} = 500 km/sec to 300 days after that nominal connection time. The five plots are aligned on their nominal connection time for V_{SW} = 500 km/sec which is the zero of the abscissa. Since the plotting interval is 500 days, all of the ~400 day synodic period is included in each plot and there is overlap into the previous synodic period and into the following synodic period. The date on each plot at the zero line is the day of nominal connection for V_{SW} = 500 km/sec.

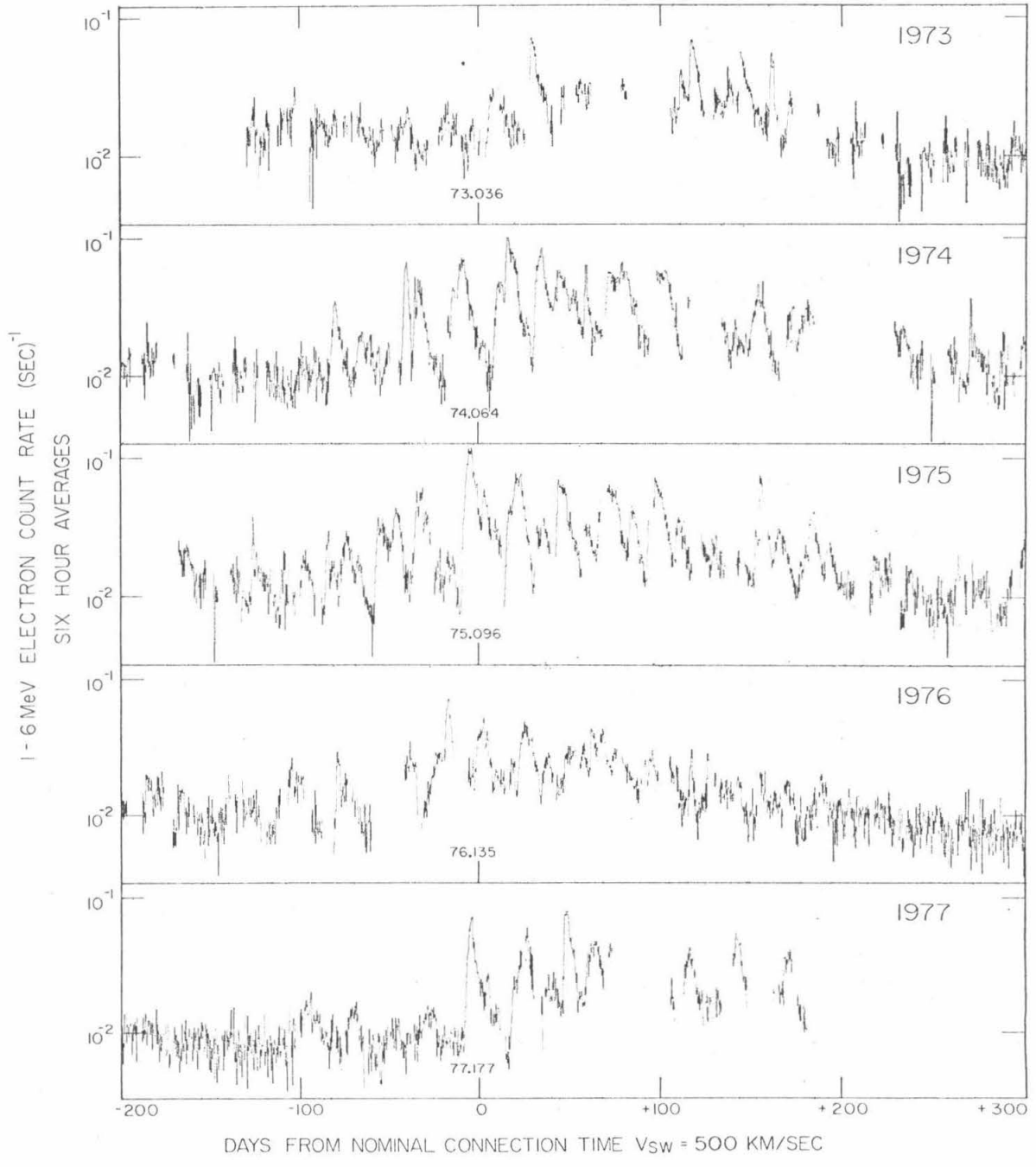
1973
1974
1975
1976
1977
73.036
74.064
75.096
76.135
77.177
10^{-1}
10^{-2}
-200
-100
0
+100
+200
+300
1-6 MeV ELECTRON COUNT RATE (SEC)$^{-1}$
SIX HOUR AVERAGES
DAYS FROM NOMINAL CONNECTION TIME V_{SW} = 500 KM/SEC

The synodic envelopes formed by the maxima of the Jovian electron increases for these five synodic periods are similar. The envelopes reach a maximum intensity around the nominal connection time for V_{SW} = 500 km/sec, generally start $<$100 days before this nominal connection time, and last $\gtrsim$ 200 days after this nominal connection time. The envelopes for these five synodic periods display changes from period to period. As reported by Hartman, et al. (1977) and Chenette, et al. (1977a,c) the synodic periods for 1975 and 1976 have Jovian increases over their complete synodic period from 150 days before the nominal connection time to more than 200 days after the nominal connection time. The three other synodic periods 1973, 1974, and 1977 have few Jovian increases before the nominal connection time in contrast to the 1975 and 1976 synodic periods which have many Jovian increases before the nominal connection time.

Since the cycle of solar activity was at a minimum during 1974, few solar particle flares occurred from 1972 through 1977 and almost continuous coverage of the interplanetary electron flux was obtained including time periods with relatively low fluxes. The lowest fluxes observed in these data are during periods of few Jovian increases usually in the period between two successive synodic periods. For example low fluxes occur from $\sim$240 days after the nominal connection time for the 1974 synodic period until $\sim$100 days before the nominal connection time for the 1975

synodic period. A similar period occurs from ~250 days after the nominal connection time for the 1976 synodic period until ~100 days before the nominal connection time for the 1977 synodic period. Plotted in Figure III-3 is the electron flux with error bars for the time period 76.322 to 77.080. The electron flux shows a slow decline down to ~6 x 10^{-3}/sec around 77.060. Hurford, et al. (1974) have reported a quiet-time energy spectrum for 0.16 to 2 MeV electrons of

$$\frac{dJ}{dE} = 0.0054 \cdot E^{-1.67} \qquad (cm^2\text{-sr-sec-MeV})^{-1}$$

which, when integrated from 1 to 6 MeV and using the effective geometrical factor for the IMP EIS, yields a count rate of ~8.5 x 10^{-3}/sec. Thus the fluxes reported here are ~40 percent lower than those fluxes reported earlier by Hurford, et al.

The electron fluxes reported here are also lower relative to the peak fluxes observed than has been previously reported (Chenette, et al., 1977c). Using the electron data reported in Figure 1 of Chenette, et al., the 1975 synodic period has a peak count rate of ~0.13/sec at ~75.100 and has minimum fluxes of ~0.014/sec around 74.330 giving a peak to minimum ratio of ~9. For the identical period the count rate observed on the IMP instruments is ~0.11/sec at ~75.096 and minimum fluxes of ~0.006/sec around ~74.351 giving a peak to minimum ratio of ~18. Thus the fluxes reported here for the time period between the

Figure III-3

Plot of the 1-6 MeV electron flux observed at 1 AU for the time period 76.322 to 77.080. Each point is the six-hour averaged flux with the fluxes from IMP-7 and IMP-8 averaged together. The error bars are the estimated 1σ statistical uncertainties in the flux measurement. This time period has no identifiable Jovian increases and includes the lowest fluxes observed over the time period of this study. The fluxes in this time period are ~40 percent lower than the fluxes reported by Hurford, et al. (1974).

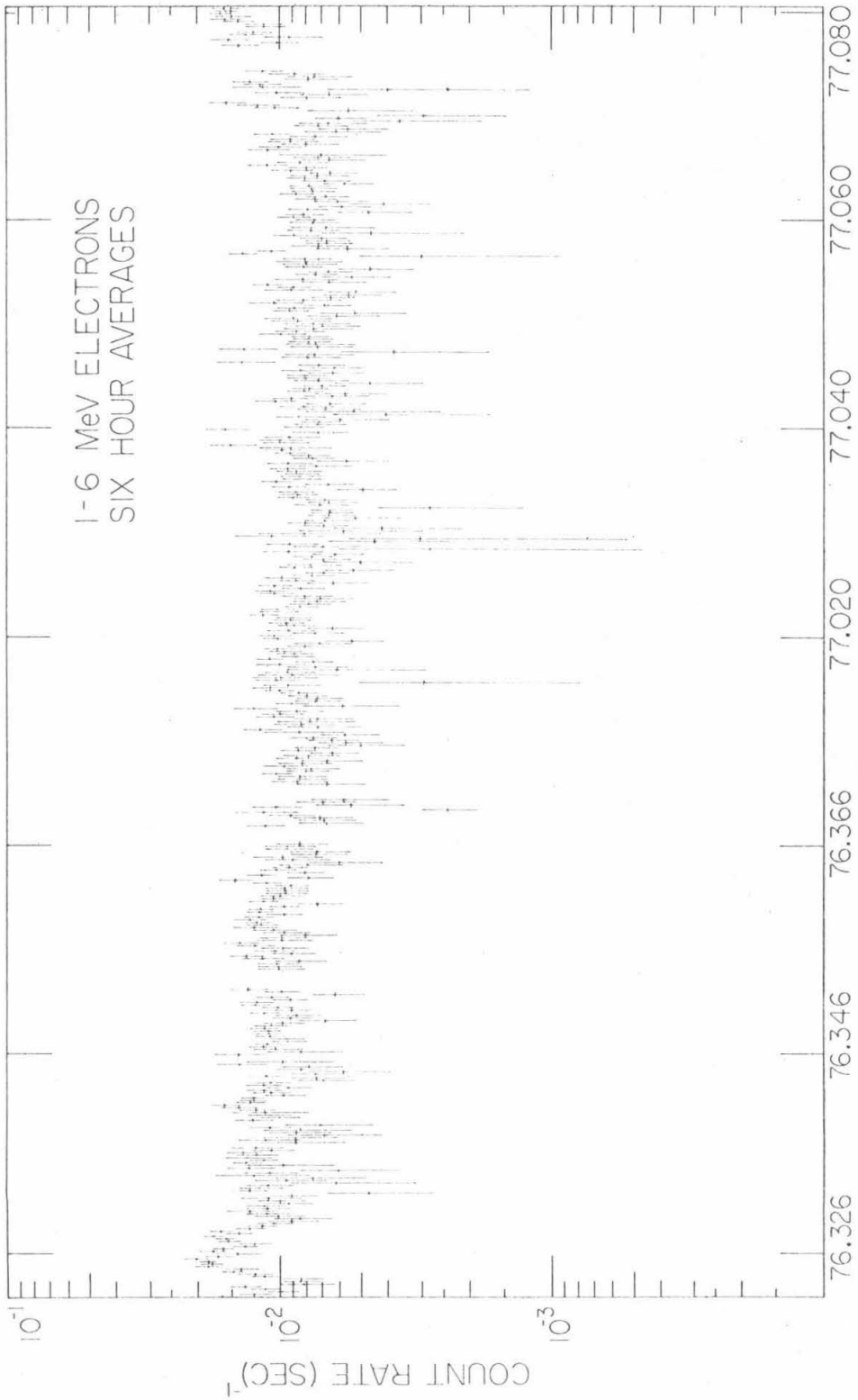
I-6 MeV ELECTRONS
SIX HOUR AVERAGES
COUNT RATE (SEC)$^{-1}$
10^{-1}
10^{-2}
10^{-3}
76.326
76.346
76.366
77.020
77.040
77.060
77.080
DAY OF YEAR

synodic periods 1974 and 1975 are ~2 times lower relative to the peak fluxes of the 1975 synodic period than previously reported.

McDonald, et al. (1972) noted the ~27 day periodicity of the electron increases. The 1975 synodic period is plotted in Figure III-4 and is identical to the plot of the 1975 synodic period that is plotted in Figure III-2. The scale at the right margin is the 1-6 MeV electron flux in $(cm^2\text{-sr-sec})^{-1}$ and the error bars at the left margin are typical statistical errors in the flux measurements. To emphasize the recurrence of the electron increases a scale of marks 27.28 days apart, the synodic rotation of the Sun as seen at Earth for the 16° latitude solar rotation of 25.38 days, is plotted above the largest increases. The increases do show the ~27 day periodicity but do not follow it precisely.

III-B. The Jovian Increases

A systematic study of the time profiles of the Jovian increases has been conducted. The information on the Jovian increases reported here provides clues to the physical processes that affect the propagation of electrons in the inner heliosphere.

Each Jovian increase observed in the electron flux at 1 AU was selected by hand with the start of the increase chosen as the time when the electron flux first displayed a systematic rise

Figure III-4

Plot of the electron flux for the 1975 synodic period with a count rate scale at the left margin and a flux scale in $(cm^2\text{-sr-sec})^{-1}$ at the right margin. The date, 75.096, is the nominal connection time for V_{SW} = 500 km/sec. The data are identical to the data plotted in Figure III-2 for the 1975 synodic period. The bars at the left margin are typical errors for a count rate of 0.01/sec and 0.05/sec. To emphasize the recurrence of the electron increases a scale of marks 27.28 days apart is plotted above the largest increases. This $\sim$27 day period is the synodic rotation of the Sun as seen at Earth.

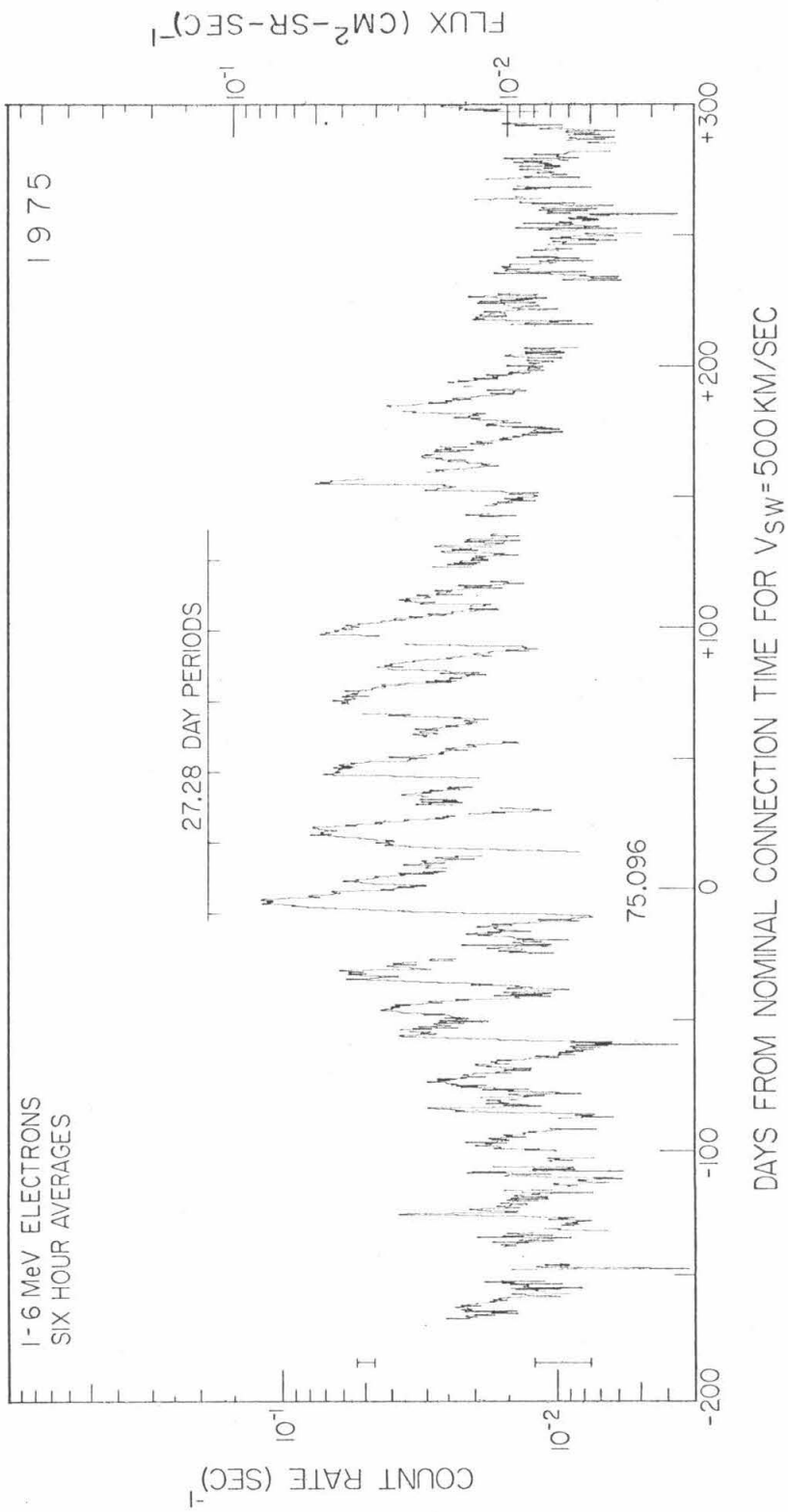
1975
1-6 MeV ELECTRONS
SIX HOUR AVERAGES
27.28 DAY PERIODS
75.096
COUNT RATE (SEC)$^{-1}$
FLUX (CM^2-SR-SEC)$^{-1}$
10^{-1}
10^{-2}
-200
-100
0
+100
+200
+300
DAYS FROM NOMINAL CONNECTION TIME FOR V_{SW}=500 KM/SEC

above the flux level in the preceding ~1-2 days. This selection procedure is biased toward recognizing large increases or abrupt increases and it may have missed small or slowly rising increases. A total of 88 increases was selected using this procedure.

These 88 Jovian increases have been classified by their rise, peak, and fall time profiles. Table III-1 is a qualitative description for the symbols used in this classification scheme and lists the number of increases in each classification. The selected increases plotted in Figure III-5 are examples of Jovian increases that illustrate the rise, peak, and fall time profiles observed in these 88 Jovian increases. The time profiles for the rise, peak, and fall were independently determined, but as noted below there is some correlation between the peak profile and the rise and fall profiles.

The 88 Jovian increases selected above are listed in chronological order and grouped into the ~13 month synodic periods in Table III-2. The five synodic periods are from 150 days before to 250 days after the time of nominal connection for V_{SW} = 500 km/sec. The plots in Figure III-2 show that these limits for the synodic period are reasonable in that the limits occur during the time that one synodic envelope is ending with low fluxes and before the time that the next synodic envelope starts. The start of each increase is given in the first column of Table III-2 as the year (e.g. 72 is 1972), the day of year (001 is Jan 1), and the

Table III-1

Classification Symbols for Time Profiles of Increases

Symbol	Description	Number of Increases
For Rise Profile		
-	Unknown	13
1	Abrupt	27
2	Diffusive	23
3	Exponential	25
For Peak Profile		
-	Unknown	10
1	Flat or Broad	35
2	Rounded or Pointed	38
3	Multiple of Other	5
For Fall Profile		
-	Unknown	20
1	Abrupt	10
2	Exponential then Abrupt	9
3	Exponential	49

Figure III-5

Plots of Jovian increases selected from the set of 88 increases. These increases were chosen to illustrate the time profiles of the rise, peak, and fall classifications of the scheme to classify the Jovian increases. The ordinate is the 1-6 MeV electron count rate and the abscissa is the time with the scale marks ten days apart. The data points are for six-hour averages. The increases plotted in Figure III-5a are for the rise profiles, Figure III-5b for the peak profiles, and Figure III-5c for the fall profiles.

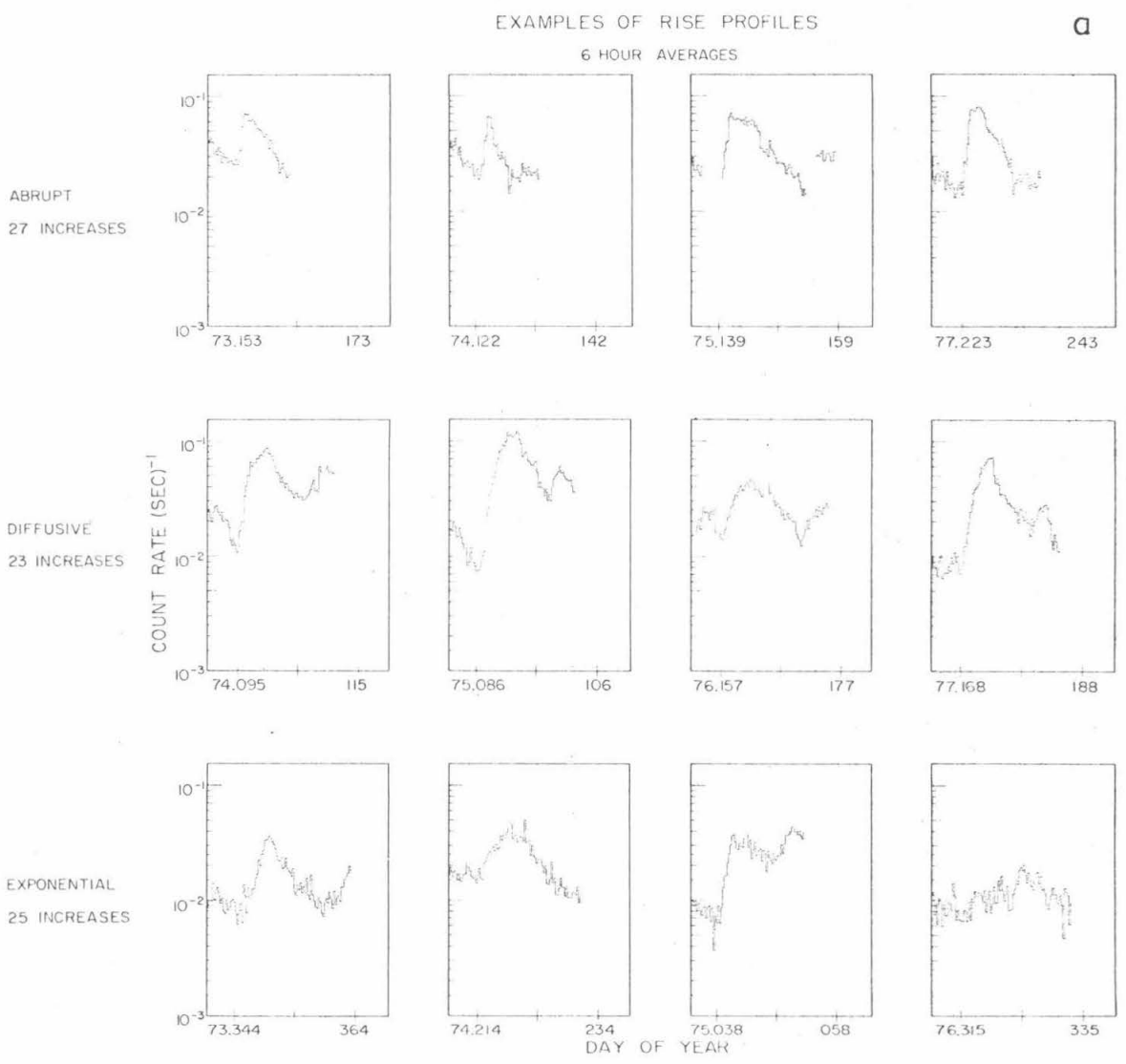
EXAMPLES OF RISE PROFILES
a
6 HOUR AVERAGES
ABRUPT
27 INCREASES
DIFFUSIVE
23 INCREASES
EXPONENTIAL
25 INCREASES
COUNT RATE (SEC)⁻¹
10⁻¹
10⁻²
10⁻³
73.153
173
74.122
142
75.139
159
77.223
243
74.095
115
75.086
106
76.157
177
77.168
188
73.344
364
74.214
234
75.038
058
76.315
335
DAY OF YEAR

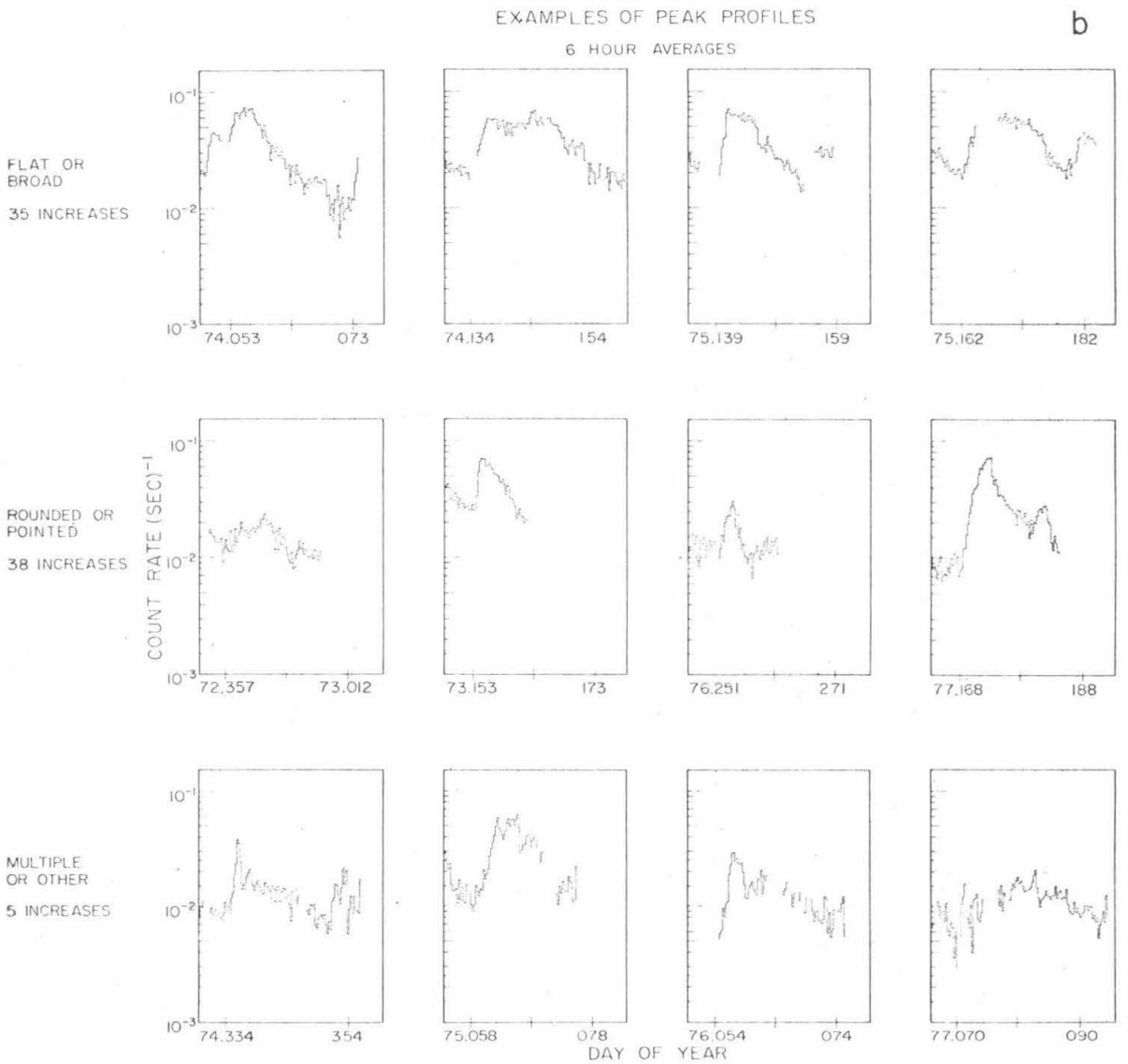
EXAMPLES OF PEAK PROFILES
6 HOUR AVERAGES
b
FLAT OR BROAD
35 INCREASES
ROUNDED OR POINTED
38 INCREASES
MULTIPLE OR OTHER
5 INCREASES
COUNT RATE (SEC)⁻¹
10⁻¹
10⁻²
10⁻³
74.053
073
74.134
154
75.139
159
75.162
182
72.357
73.012
73.153
173
76.251
271
77.168
188
74.334
354
75.058
078
76.054
074
77.070
090
DAY OF YEAR

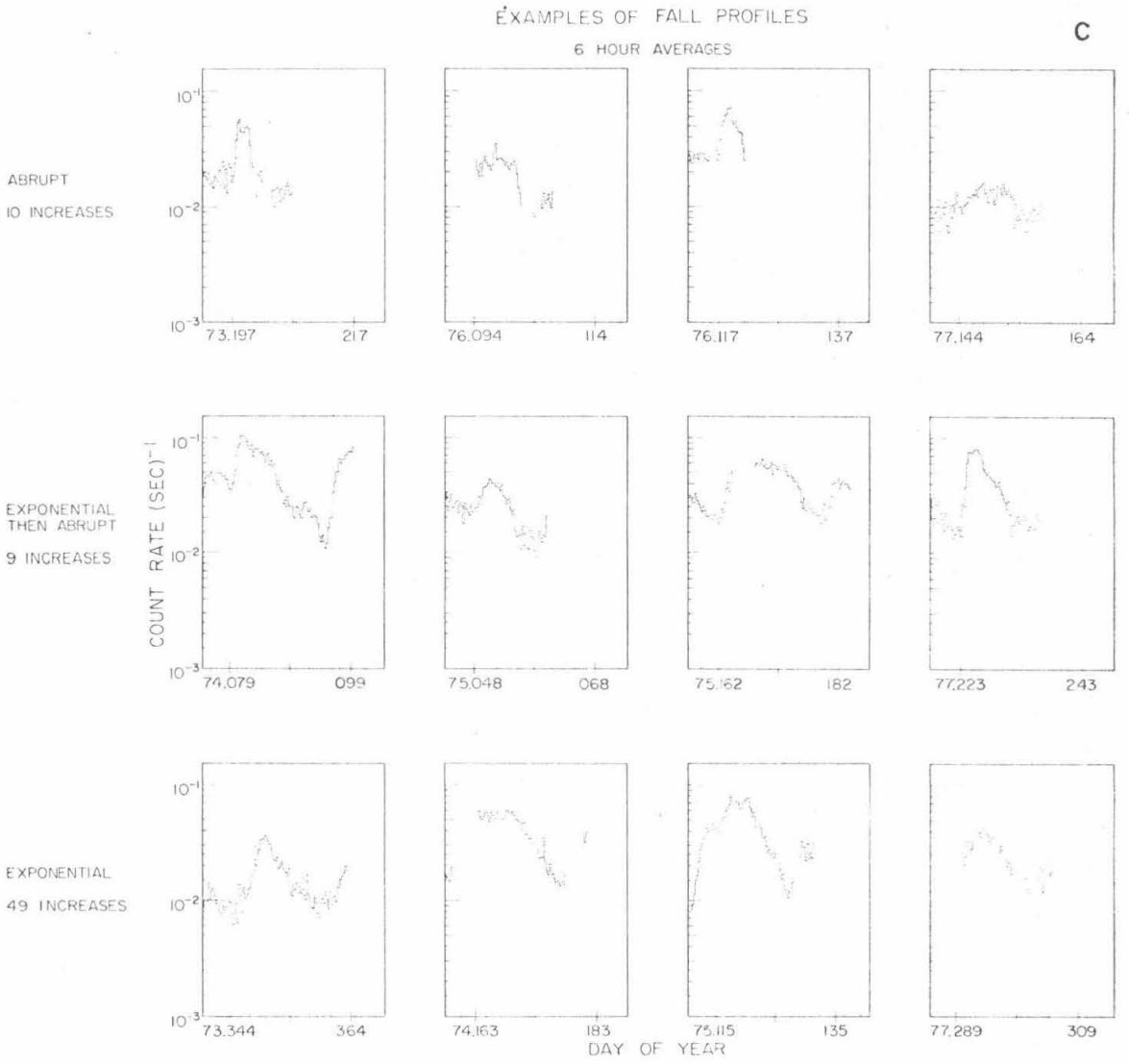
EXAMPLES OF FALL PROFILES
6 HOUR AVERAGES
C
ABRUPT
10 INCREASES
EXPONENTIAL
THEN ABRUPT
9 INCREASES
EXPONENTIAL
49 INCREASES
COUNT RATE (SEC)⁻¹
10⁻¹
10⁻²
10⁻³
73.197
217
76.094
114
76.117
137
77.144
164
74.079
099
75.048
068
75.162
182
77.223
243
73.344
364
74.163
183
75.115
135
77.289
309
DAY OF YEAR

Table III-2

List of the 88 Jovian increases observed in the non-solar interplanetary 1-6 MeV electron flux at 1 AU. The increases are listed chronologically by their start times and are grouped into the five synodic periods. A synodic period is from 150 days before to 250 days after the nominal connection time for V_{SW} = 500 km/sec. In the first column is the date of the increase start. The format is the year (e.g. 1972 is 72), the day-of-year (e.g. Jan 1 is 001), and the six-hour period (e.g. 00, 06, 12, or 18). The column labeled "L" is the length of the increase rounded up to the nearest day. A dash in this column signifies that the length could not be determined due to data gaps at the start or end of an increase. The symbols used for the classification of the increases are listed in Table III-1. The symbols for each increase are listed in the columns headed "R," "P," and "F" where these signify the classification symbol for the rise, peak, and fall profiles respectively. The last three columns are the time of the start of the increase from the nominal connection time for V_{SW} = 400, 500, and 600 km/sec.

Table III-2

Jovian Increases At 1 AU

Increase Date	L (days)	R	P	F	Days From Nominal Connection V_{SW}= 400	500	600 km/sec
					Synodic Period 1973		
72.357.12	10	3	2	3	-98	-44	-9
73.014.00	7	3	2	1	-75	-21	14
73.040.00	15	2	1	3	-50	4	39
73.065.00	12	1	2	3	-25	29	64
73.147.18	5	1	2	3	58	112	147
73.153.00	8	1	2	3	63	117	152
73.179.00	9	1	2	3	89	143	178
73.196.18	5	1	1	1	107	161	196
73.206.06	-	3	2	-	116	170	205
					Synodic Period 1974		
73.325.18	9	3	2	3	-156	-103	-69
73.344.06	14	3	2	3	-137	-84	-50
73.361.12	13	2	2	-	-120	-67	-33
74.009.18	-	3	-	-	-107	-54	-20
74.021.12	6	2	2	2	-95	-42	-8
74.028.00	18	2	2	3	-88	-35	-1
74.049.00	4	1	2	-	-67	-14	20
74.052.18	16	2	1	3	-64	-11	23
74.072.12	7	2	1	-	-45	8	42
74.079.06	15	2	2	2	-38	15	49
74.094.18	11	2	2	3	-22	31	65
74.106.00	16	3	1	3	-11	42	76
74.122.12	5	1	2	1	5	58	92
74.134.12	23	3	1	3	17	70	102
74.162.18	15	-	1	3	46	99	133
74.214.00	14	3	2	3	97	150	184
74.234.18	-	-	-	-	118	171	205
74.240.06	-	3	-	-	123	176	210
74.297.00	6	1	1	2	180	233	267

Increase Date	L (days)	R	P	F	Days From Nominal Connection V_{SW}= 400	500	600 km/sec
					Synodic Period 1975		
74.334.06	17	1	3	3	-181	-126	-92
74.351.00	4	1	3	-	-164	-109	-75
74.361.12	8	3	1	3	-154	-99	-65
75.010.18	8	2	2	1	-140	-85	-51
75.018.12	9	2	2	3	-132	-77	-43
75.028.00	10	2	2	3	-122	-67	-33
75.038.12	9	3	1	3	-112	-57	-23
75.048.00	7	2	2	2	-102	-47	-13
75.058.06	12	3	3	-	-92	-37	-3
75.086.06	11	2	1	3	-64	-9	25
75.098.00	11	2	2	3	-53	2	36
75.110.18	4	3	-	-	-40	15	49
75.115.06	11	3	1	3	-36	19	53
75.127.06	9	-	1	3	-24	31	65
75.139.06	14	1	1	3	-12	43	77
75.155.00	6	-	1	3	4	59	93
75.161.18	17	3	1	2	11	66	100
75.180.00	9	1	2	3	29	84	118
75.189.18	14	1	2	3	39	94	128
75.205.18	8	1	1	3	55	110	144
75.248.12	3	1	2	-	97	152	186
75.251.12	7	1	2	3	100	155	189
75.259.12	13	3	2	3	108	163	197
75.273.06	5	-	-	-	122	177	211
75.278.18	8	1	2	3	128	183	217
75.287.12	7	-	2	3	136	191	225
75.314.06	5	1	1	-	163	218	251
75.331.12	15	-	1	3	180	235	269

Increase Date	L (days)	R	P	F	Days From Nominal Connection V_{SW}= 400	500	600 km/sec
					Synodic Period 1976		
75.358.06	6	-	-	-	-197	-141	-105
76.021.18	16	3	1	-	-169	-113	-77
76.054.06	16	1	3	3	-136	-80	-44
76.094.00	8	-	1	1	-96	-40	-4
76.104.12	12	3	1	-	-86	-30	6
76.116.18	5	2	2	1	-74	-18	18
76.133.00	10	3	1	3	-57	-1	35
76.156.18	13	2	1	3	-34	22	58
76.170.00	7	2	2	3	-21	35	71
76,183.00	7	1	1	-	-8	48	84
76.197.06	5	1	2	3	6	62	98
76.202.18	7	-	1	1	12	68	104
76.209.18	15	1	-	3	19	75	111
76.226.18	8	-	1	3	36	92	128
76.241.00	-	-	-	-	50	106	142
76.251.12	5	2	2	1	60	116	152
76.261.12	-	1	-	-	70	126	162
76.289.00	6	1	-	1	98	154	190
76.304.00	7	1	1	2	113	169	205
76.315.00	13	3	2	3	124	180	216
					Synodic Period 1977		
77.070.12	19	3	3	3	-165	-106	-68
77.101.12	9	2	1	2	-134	-75	-37
77.123.00	10	3	1	3	-112	-53	-15
77.144.00	9	3	1	2	-91	-32	6
77.168.00	11	2	2	3	-67	-8	30
77.179.06	3	2	2	1	-57	2	40
77.193.06	14	2	2	3	-43	16	54
77.222.18	8	1	1	3	-13	46	84
77.235.00	10	2	1	3	-1	58	96
77.289.12	11	3	2	3	53	112	150
77.316.12	8	-	1	2	80	139	177
77.344.18	10	1	1	-	109	168	206

hour of the day (0, 6, 12, 18). The resolution in time is 6 hours because the flux data are averaged over 6 hour intervals.

The second column lists the duration of an increase rounded up to the nearest day. A dash signifies that the length could not be measured due to data gaps at the start or end of an increase. The length or duration of an increase is the time in days from the start of the increase until the end of the increase. The end was chosen as either the time when the next increase started or when the systematic decrease in the flux stopped and the flux was at a constant level. If the start of the next increase determines the end of the previous increase, then the increase length is a measure of the time between successive increase starts. If the end was determined by when the flux stopped decreasing, then the increase length is a measure of the time that the flux in an increase is either above the instrument sensitivity or above a background of electrons.

Columns 3, 4, and 5 list the rise, peak, and fall time profile classifications for each increase. A dash in any of these three columns indicates that for that increase the time profile corresponding to that column could not be determined either because of data gaps or because the increase did not have a consistent trend.

The rise time profile classifications are listed in column 3. The rise is that part of the increase from its start to its first

maximum. As in Table III-1 an increase rise labeled with a 1 is an abrupt rise of the electron flux reaching a maximum in typically less than 18 hours. An increase rise labeled with a 2 is a diffusive rise. These rise time profiles are described as diffusive because they are similar to the time profiles of the particle flux at 1 AU predicted by the convection-diffusion model (Conlon, 1978) which is discussed in a later section of this paper. The last rise time profile is exponential and is labeled with a 3. The exponential rises have an exponential time constant varying between 1-3 days.

The peak time profile classifications are listed in column 4. The peak is that part of the increase around the maximum of the increase. A peak time profile labeled with a 1 is a flat or broad profile with no sharp or large peaks. The peak profile labeled with a 2 is rounded or pointed, while the peak profile labeled 3 has multiple peaks or does not fit into one of the other classifications. The rounded or pointed peak profiles tend to occur with abrupt and diffusive rises and with abrupt falls.

The fall time profiles of the Jovian increases are listed in column 5. The fall part of an increase is from the last maximum to the end of the increase. A fall time profile labeled 1 is an abrupt decrease similar to the abrupt rise time profile. A fall time profile labeled with a 2 is a short exponential decay followed by an abrupt decrease. A fall profile labeled with a 3 is an exponential decay. The majority of increases are classified as

exponential decays with time constants varying from 4-9 days.

The last three columns of Table III-2 give the start time of each increase in days relative to the nominal connection time of each synodic period for solar wind speeds of V_{SW} = 400, 500, and 600 km/sec.

IV. Model Discussion

As reviewed in Section I there have been attempts to explain both qualitatively and quantitatively the occurrence and time profiles of Jovian increases in the vicinity of Jupiter and at 1 AU. The convection-diffusion propagation model with corotating interaction regions (CIR's) originally developed by Conlon (1978) can be used to calculate both the time profiles of individual increases and the envelope of the synodic period while neither the scatter free diffusion model (Gold and Roelof, 1976) nor the field-line random walk model (Jokipii, 1976) are as developed. This discussion will therefore concentrate on how aspects of the convection-diffusion propagation model can be used to explain the characteristics of the Jovian electron increases observed at 1 AU.

First will be a brief review of the convection-diffusion model and corotating interaction regions. Then the Jovian increases listed in Table III-2 will be examined for systematic variations within the synodic period and compared to the predictions of the convection-diffusion model. The barrier effect predicted for the CIR's at Jupiter and possibly Earth will be investigated for the increases occurring in the 1974 synodic period. Then magnetic field strength enhancements observed at 1 AU will be correlated with Jovian increases and other changes in the electron flux, also for the

fluxes observed in the 1974 synodic period. Next the convection-diffusion model will be used to calculate the expected envelope of the maxima of the increases at 1 AU. Finally three Jovian increases at 1 AU will be fit with the rise profiles predicted by the convection-diffusion model and a range of values for the diffusion coefficients determined.

IV-A. The Convection-Diffusion Propagation Model

A convection-diffusion model for the propagation of Jovian electrons has been proposed (Conlon, 1978; Chenette, et al., 1977c) to explain the distribution of Jovian electrons observed at 1 AU. This model uses a Fokker-Planck equation (Parker, 1963) that includes diffusion, convection, and adiabatic deceleration. This propagation model and its variations discussed here are described in more detail in Appendix C. The diffusion tensor is assumed to be diagonal and to be independent of position, energy, and time. The model also assumes that Jupiter is a point source of constant strength, that the electron spectrum is a power law in energy, and that the divergence of the solar wind is a constant.

The coordinate system used here for this model is a Cartesian coordinate system with the orgin at Jupiter. The x coordinate is the perpendicular distance from Jupiter to the ideal spiral field line which is connected to Earth. The x coordinate is

positive in the direction of increasing heliocentric radius. The y coordinate is the distance along the ideal spiral field line from the x coordinate intersection to the position of Earth. The y coordinate is positive in the direction of decreasing heliocentric radius.

The above aspects of the model allow a calculation of the efficiency with which electrons propagate from the source, Jupiter, to other points in the heliosphere. Since the source is assumed to be constant in this convection-diffusion model, the occurrence of Jovian increases is explained qualitatively by having the source and the point of observation separated by barriers to electron propagation. An increase occurs immediately after a barrier passes the source position or the observation point and both positions are within the same bounded region of space.

Corotating interaction regions (CIR's) were used as barriers by Conlon (1978) in fitting three rise time profiles observed by Pioneer 11. CIR's were first observed by Smith and Wolfe (1976) and have previously been used by Conlon and Simpson (1977) to explain some features in the electron flux for both the pre-encounter and post-encounter periods of Pioneer 10 and Pioneer 11. CIR's typically form beyond ~ 2 AU from the interaction of the solar wind plasma in a high-speed solar wind stream overtaking slower moving plasma (Smith and Wolfe, 1976). The interaction region has discontinuities in the solar wind speed, increases in the

solar wind particle density, and enhanced magnetic fields. Spikes in the proton flux have also been observed (Barnes and Simpson, 1976) at the passages of CIR shocks and were used (Pyle and Simpson, 1977) to indicate the times that CIR's passed the Pioneer spacecraft when solar wind data were not available.

This convection-diffusion model has been used to model three phenomena: the electron intensity increases observed near Jupiter (Chenette, et al., 1977c, Conlon, 1978); the rise time profiles of Jovian increases observed by Pioneer 11 within $\sim$1.2 AU of Jupiter (Conlon, 1978); and the asymmetric envelope formed by the maxima of Jovian electron increases at 1 AU over a Jovian synodic period (Chenette, et al., 1977c; Conlon, 1978).

IV-B. The Distribution of the Observed Time Profiles Within a Synodic Period

The convection-diffusion propagation model described in Appendix C predicts a diffusive rise time profile throughout the Jovian synodic period. The number of observed increases with abrupt, diffusive, and exponential rise time profiles are about equal as shown in Table III-1. This says that there are other physical processes besides those in the convection-diffusion model that affect the electron propagation from Jupiter to Earth.

To investigate these possible processes the distributions of

the increase start times during the synodic period for each of the categories of the rise time profiles were examined. These distributions are plotted in Figure IV-1. The electron count rate for the 1975 Jovian synodic period is plotted for reference in the top panel. The lower panels show the distribution of each category of rise time profile for all of the synodic periods. The start time for each of the 88 increases has been plotted relative to the nominal connection time of Earth and Jupiter for a solar wind speed of V_{SW} = 500 km/sec. The choice of a solar wind speed does not significantly alter these distributions. For instance, using V_{SW} = 420 km/sec would only shift the nominal connection time, the zero point, about 40 days to the right on the plot. The start times have been sorted into 10 day bins to form these distributions.

The second panel down is the distribution of the increase start times for all of the 88 Jovian increases. The increases are approximately uniformly distributed throughout the synodic period with 32 increases occurring before the nominal connection time for V_{SW} = 500 km/sec and 56 increases occurring after this nominal connection time. A convenient measure for the distribution of the occurrences of Jovian increases is the number of increases per 100 days. For the distributions of all the increases, the 150 day period before the nominal connection time has a rate of occurrence of (21.4 ± 3.8)/100 days and the 250 day period after the nominal connection time has a rate of occurrence of

Figure IV-1

Distribution of the rise time profiles of the Jovian increases throughout the synodic period. Plotted for reference in the top panel is the electron flux for the 1975 synodic period. The abscissa is the number of days from the nominal connection time for a solar wind speed of V_{SW} = 500 km/sec. The lower panels are the distributions over the synodic period for each of the classifications of rise time profiles. The number at the left in each plot is the number of increases that start before the nominal connection time and the number at the right is the number of increases that start after the nominal connection time.

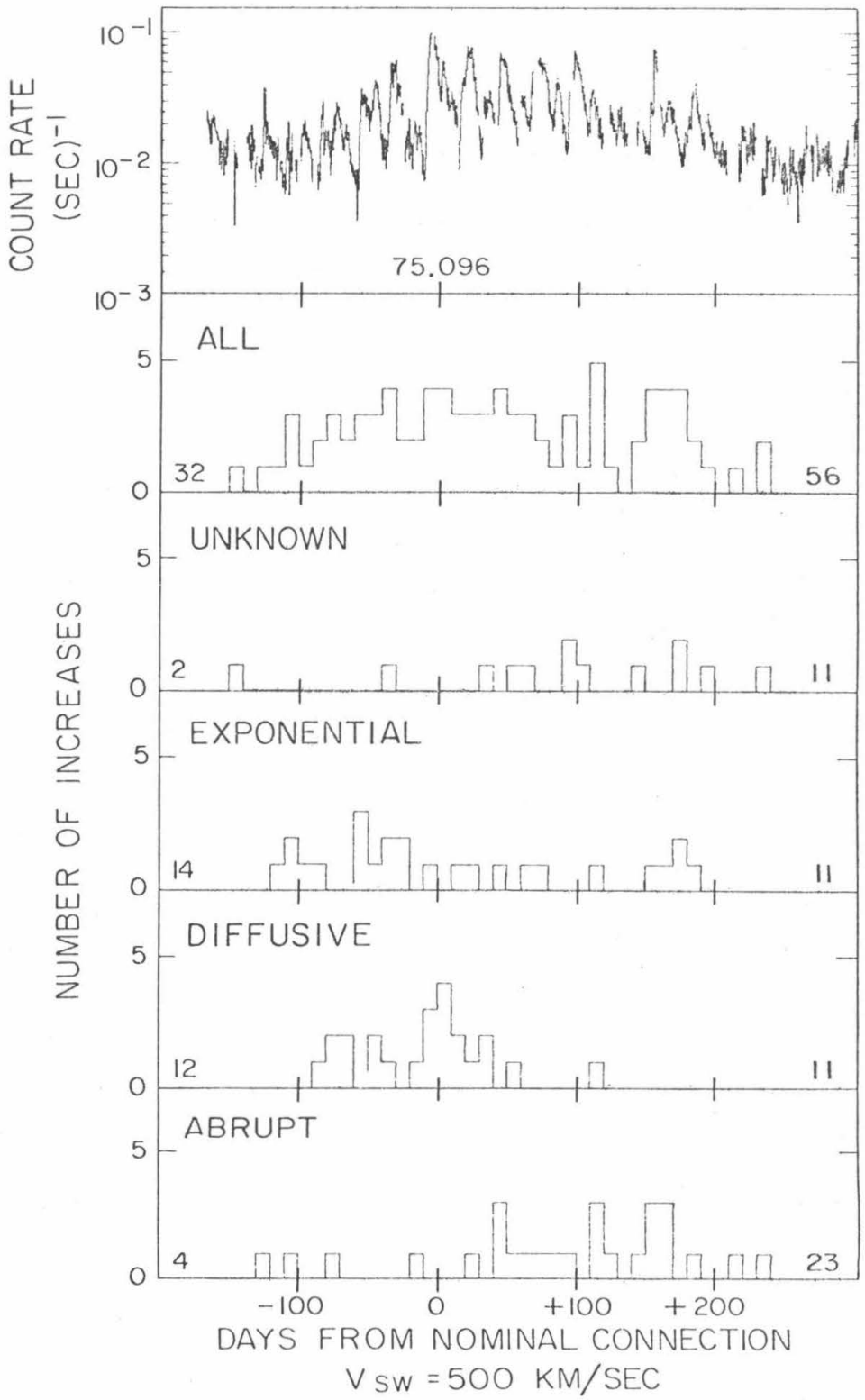
COUNT RATE
(SEC)⁻¹
10⁻¹
10⁻²
10⁻³
75.096
ALL
32
56
UNKNOWN
2
11
EXPONENTIAL
14
11
DIFFUSIVE
12
11
ABRUPT
4
23
NUMBER OF INCREASES
5
0
-100
0
+100
+200
DAYS FROM NOMINAL CONNECTION
V SW = 500 KM/SEC

(22.4±3.0)/100 days. Thus the rate of occurrence is approximately constant over the whole synodic period confirming the visual appearance of the distribution shown in Figure IV-1.

The next panel down is for those increases whose rise time profiles could not be determined. Next are the increases with exponential rise time profiles. Even though the increases with exponential rise time profiles occur over the whole synodic period, 14 increases occur in the 150 days before the nominal connection time for a rate of occurrence of (9.3± 2.5)/100 days while 11 increases occur in the 250 days after the nominal connection time for a rate of occurrence of (4.4± 1.3)/100 days. Thus increases with exponential rise time profiles occur twice as frequently before the nominal connection time than after the nominal connection time.

In the next panel the increases with diffusive rise time profiles tend to occur near the nominal connection time. The 12 increases occurring before the nominal connection time are within 90 days of the nominal connection time and 10 of the 11 increases occurring after the nominal connection time are within 60 days of the nominal connection time. Using the mid-point of the 10 day bins, the distribution of the increases with diffusive rise time profiles relative to the nominal connection time has an average occurrence of 9 days before the nominal connection time with a sigma of 48 days.

Finally, in the bottom panel the increaseswith abrupt rise time profiles tend to occur after the nominal connection time. The 4 increases occurring before the nominal connection time give a rate of occurrence of (2.7 ± 1.3)/100 days and the 23 increases occurring after the nominal connection time give a rate of occurrence of (9.2 ± 1.9)/100 days. Thus, increases with abrupt rise time profiles occur ~ 3.5 times as frequently after the nominal connection time than before the nominal connection time. In fact 70 percent (19 out of 27) of the increases with abrupt rise time profiles occur in the interval from 40 days to 160 days after the nominal connection time.

The diffusive rise time profile predicted by the convection-diffusion model only occurs around the nominal connection time. At this time Earth and Jupiter are connected most efficiently with the distance along a field line at a minimum and the distance perpendicular to the average spiral field line near zero. This time period also corresponds to the region near Jupiter where Jovian increases seen on Pioneer 11 were fit with time profiles predicted by the convection-diffusion model (Conlon, 1978).

The other aspect of the convection-diffusion model is that corotating interaction regions act as barriers to electron propagation (Conlon and Simpson, 1977). The abrupt rise time profiles that tend to occur after the nominal connection time can be understood with this concept. Figure IV-2 shows two schematic

Figure IV-2

Schematic drawing of two CIR's acting as barriers to electron propagation. The relative positions of Earth and Jupiter are for the time period after the nominal connection time. Figure IV-2a shows CIR_1 passing Jupiter after which Earth and Jupiter will be in the two separate regions bounded by CIR_1 and CIR_2. The shaded region behind CIR_1 and in front of CIR_2 contains Jupiter and will now start filling up with electrons. In Figure IV-2b the CIR's have corotated so that CIR_1 is passing Earth at which time Earth will enter the shaded region which Jupiter has been filling with electrons and will see an abrupt increase in the electron flux at 1 AU.

a
JUPITER
CIR1
EARTH
SUN
CIR2
b
CIR1
JUPITER
EARTH
SUN
CIR2

snapshots of the position of Earth and Jupiter for the time period after the nominal connection time and the positions of two CIR's. The CIR's act as barriers to electron propagation so that in Figure IV-2a the CIR labeled CIR_1 passes Jupiter and with the CIR labeled CIR_2 separates Earth from the shaded region containing Jupiter. While the CIR's corotate the shaded region behind CIR_1 is being filled with electrons from Jupiter. When CIR_1 passes Earth, as shown in Figure IV-2b, the flux first seen at Earth will be high since the shaded region has been filled partially with electrons, and thus an abrupt increase occurs at Earth. It is possible that the exponential rise time profiles seen before the nominal connection time are due to the source filling up a region between two CIR's.

Neither the peak time profiles nor the fall time profiles show any systematic distribution over the synodic period similar to the distribution of the rise time profiles. The fall time profiles being mainly exponential may be due to the decay of electrons after the source, Jupiter, has exited the region between two CIR's. The occasional abrupt fall suggests that sometimes a barrier passes Earth during the decay phase of an increase. The flat or broad peak time profiles may indicate that the flux within the region between two CIR's has reached an equilibrium value. However, only the two Jovian increases at 74.134.12 and 74.162.18 have a flat peak that lasts for more than $\sim$1 day.

IV-C. Occurrence of Jovian Increases

IV-C-1. Correlation of Jovian Increases with Corotating Interaction Regions

Corotating interaction regions (CIR's) have been suggested by Conlon and Simpson (1977) to form "impenetrable barriers" to the propagation of Jovian electrons. They found that the occurrence of electron increases observed by the Pioneer 10 spacecraft after the Jupiter encounter could be correlated with the passage of CIR's either past the Pioneer 10 spacecraft or past the position of Jupiter. These results suggest that electron increases observed at Earth may also be correlated with the passage of CIR's past the position of Jupiter or with the times that the ideal spiral field lines associated with the CIR's pass Earth. Chenette and Simpson (1978) used the information on CIR's from Pioneer 10 and Pioneer 11 to predict the passage times of CIR's past Jupiter and Earth. Using the idea that CIR's form barriers to electron propagation, they suggested that the timing of most of the increases seen at 1 AU could be explained by CIR's passing Jupiter and CIR precursors passing Earth.

The times that the CIR's occurred at Pioneer 11 for the period 73.330 through 74.284 were taken from Figure 6 of Conlon (1978) which is reproduced here as Figure IV-3. Using daily snapshot

Figure IV-3

Plots of the 3-6 MeV electron counting rate observed by Pioneer 11. The data have been averaged over six-hour intervals. The times of CIR passages at Pioneer 11 are indicated by the hatched areas. The times that the trailing edges of the CIR's reached Jupiter are indicated by the vertical lines. From Figure 6 of Conlon (1978).

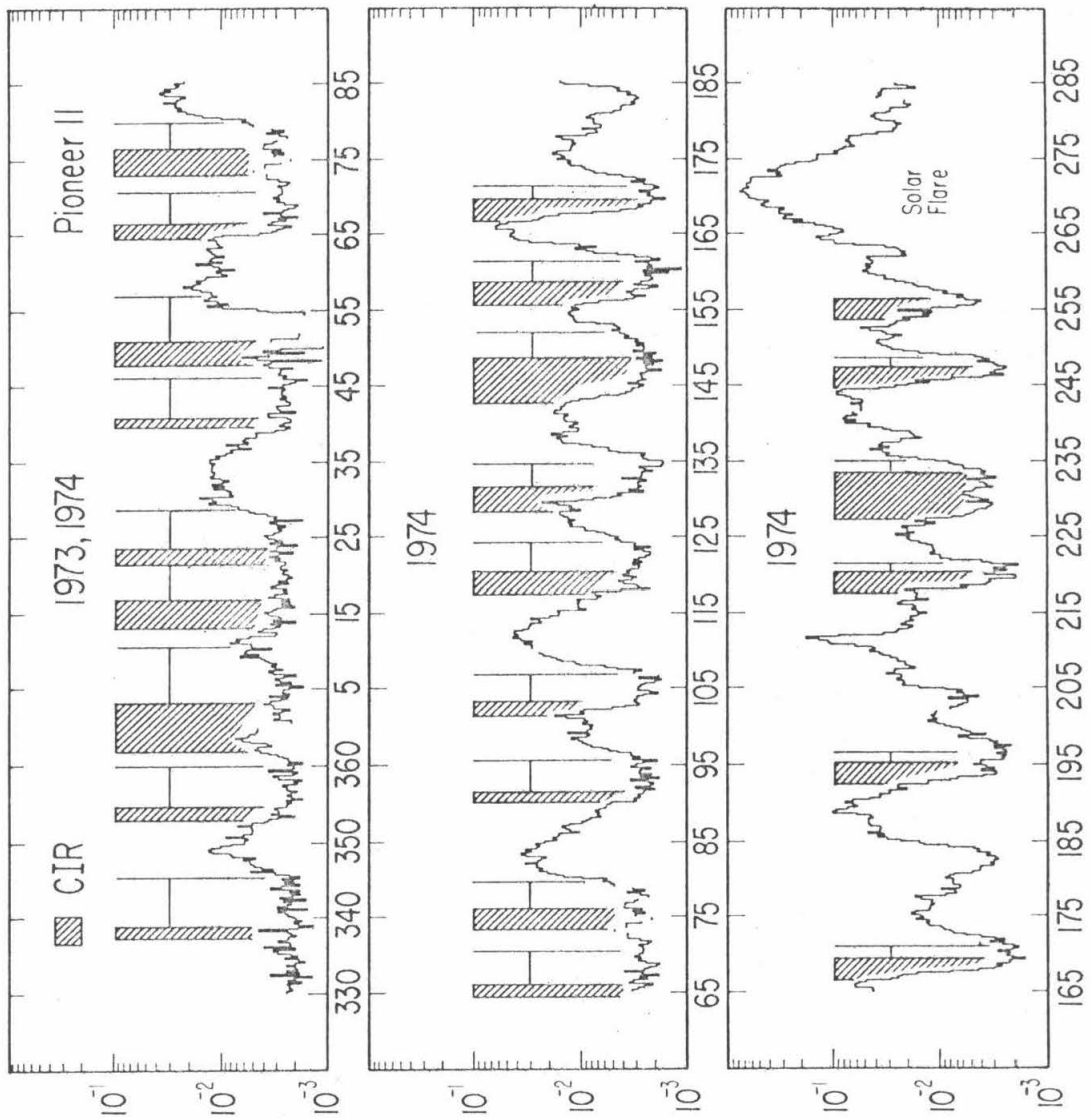
Pioneer 11
1973, 1974
CIR
1974
1974
Solar Flare
3-6 MeV Electron Counting Rate (Counts/sec)
Day of Year

solar wind speeds, Conlon estimated the time that the trailing edge of the previous CIR would pass Jupiter. These times are the vertical lines in Figure IV-3 and are connected by horizontal lines to the previous CIR passage times at Pioneer 11 indicated by the hatched areas. The time difference between the time that the trailing edge of a CIR passed Pioneer 11 and the time that the trailing edge passed Jupiter was measured from Figure IV-3. Then using this time difference and Equation B-6 of Appendix B the solar wind speed associated with the CIR was calculated. For the CIR that passed Pioneer 11 on 74.013 the correct solar wind speed cannot be calculated since a second CIR was plotted in Figure IV-3 before the first CIR reaches Jupiter. Therefore this CIR was not used in looking for correlations of CIR's with the electron flux at 1 AU.

With these solar wind speeds Equation B-6 was used to calculate the time that the ideal spiral field line associated with the CIR passed Earth. The positions of Pioneer 11, Jupiter, and Earth were furnished by Penzo (1975a,b). Table IV-1 lists the 19 CIR's for which solar wind speeds could be determined in the manner described above. The CIR's are labeled by the day that their front edge reached Pioneer 11. Included in Table IV-1 are the front and rear CIR passage times at Pioneer 11, the rear CIR passage time at Jupiter all obtained from Figure IV-3, and both the calculated solar wind speed and the rear CIR passage time at Earth. The

Table IV-1

Passage Times Of CIR's

CIR Date	V_{SW} (km/sec)	Time Of CIR At: Pioneer 11 Front	Pioneer 11 Rear	Jupiter Rear	Earth Rear
73.337	560	73.337.03	73.338.19	73.345.07	73.340.21
73.353	632	73.352.18	73.354.15	73.359.22	73.358.01
73.362	432	73.361.21	74.003.04	74.010.15	74.004.07
74.013	661*	74.012.10	74.016.22	74.021.09	74.021.22
74.021	563	74.021.09	74.023.13	74.028.16	74.027.16
74.040	506	74.039.12	74.040.18	74.046.01	74.044.21
74.048	429	74.047.16	74.050.19	74.056.18	74.053.16
74.065	566	74.064.10	74.066.09	74.070.12	74.072.15
74.073	628	74.072.18	74.076.06	74.079.16	74.083.19
74.090	504	74.090.03	74.091.15	74.095.16	74.098.00
74.101	543	74.101.13	74.103.12	74.107.00	74.111.03
74.118	456	74.117.13	74.120.12	74.124.09	74.127.01
74.128	531	74.128.09	74.131.16	74.134.16	74.140.09
74.143	434	74.142.16	74.148.16	74.152.01	74.155.19
74.156	499	74.155.13	74.158.16	74.161.09	74.168.00
74.167	699	74.166.16	74.169.15	74.171.07	74.182.19
74.193	731	74.192.12	74.195.12	74.196.19	74.210.10
74.218	707	74.217.16	74.220.10	74.221.12	74.236.10
74.227	532	74.227.09	74.233.15	74.235.00	74.247.09
74.244	494	74.244.10	74.247.10	74.248.16	74.260.22

* For this CIR the correct solar wind speed could not be calculated.

estimated error in determining the CIR passage time at Jupiter from Figure IV-3 is $\lesssim 0.5$ day and the error in calculating the CIR passage time at Earth is ~ 0.8 day on 73.330, increasing to ~ 1.3 days on 74.085 and to ~ 5 days on 74.265.

Notice that except for the CIR at 73.362, from 73.353 until 74.118 Earth and Jupiter are within ≤ 4 days of being on the same spiral field line. This occurs because a change of 1 day in the corotation time is equivalent to a change of ~ 15 days at Earth. During this time period then any correlation of CIR's at Jupiter with increases at 1 AU will also be a correlation at Earth to within ~ 4 days. Note that even for the CIR at 73.362 Earth and Jupiter are within $\lesssim 6$ days of being on the same spiral field line. This larger difference of 6 days as compared to typically ~ 4 days is due to the low solar wind speed of $V_{SW} \approx 432$ km/sec for this CIR. The low solar wind speed of $V_{SW} \approx 429$ km/sec on 74.048 does not have as large an effect since Earth and Jupiter are nearer the nominal connection time.

Plotted in Figure IV-4 are the solar wind speed, V_{SW}, the interplanetary magnetic field strength, $|B|$, and direction, ϕ_B, and the electron flux all measured at 1 AU. The solar wind and magnetic field data are from the National Space Science Data Center Omnitape (King, 1978). The time period covered in these plots is from 73.324 to 74.184 and covers the 1974 Jovian synodic period from 105 days before the nominal connection time

Figure IV-4

Plots of the solar wind speed, the interplanetary magnetic field, and the electron flux observed at 1 AU. Figure IV-4a covers the time period 73.324 to 74.033, Figure IV-4b the time period 74.034 to 74.108, and Figure IV-4c the period 74.109 to 74.183. The data are averaged over six-hour intervals except for the magnetic field direction which is the one hour average direction at the end of the six-hour interval. The top plot is the solar wind speed, V_{SW}. Next down are the magnetic field strength, $|B|$, and the magnetic field direction, ϕ_B . At the bottom the 1-6 MeV electron flux at 1 AU is plotted. The error bars are the 1σ error estimates. The open horizontal bars indicate the magnetic field enhancements selected by the criteria outlined in the text. The horizontal lines connecting short vertical marks are the time periods that CIR's are passing Jupiter and the calculated times that these CIR's would have been at 1 AU. The length of the CIR's is the CIR width as seen by Pioneer 11. The arrows point to the times of nominal connection for V_{SW} = 400, 500, and 600 km/sec.

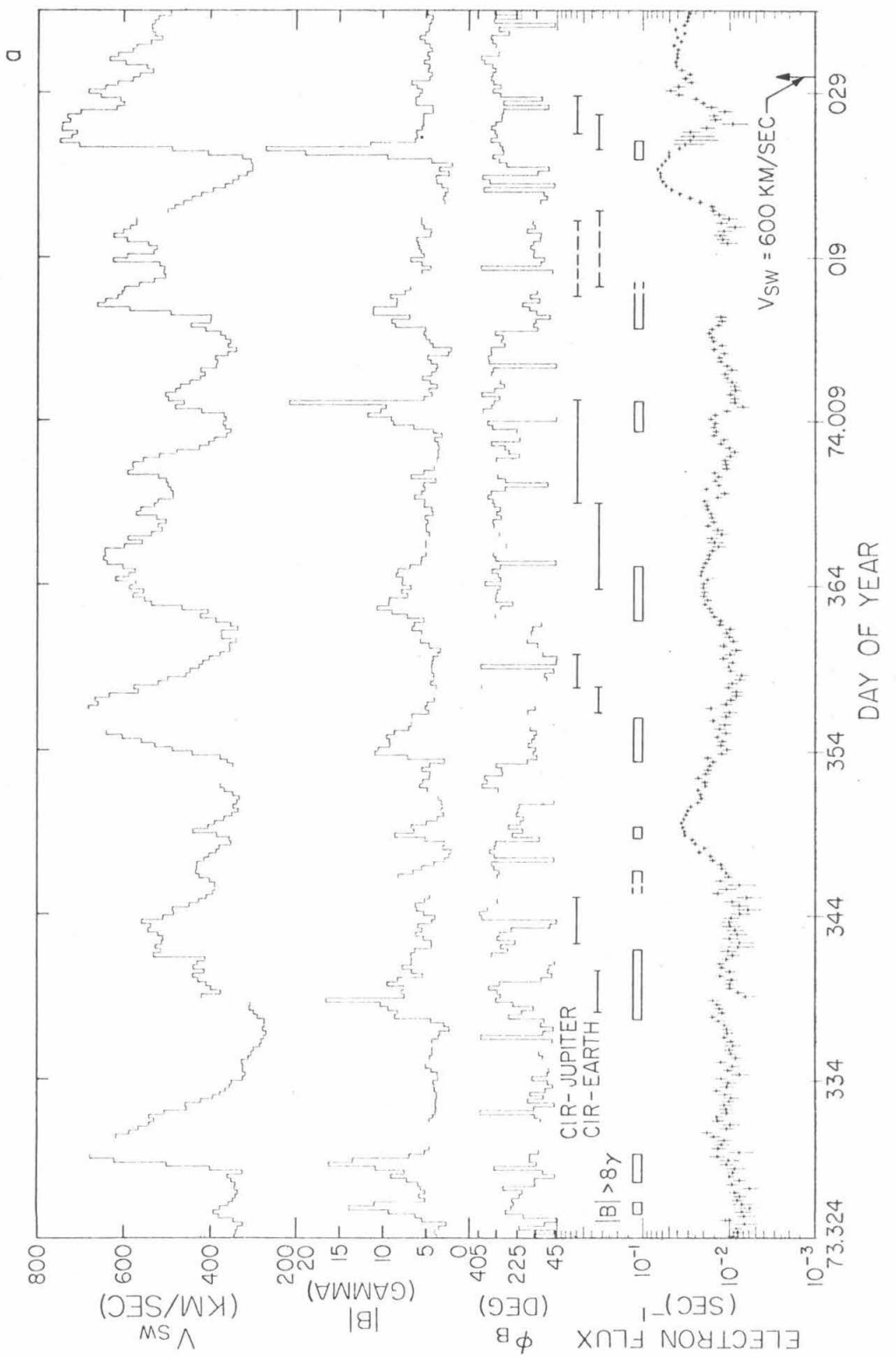
a
800
600
400
V_{SW} (KM/SEC)
200
20
15
10
5
0
|B| (GAMMA)
405
225
45
ϕ_B (DEG)
CIR-JUPITER
CIR-EARTH
|B| >8γ
10^{-1}
10^{-2}
10^{-3}
ELECTRON FLUX (SEC)$^{-1}$
V_{SW} = 600 KM/SEC
73.324
334
344
354
364
74.009
019
029
DAY OF YEAR

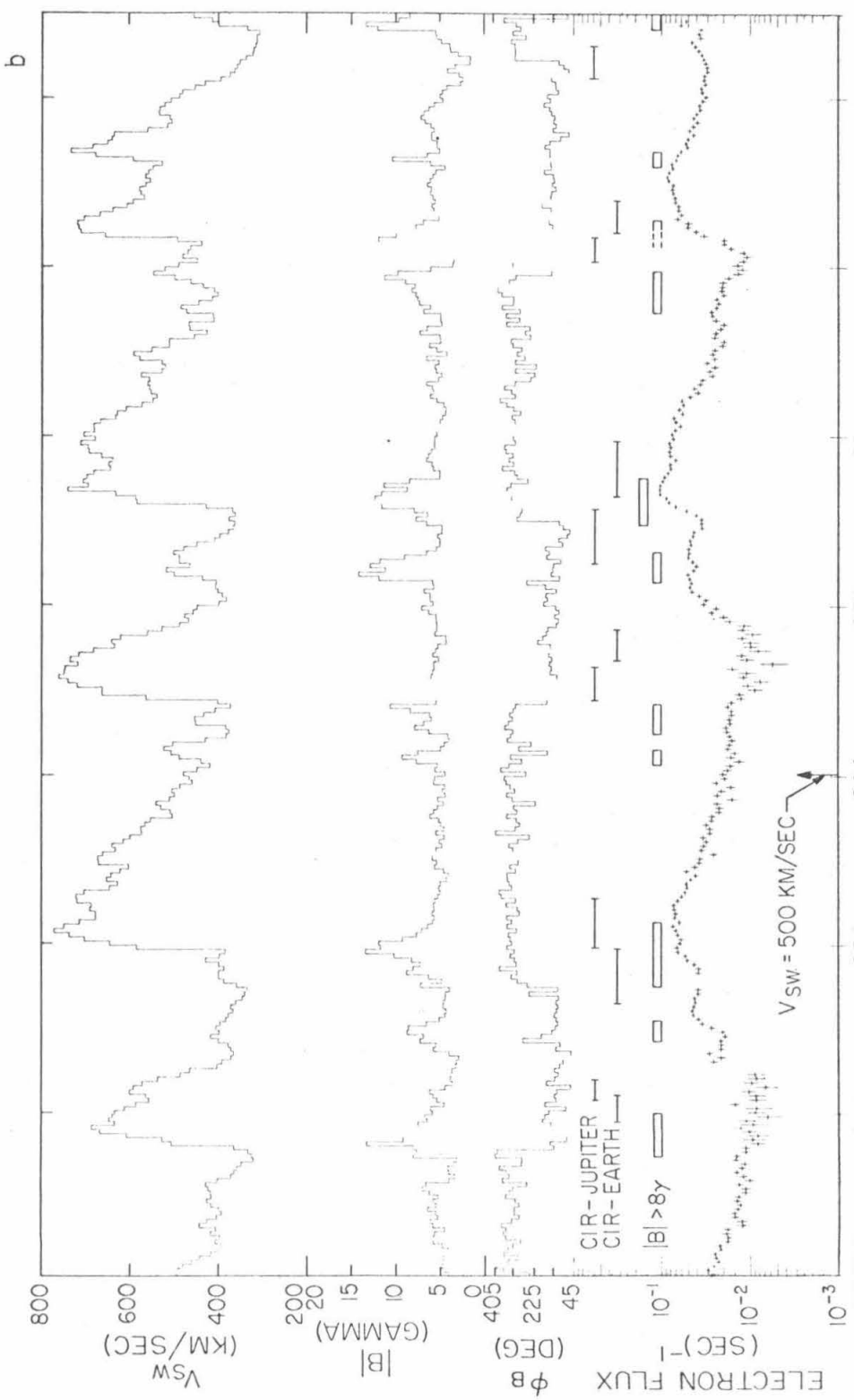
b
V_{SW} (KM/SEC)
|B| (GAMMA)
ϕ_B (DEG)
ELECTRON FLUX (SEC)$^{-1}$
CIR-JUPITER
CIR-EARTH
|B| >8γ
V_{SW} = 500 KM/SEC
DAY OF YEAR
74.034
044
054
064
074
084
094
104

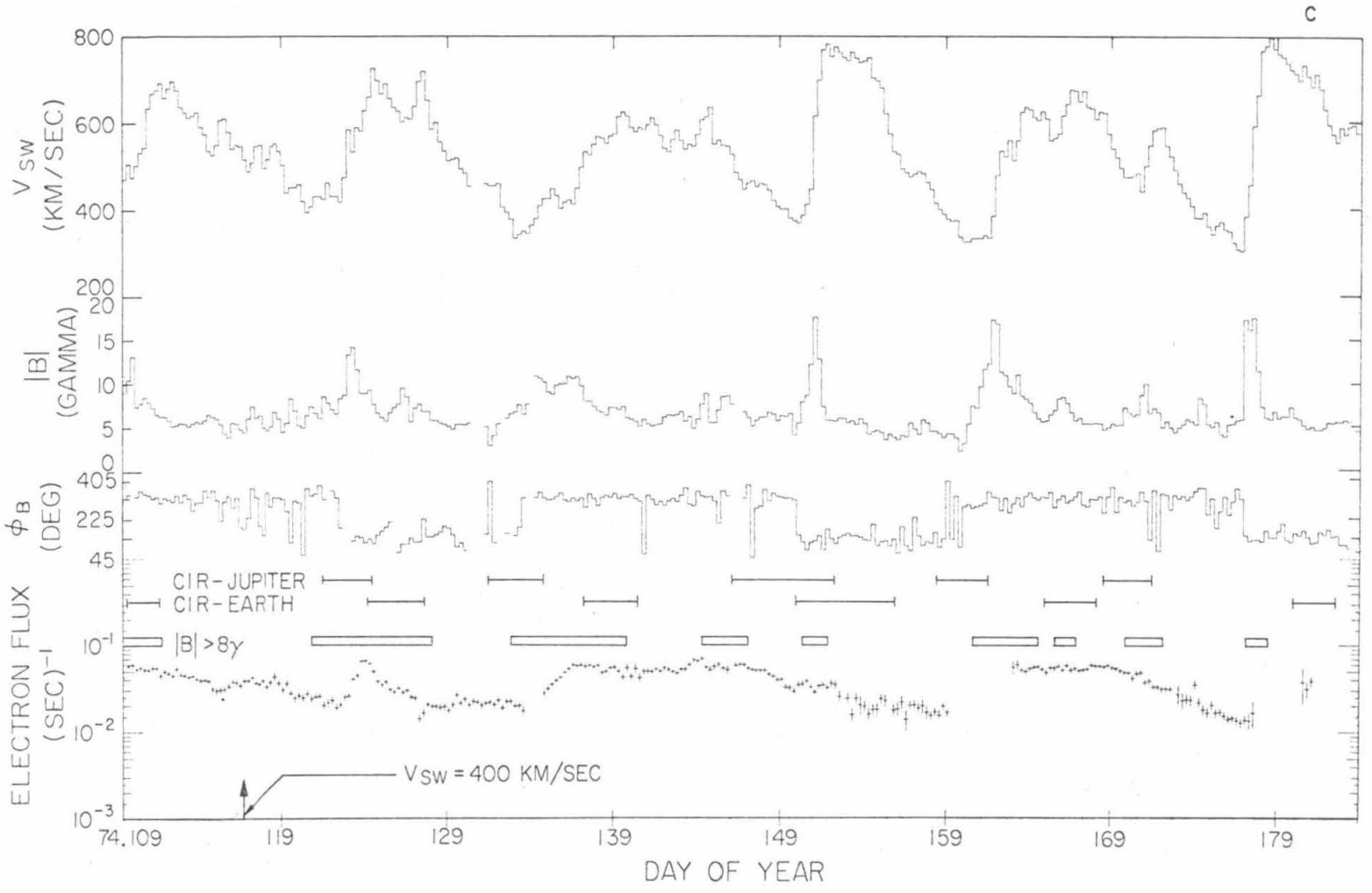
c
800
600
400
200
V_{SW} (KM/SEC)
20
15
10
5
0
|B| (GAMMA)
405
225
45
ϕ_B (DEG)
CIR-JUPITER
CIR-EARTH
|B| >8γ
10^{-1}
10^{-2}
10^{-3}
ELECTRON FLUX (SEC)$^{-1}$
V_{SW} = 400 KM/SEC
74.109
119
129
139
149
159
169
179
DAY OF YEAR

for V_{SW} = 500 km/sec to 120 days after this nominal connection time. The data are for six-hour averages with the solar wind speed at the top, below it the magnetic field strength and direction, and at the bottom the electron flux at 1 AU. The nominal connection times for V_{SW} = 400, 500, and 600 km/sec are plotted at the bottom of Figure IV-4 as arrows.

The CIR's listed in Table IV-1 for the time period covered in Figure IV-4 are plotted as horizontal lines above the electron flux. The front and rear passage times of a CIR past Earth or Jupiter are shown as short vertical marks at the ends of the horizontal lines. In Figure IV-4 the dotted lines at ~74.019 indicate the CIR at 74.013 on Pioneer 11 for which the correct solar wind speed could not be calculated.

The convection-diffusion model predicts that an increase at 1 AU should occur after a CIR acting as a barrier to electron propagation passes Earth or Jupiter such that after its passage both Earth and Jupiter are within the same region of space. The situations for before and after the nominal connection time are shown in the schematic drawings of Figure IV-5. The solid lines for CIR_1 and CIR_2 are the CIR positions relative to Earth and Jupiter just prior to an increase while the dotted lines are the CIR positions just after an increase. Before the increase the CIR's drawn as solid lines are separating Earth and Jupiter while after the increase the CIR's drawn as dotted lines place Earth

Figure IV-5

Schematic drawings of CIR's acting as barriers to electron propagation from Jupiter to Earth. Figure IV-5a is for the time period before the nominal connection time and Figure IV-5b is for the time period after the nominal connection time. The solid lines are the positions of the CIR's prior to the increase and the dotted lines are the CIR positions just after the increase starts. For the time period before nominal connection Earth is in the region behind CIR_1 and ahead of CIR_2. An increase occurs for this time period when CIR_1 passes Jupiter. The time period after nominal connection is similar except that the roles of Earth and Jupiter are exchanged with an increase occurring when CIR_1 passes Earth.

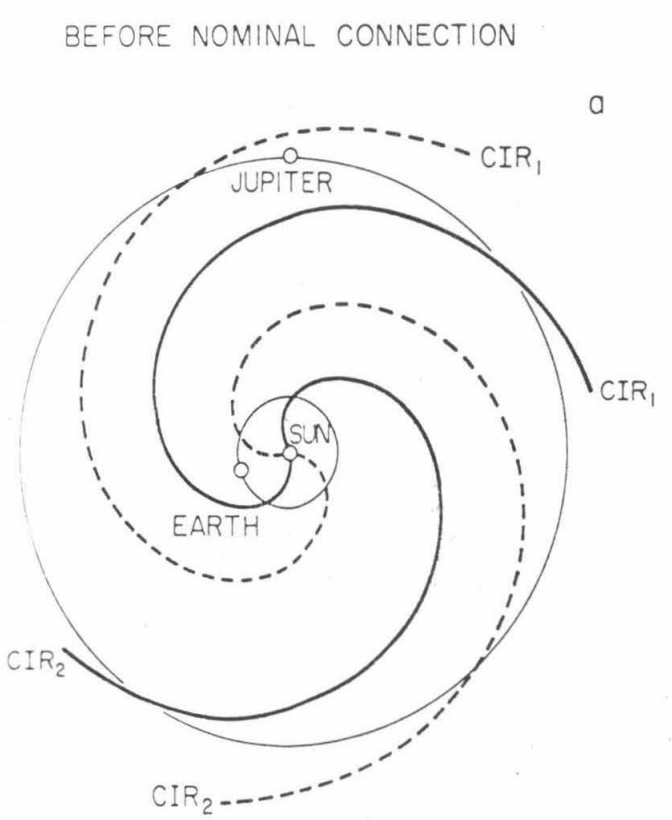
BEFORE NOMINAL CONNECTION
a
CIR1
JUPITER
CIR1
SUN
EARTH
CIR2
CIR2

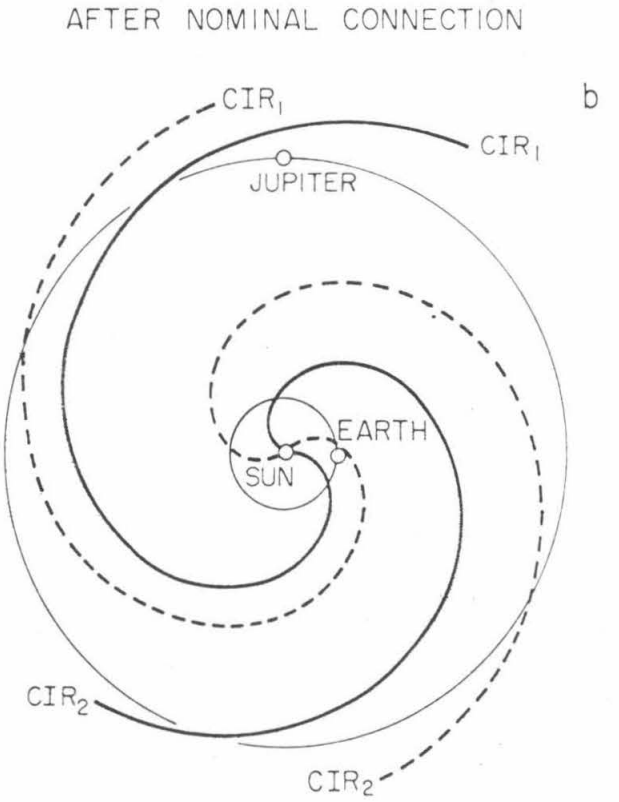
AFTER NOMINAL CONNECTION
b
CIR1
CIR1
JUPITER
EARTH
SUN
CIR2
CIR2

and Jupiter in the same region of space.

For the time period before the nominal connection time Earth is behind CIR_1 but ahead of CIR_2 while Jupiter is ahead of CIR_1 and behind CIR_2. When CIR_1 passes Jupiter then both Jupiter and Earth are within the region of space behind CIR_1 and ahead of CIR_2. Thus, for the time period before the nominal connection time an increase should occur when the CIR passes Jupiter.

For the time period after the nominal connection time the situation is similar except that now Jupiter is behind CIR_1 and ahead of CIR_2 while Earth is ahead of CIR_1 but behind CIR_2. When CIR_1 passes Earth then both Earth and Jupiter are within the region of space behind CIR_1 and ahead of CIR_2. During the time period after the nominal connection time an increase should occur when the CIR passes Earth.

Sixteen CIR's occur in the time period shown in Figure IV-4. As discussed earlier the CIR at ~74.019, labeled 74.013 at Pioneer 11, is not used in the correlation since its solar wind speed could not be calculated. The other CIR's form two groups with a boundary at about the nominal connection time for V_{SW} = 500 km/sec. The CIR's occurring from ~73.339 to 74.064 have the CIR passing Earth before passing Jupiter. These CIR's occur in the before nominal connection time period discussed above in Figure IV-5. The CIR's occurring from 74.064 to ~74.183 have the CIR passing Jupiter before passing Earth. These CIR's occur in the after nominal

connection time period discussed above in Figure IV-5.

The before nominal connection group is composed of six CIR's since the CIR at ~74.019 is not used. These CIR's should have an electron increase after the CIR passes Jupiter. Except for the CIR at 74.054 all the CIR's precede by ~1 day a Jovian increase listed in Table III-2. The CIR at 74.054 is at the peak of the increase starting at ~74.053. During the before nominal connection period the prediction of the convection-diffusion model with CIR barriers is good except for the increase nearest the nominal connection time.

If CIR's act as barriers both at Jupiter and at Earth then a CIR at Earth during the before nominal connection time period should cut off an increase. Of the six CIR's at Earth only the ones at 73.364, 74.026, and 74.051 have their front edge within ~1 day of a peak in the electron flux. These three all occur after the peak of the increase. The other three CIR's at Earth are not associated with the beginning of a decrease in the flux or with the peak of an increase. Thus, some of the decreases in the electron flux at 1 AU can be explained by a CIR passing Earth and separating Earth and Jupiter. These three expained decreases all occur $\gtrsim$1 day before the calculated CIR passage time at Earth which is consistent with the error in the calculated CIR passage time at Earth of ~0.8 to ~1.3 days during this time period. However, there are many other decreases in the electron

flux, for example at 73.349, 74.009, and 74.029, which remain to be explained.

The after nominal connection group is composed of nine CIR's. During this time period an increase should occur after the CIR passes Earth. The error in the calculated CIR passage time at Earth increases from ~1.3 days on 74.085 to ~2.7 days on 74.205 for this time period. Only the CIR's on 74.072 and 74.095 are associated with the rise time profile of an increase. The CIR's at 74.080, 74.107, 74.124, 74.137, and 74.165 all occur just after the peak of an increase. The CIR at 74.150 occurs between increases and the CIR at 74.180 occurs within a gap in the electron data. Thus, of the eight CIR's at Earth that occur with electron data only two are associated with the rise time profile of an increase and these two occur near the nominal connection time. One CIR occurs between increases and six CIR's occur just after the peak of an increase. The error in calculating the CIR passage times at Earth will not change the timing of the CIR passages enough to place the CIR rear passage at the rise profile of the increases. It is possible that the solar wind speed calculated from Figure IV-3 cannot be used to calculate the CIR passage times back from ~4 AU to 1 AU because the solar wind speed may be changing as the solar wind goes from 1 AU outward. If, however, the procedure used to find the CIR passage times at Earth is

appropriate, then the convection-diffusion model with CIR barriers does not explain the increase occurrences for the time period after the nominal connection time.

Since CIR's do not form until $>$ 2 AU from the sun, the characteristic shocks of CIR's are not seen at 1 AU. In the above discussion the times that CIR's passed Earth are more accurately the times that the ideal magnetic spiral field lines associated with the CIR's passed Earth.

IV-C-2. Correlation of Jovian Increases with Magnetic Field Enhancements

Since the convection-diffusion propagation model with CIR's acting as barriers does not explain all of the increases and changes in the electron flux at 1 AU, other physical mechanisms or parameters may be important. Since CIR's contain enhanced magnetic fields another possible barrier to electron propagation at 1 AU may be enhancements in the interplanetary magnetic field.

An examination of Figure IV-4 shows many magnetic field enhancements. Most such enhancements are associated with the front edge of a high-speed solar wind stream, as at 73.328 or 74.025, while some are not, as at 74.049. Since CIR's develop from the interaction of a high-speed stream overtaking lower speed plasma, some of the magnetic field enhancements should be associated with CIR's. However, there are more magnetic field enhancements in the time period in Figure IV-4 than the sixteen CIR's. Also, some enhancements are associated with sector boundaries as at 74.025, 74.042, and 74.150. A sector boundary is indicated by a 180° change in the direction of the interplanetary magnetic field.

An enhancement in the magnetic field, $|B|$, was identified by the following criteria:

1-at least one six-hour interval has $|B| \geq 8\,\gamma$,

2-at least two adjacent six-hour intervals have $|B| \gtrsim 6.5\,\gamma$, and

3-if two enhancements are separated by only one or two six-hour intervals with $|B| < 6.5\,\gamma$, then these two enhancements are merged into one enhancement or if a six-hour interval with $|B| \gtrsim 6.5\,\gamma$ is separated from an enhancement by one or two six-hour intervals with $|B| < 6.5\,\gamma$, then it is included in the enhancement.

The third criterion will include as part of the enhancement the one or two six-hour intervals that formed the separation mentioned.

The selection criteria stated above were checked by looking at the distribution of the magnetic field strength for all the six-hour intervals in Figure IV-4. The distributions of all the $|B|$ values, the $|B|$ values outside of $|B|$ enhancements, and the $|B|$ values inside of $|B|$ enhancements are shown in Figure IV-6. The top panel is the distribution of $|B|$ for all the six-hour intervals in Figure IV-4 and shows that the magnetic field strength is generally $\sim 5.5\,\gamma$ with a range from $\sim 2\,\gamma$ to $> 14\,\gamma$. The middle panel is the distribution of $|B|$ outside of $|B|$ enhancements and shows that the criteria for identifying $|B|$ enhancements selects all six-hour intervals with $|B| \gtrsim 8.5\,\gamma$ and most with $|B| \gtrsim 6.5\,\gamma$. The bottom panel shows the distribution of $|B|$ inside of $|B|$

Figure IV-6

Distributions of the magnetic field strength, $|B|$, for the six-hour averages over the time period plotted in Figure IV-4. The top panel is the distribution of all the $|B|$ values. The middle panel is the distribution for the $|B|$ values outside of $|B|$ enhancements. The bottom panel is the distribution for the $|B|$ values within the identified $|B|$ enhancements.

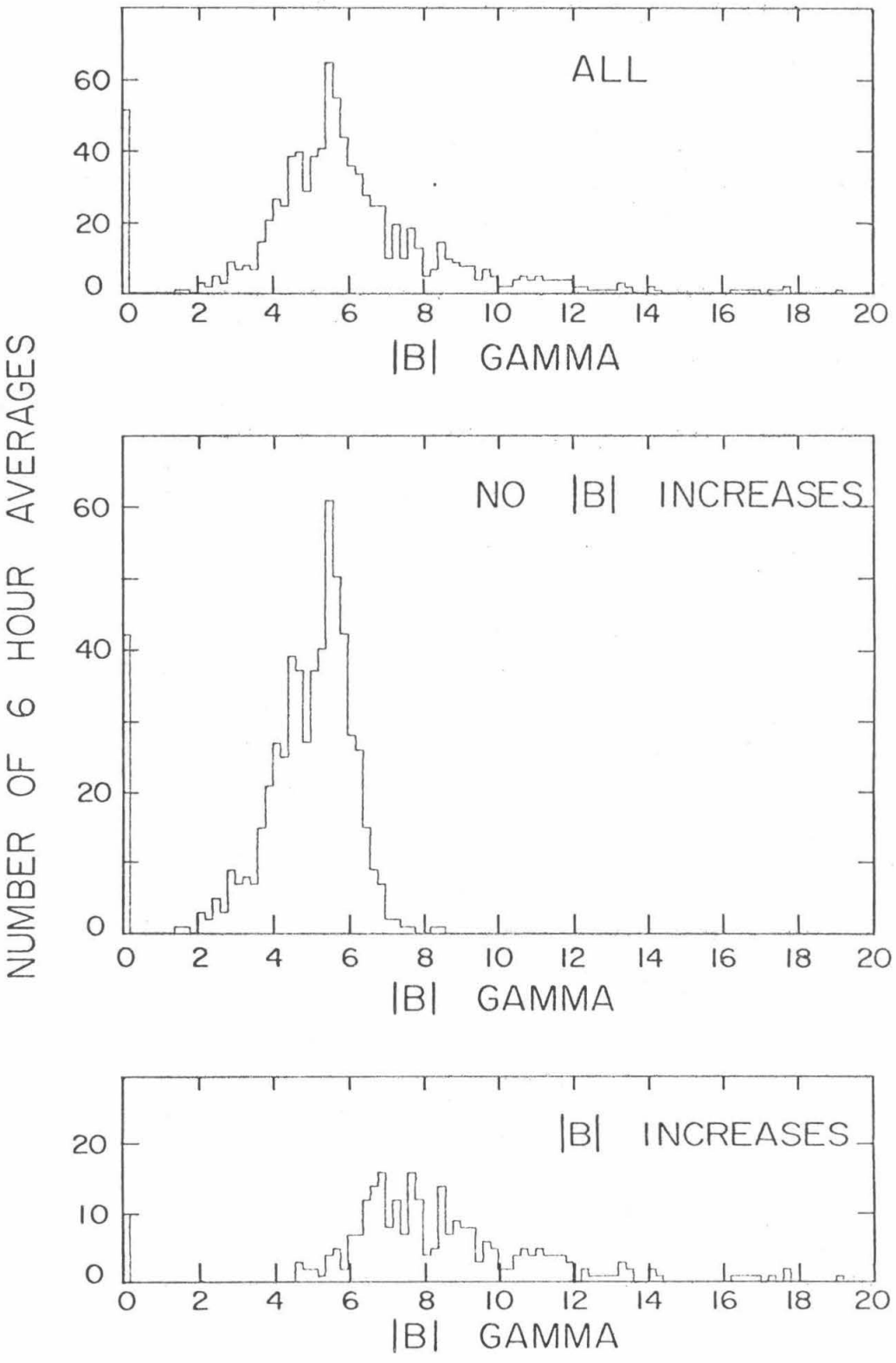
ALL
NO |B| INCREASES
|B| INCREASES
NUMBER OF 6 HOUR AVERAGES
|B| GAMMA
|B| GAMMA
|B| GAMMA
0
20
40
60
10
0 2 4 6 8 10 12 14 16 18 20

enhancements and shows that most of the selected six-hour intervals have $|B| > 6.4\,\gamma$ with data gaps and some six-hour intervals with $B \lesssim 6.4\,\gamma$ included due to the third criterion.

The 29 |B| enhancements selected by the above criteria are listed in Table IV-2 with their start and end times. Also included in Table IV-2 are the times of the maximum magnetic field strength, $|B|_{MAX}$, within the enhancement and the maximum field. The start and end times of a |B| enhancement have been labeled with the letter "S" if a sector boundary occurred near the edge of the |B| enhancement. Of the 29 |B| enhancements in Table IV-2, sixteen enhancement starts show some association with a sector boundary while only three enhancement ends show some association.

Some enhancements such as the one at 74.008.12 have a second maximum in |B| and the time of this second maximum is enclosed in parentheses in Table IV-2. Three enhancements have gaps in the |B| data and are noted in Table IV-2. The |B| enhancements in Table IV-2 are plotted in Figure IV-4 as open bars. The dotted bars for the enhancements at 73.346.06, 74.014.18, and 74.095.12 indicate that a portion of the enhancement was missing because of the data gaps. The last column of Table IV-2 lists the association of these |B| enhancements with increases and other changes in the electron flux at 1 AU.

The |B| enhancements have been correlated with slope changes in the rise time profiles of the Jovian increases. The time of a

Table IV-2

|B| Enhancements

Start[1]	End	Time of $\|B\|_{MAX}$[2]	$\|B\|_{MAX}$	Association[3]
73.325.12 S	73.326.00	73.325.18	14	
73.327.12	73.329.00	73.328.12	16	I *
73.337.18 S	73.341.18 S	73.338.18	17	A *
73.346.06 (73.345.06)[4]	73.346.12	73.346.06 [73.345.06][4]	8	Start *
73.348.18 S	73.349.06	73.348.18	9	I *
73.353.12 S	73.356.00	73.353.18	11	End *
73.362.00 S	73.365.00	73.362.12 (73.364.12)	11 9	I * Fall *
74.008.12	74.010.00	74.010.00 (74.009.06)	21 12	Start A *
74.014.18 S	74.017.00 (74.017.18)[5]	74.015.18	11	
74.025.00 S	74.025.18	74.025.12	24	
74.041.06 S	74.043.18	74.042.00	13	A
74.048.06 S	74.049.06	74.048.18	9	Start *
74.051.12 S	74.055.00	74.053.12	13	I *
74.064.18	74.065.06	74.065.00	9	End *
74.066,12	74.068.00 S	74.068.00	11	A *

Start[1]	End	Time of $\|B\|_{MAX}$[2]	$\|B\|_{MAX}$	Association[3]	
74.075.12	74.077.00	74.075.18	14	I	
74.078.18 S	74.081.06	74.080.06	12	I	*
74.091.06	74.093.12 S	74.093.00	11	A	*
74.095.12 (74.094.12)[4]	74.096.12	74.095.12 [74.094.12][4]	12	I	*
74.100.00	74.100.12	74.100.06	11	I	
74.108.00	74.111.00	74.108.06 (74.109.12)	13 13	I A	
74.120.18 S	74.127.18	74.123.06 (74.126.06)	14 9	I A	*
74.132.18 S	74.139.12	74.134.06 (74.136.06)	11 11	Start I	*
74.144.06[3]	74.146.18	74.144.12 (74.145.18)	9 9	Fall	
74.150.06 S	74.151.12	74.151.00	18	A	
74.160.12 S	74.164.06	74.161.18	17		
74.165.12	74.166.12	74.166.00	8		
74.169.18	74.171.18	74.171.00	10	Fall	
74.177.00 S	74.178.00	74.177.12	18	Start	

Table IV-2 notes

1- The start and end times of the |B| enhancements are in the same format that was used for the increases listed in Table III-2. An "S" signifies an association of the start or end of a |B| enhancement with a sector boundary.

2- Some of the |B| enhancements have a second maximum which is listed in parentheses.

3- The symbols used to indicate the type of association are:

I-associated with a slope change listed in Table IV-3;
A-associated with an abrupt change in the flux listed in Table IV-4;
Start-associated with the start of an increase;
Fall-associated with the fall of an increase;
End-associated with the end of an increase;
*-indicates a good association.

4- The start time of the |B| enhancement is unknown due to a gap in the |B| data from the date in parentheses until the listed start date. Note that $|B|_{MAX}$ may occur within this gap and that the earliest occurrence of $|B|_{MAX}$ is listed in brackets.

5- The end time of the |B| enhancement is unknown due to a gap in the |B| data from the listed date until the date in parentheses.

slope change was defined as the time that the flux in the rise time profile of an increase had a discontinuous change in slope in the plots in Figure IV-4. For example the increase starting at 73.344.06 has a rise time profile with almost constant slope in Figure IV-4 from 73.346.06 to 73.348.18. At 73.349.00 the increase has a rounded profile and then has a discontinuity in the slope at 73.349.12. This time was taken as the time of the slope change. The increase at 74.021.12 has a slightly different slope change. It has a smoothly varying rise profile until 74.024.06 when the slope changes in a discontinuous manner. The times of the slope changes for the other increases were determined in a similar manner.

An association of a $|B|_{MAX}$ with a slope change is noted as good if the $|B|_{MAX}$ occurs $\lesssim 1$ day before the slope change. This definition is reasonable since the correlation is done to look for a possible barrier effect of the |B| enhancements.

The slope changes are listed in Table IV-3 with the increase start time, the slope change time, and the association of the |B| enhancement with the slope change. The rise profile for the increase at 74.162.18 occurs in a gap in the flux data and the time of its slope change is unknown but $|B|_{MAX}$ does occur in the data gap. This increase and slope change are not used in this correlation. Fifteen slope changes with known occurrence times are listed in Table IV-3, including the two slope changes for the increase at 74.106.00. Four of the slope changes occur >24 hour from the time of

Table IV-3

Slope Changes In The Rise Profiles

Increase[1] Start Time	Slope Change[2] Time	Time Of Nearest $\|B\|_{MAX}$	$\Delta\tau$[3] Hours
73.325.18	73.329.00	73.328.12	12 $^{+24}_{-12}$
73.344.06	73.349.12	73.348.18	18 $^{+\ 0}_{-12}$
73.361.12	73.363.00	73.362.12	12 $^{+12}_{-60}$
74.009.18	74.014.06	74.015.18	-36 $^{+24}_{-30}$
74.021.12	74.024.06	74.025.12	-30 $^{+12}_{-\ 6}$
74.028.00	74.029.00	None[4]	
74.049.00	74.050.00	74.048.18	36 $^{+12}_{-12}$
74.052.18	74.053.18	74.053.12	6 $^{+48}_{-36}$
74.072.12	74.075.00	74.075.18	-18 $^{+\ 6}_{-30}$
74.079.06	74.080.12	74.080.06	6 $^{+36}_{-24}$
74.094.18[5]	74.096.06	74.095.12	18 $^{+\ 0}_{-24}$
	74.099.06	74.100.06	-24 $^{+\ 6}_{-\ 6}$
74.106.00	74.107.06	74.108.06	-24 $^{+\ 6}_{-56}$
74.122.12	74.123.18	74.123.06	12 $^{+60}_{-108}$
74.134.12	74.136.12	74.136.06[6]	6 $^{+84}_{-78}$
74.162.18	74.159.00 -74.164.00[7]	74.161.18	$^{54}_{-66}$

Table IV-3 notes

1- The increase start time is from Table III-2.

2- The slope change time is the time that the rise time profile of an increase had a discontinuous change in slope as plotted in Figure IV-4.

3- Δt is the difference of the slope change time from the time of the nearest $|B|_{MAX}$. The $\pm$ values are the range for for the |B| enhancement. For example the slope change at 73.320.00 occurred 12 hours after the time of $|B|_{MAX}$, 36 hours after the start of the |B| enhancement, and 0 hours before the end of the |B| enhancement.

4- The closest enhancements are at 74.025.12, over three days earlier, and at 74.042, thirteen days later.

5- This increase has two slope changes on its rise time profile. Since both slope changes fit the definition, both are listed in this table.

6- Second $|B|_{MAX}$ of the broad enhancement at 74.132.18.

7- $|B|_{MAX}$ occurs within a gap in the flux data from 74.159.00 to 74.164.00. For this slope change Δt is the range of possible times to the $|B|_{MAX}$ and no $\pm$ values are listed. The width of the |B| enhancement is 90 hours.

a $|B|_{MAX}$. The slope change at 74.029.00 is not associated closer than 3 days to a $|B|_{MAX}$. The slope change at 74.014.06 occurs at the same time as a sector change and the slope change at 74.024.06 occurs 6 hours before a sector change. The start of the increase at 74.049.00 occurs 6 hours after $|B|_{MAX}$. So of the four slope changes that occur relatively far from the time of a $|B|_{MAX}$, one does not have a $|B|_{MAX}$ association, two have good associations with sector boundaries, and though the last slope change does not have a $|B|_{MAX}$ association, the start of the increase does have a good association with $|B|_{MAX}$.

For the other eleven slope changes, eight $|B|_{MAX}$ occur ≤ 18 hours before the slope change time and therefore these $|B|_{MAX}$ display good associations. For the other three slope changes, their $|B|_{MAX}$ occur after the slope change time and thus these $|B|_{MAX}$ do not display good associations. The eleven $|B|$ enhancements for which their $|B|_{MAX}$ displayed an association with a slope change are indicated by the letter "I" in the last column of Table IV-2 with the eight good associations noted by an asterisk.

For a model including barriers to electron propagation, the passage of a barrier past Earth should either place Jupiter and Earth within the same region of space so that an increase may occur or the passage would separate Earth and Jupiter so that an increase would have a peak, a slope change, or a fall. Slope changes due to barriers can occur throughout the whole synodic period.

Table IV-3 only lists the associations of |B| enhancements with slope changes. Eleven slope changes show some association with $|B|_{MAX}$ and of these eight have good associations. Of the four slope changes that have no association with $|B|_{MAX}$, two have an association with sector boundaries. Since the sector boundaries in these two cases occur just before |B| enhancements, perhaps the leading edge of the |B| enhancement can also indicate the time that a barrier passed Earth. The eight good associations of slope changes with $|B|_{MAX}$ occur over most of the time period in Figure IV-4. This distribution in occurrence is consistent with the idea that |B| enhancements are a barrier signature.

There are a number of abrupt changes in the electron flux occurring in a time interval of less than 18 hours for the time period shown in Figure IV-4. The abrupt fall in the flux at 73.339.00 is an example of one of these abrupt changes. Nine abrupt changes have been noted in the flux plotted in Figure IV-4 and are listed in Table IV-4 with their date, time interval, Δt , for the flux change, and the factor of the flux change. To see if these abrupt changes associate with |B| enhancements, the time of the nearest $|B|_{MAX}$ is also listed in Table IV-4 along with the time difference from the time of $|B|_{MAX}$ to the time of the abrupt change.

For five abrupt changes, a $|B|_{MAX}$ occurs $\leq$ 6 hours before the time of the abrupt change. These five abrupt changes have

Table IV-4

Abrupt Changes in the Electron Flux

Time of Abrupt Change	ΔT[1] Hours	Factor[2]	Time Nearest $\|B\|_{MAX}$	Δt[3] Hours
73.339.00	6	0.43	73.388.18	6^{+24}_{-72}
74.009.06	12	0.50	74.009.06[4]	0^{+18}_{-18}
74.041.12	18	~0.63[5]	74.042.00	-12^{+18}_{-42}
74.046.12[6]	12	2.9	74.048.18	-54^{+12}_{-12}
74.068.06	18	0.55[5]	74.068.00	6^{+36}_{-0}
74.093.06	12	0.69[5]	74.093.00	6^{+42}_{-12}
74.108.06	6	1.6	74.108.06[7]	0^{+6}_{-66}
74.127.06	6	0.59	74.126.06[4]	24^{+132}_{-36}
74.152.06	18	~0.69[5]	74.151.00	30^{+18}_{-12}

[1] ΔT is the time interval for the flux to abruptly change.

[2] "Factor" is the multiplicative factor for the flux change.

[3] Δt is the time difference in hours of the time of the abrupt change from the time of the nearest $|B|_{MAX}$. The $\pm$ values are the range for Δt for the |B| enhancement.

[4] Second $|B|_{MAX}$ of an enhancement.

[5] This is an abrupt fall in the flux occurring near the end of an increase.

[6] This abrupt change occurs over a gap from 74.046.12 to 74.047.00.

[7] First $|B|_{MAX}$ of an enhancement.

good associations with $|B|_{MAX}$. The two abrupt changes at 74.127.06 and 74.152.06 have poor associations. The abrupt change at 74.041.12 occurs both within 6 hours of the sector change at 74.041.18 and within 6 hours of the |B| enhancement edge. This abrupt change may be associated with the enhancement edge rather than with $|B|_{MAX}$. Note that the abrupt changes at 74.068.06 and 74.093.06 also both occur at a sector change and an enhancement edge. The abrupt change at 74.047.12 occurs in a gap in the flux data and is not associated with either a |B| enhancement or a sector change.

Out of the nine abrupt changes in the flux listed in Table IV-4, five display a good association with $|B|_{MAX}$, two display a poor association, one displays an association with a sector change and an enhancement edge, and one shows no association. The eight |B| enhancements that have some association with abrupt changes in the flux are listed in the last column of Table IV-2 by the letter "A" with the good associations noted by an asterisk.

The occurrence of |B| enhancements may also have an association with increase starts. For the time period before the nominal connection time, |B| enhancements may indicate the time of an increase start if the enhancements occur shortly after a CIR passage time at Jupiter. The enhancement at 73.346.06 fits this character since it occurs both just after the time the CIR at 73.343 passes Jupiter and before the increase rise starting around 73.346.12. The

enhancements at 74.008.12, 74.048.06, 74.132.18, and 74.177.00 show a similar pattern though CIR's are also associated with the increase starts for all but the enhancement at 74.048.06. These associations are noted in the last column of Table IV-2 by the word "Start" with an asterisk indicating the better associations for 73.346.12 and 74.048.06.

The |B| enhancements should also be associated with the falls or ends of increases. The two enhancements at 73.353.12 and 74.064.18 are associated with the end of an increase when the flux stops falling and becomes approximately constant. Both $|B|_{MAX}$ are good associations and occur within 24 hours of the increase ends at 73.353.18 and 74.064.06 respectively. The association of these two |B| enhancements with increase ends are noted in the last column of Table IV-2 by the word "End" with an asterisk to indicate the good associations. The two enhancements at 74.144.06 and 74.169.18 are associated with the beginning of an increase fall. Both however display poor associations. The second $|B|_{MAX}$ of the enhancement at 73.362.00 occurs ~12 hours before the beginning of an increase fall at ~73.364.30 and has a good association. These associations are noted in the last column of Table IV-2 by the word "Fall" with an asterisk indicating the good association at 73.364.12.

Only 5 of the 29 |B| enhancements listed in Table IV-2 have no association with any of the features in the electron flux discussed

above. This is evidence that the occurrence of |B| enhancements at 1 AU, especially the maxima of these enhancements, indicate the times that barriers to electron propagation pass Earth.

For the time period before the nominal connection time a |B| enhancement associated with a CIR will pass Earth before the CIR passes Jupiter. Thus if the |B| enhancement indicates the passage of a barrier past Earth, then Earth will be separated from the region of falling fluxes that contained the previous increase and the flux level should be approximately constant until the CIR passes Jupiter.

The observed V_{SW} must be used to determine whether the sequence of the CIR's, enhancements, and increases is before or after the nominal connection time. For example the CIR and enhancement on ~74.124 were ~ 60 days after the nominal connection time for V_{SW} = 500 km/sec. However, the CIR and the of the enhancement passed Jupiter and Earth at about the same time. Since for this CIR V_{SW} = 456 km/sec, this sequence was around the nominal connection time for $V_{SW} \approx$ 400 km/sec. Thus, the timing of the enhancements and CIR's is consistent when the observed V_{SW} is used.

On ~73.345 a CIR passed Jupiter. Since $V_{SW} \approx$ 560 km/sec for this CIR, this time period was before the nominal connection time. Since Earth and Jupiter were in the same region, the increase on 73.344.06 started. The increase was cut off on 73.348.18 by the |B| enhancement that passed Earth at that time. The electron flux decreased since Earth and Jupiter were separated by the |B| enhancement. Note that this

enhancement was not associated with a CIR at Jupiter. On 73.353.12 a |B| enhancement passed Earth and the flux leveled off. This enhancement was associated with a high speed solar wind stream on ~73.354 and probably with the CIR that passed Jupiter on ~73.357. Since for this CIR V_{SW} = 632 km/sec, this sequence is also in the time period before the nominal connection time. If this CIR and enhancement were the same barrier, then the low fluxes from ~73.354 to ~73.359 were due to Earth entering a region that did not have an electron source in it for about half a corotation time or ~13 days. After the CIR passed Jupiter, an increase occurred on 73.361.12. The |B| enhancement that occurred at Earth on 73.362.00 again separated Earth and Jupiter and the increase was cut off. This sequence is consistent with the view that the CIR's indicate the times that barriers pass Jupiter and |B| enhancements at 1 AU indicate the times that barriers pass Earth.

The sequence from ~74.064 to ~74.076 is similar. Since for the CIR on ~74.070 V_{SW} = 566 km/sec, this sequence is around the nominal connection time. The enhancement on 74.064.18 occurred as the decrease ended. The enhancement on 74.066.12 was associated with the high speed stream, the sector boundary, and the CIR on ~74.070. When the $|B|_{MAX}$ of this enhancement passed Earth on 74.068.00, the flux decreased. After the trailing edge of the CIR passed Jupiter on 74.070, an increase occurred on 74.072.12. Since this time period is around the nominal connection time, the enhancement and CIR passed Earth and Jupiter at about the same time. On 74.075.18 a $|B|_{MAX}$ occurred as the increase reached its maximum.

For the time period after the nominal connection time a |B| enhancement associated with a CIR should pass Earth after the CIR passed Jupiter and an abrupt increase should be seen. However, in Table IV-2 for the time period after 74.064 only two enhancements were associated with increase starts while most were associated with slope changes, abrupt changes, or starts of the fall profiles.

For the increase on 74.094.18 the enhancement on 74.095.12 occurred at the same time as the CIR on ~74.095 passed Jupiter. This CIR had a solar wind speed of $V_{SW} \approx 504$ km/sec. This sequence occurred only ~30 days after the nominal connection time for $V_{SW} = 500$ km/sec and is consistent with being in the time period around the nominal connection time rather than after the nominal connection time. When the |B| enhancement on 74.091.06 passed Earth, the flux dropped. The increase occurred after the CIR on ~74.095 passed Jupiter and the flux had a slope change on 74.096.06 at a |B| enhancement. The enhancement on 74.095.12 was probably associated with the CIR. On 74.100.00 an enhancement passed Earth and the flux decreased as Earth was no longer within the region containing the electron increase. The next increase was observed at Earth when the CIR on ~74.107 passed Jupiter.

IV-D. The Convection-Diffusion Model Applied to the Synodic Period Envelope and the Increase Rise Time Profiles

IV-D-1. Predicted Synodic Envelopes

The convection-diffusion model has been used (Chenette, et al., 1977c; Conlon, 1978) to reproduce qualitatively the ~13 month Jovian synodic period envelope of the maxima of the 1 AU electron intensity increases. After Jupiter has been in a region of space a long time the input of electrons from the source equals the loss of electrons and the flux density is in equilibrium. This "equilibrium number density" is reached at 1 AU for model increase profiles after ~30 days (see Figure C-2 of Appendix C) and is calculated from the asymptotic solution given in Equation C-6 of Appendix C. The envelope calculated from the "equilibrium number density" was fit to only the 1975 synodic period and the variations between the synodic periods visible in Figure III-2 were not explained.

For a diffusive process the time scales as $t \propto \frac{L^2}{K}$ where t is the time, L is the distance from the source, and k is the diffusion coefficient. The increase at 74.107 on Pioneer 11 that was fit by Conlon (1978) took $\gtrsim$ 5 days to reach the asymptotic part of the increase profile. The distance of Pioneer 11 from Jupiter in the direction perpendicular to the average spiral

magnetic field line was L_{P11}=1.2 AU. Earth is about L_E=15 AU from Jupiter in the direction parallel to the average spiral field line. The scaling from Pioneer 11 to Earth for the time to reach the equilibrium or asymptotic part of the increase profile is then

$$t_E = t_{P11} \cdot \left(\frac{L_E}{L_{P11}}\right)^2 \cdot \left(\frac{K_x}{K_y}\right)$$

where k_x and k_y are the perpendicular and parallel diffusion coefficients respectively. Using the values of $k_x = 1 \times 10^{21}$ cm^2/sec and $k_y = 5 \times 10^{22}$ cm^2/sec, the time at Earth, t_E, is $\sim$3 times the time at Pioneer 11. For this example the time to reach the equilibrium part of an increase profile for increases at Earth is $t_E \gtrsim 15$ days. The sampling of Jovian increases shown in Figure III-5 rarely have a time from start to peak of $\gtrsim 7$ days. So though increases near Jupiter have time to reach equilibrium the increases at Earth do not have time to reach equilibrium.

In fact for the 88 Jovian increases observed at 1 AU, diffusive profiles for the onset of the increases occurred only around the nominal connection time, and even at the nominal connection time there were no increases that reached the asymptotic part of the predicted increase profiles plotted in Figure C-2. This may be due to a barrier or propagation inhibiting region occurring

between Earth and Jupiter late in the Jovian increase thus separating Earth and Jupiter and preventing the increases from reaching the equilibrium level. This says that the "equilibrium number density" solution used above is not appropriate to calculate the synodic envelope of Jovian electron increases at 1 AU and instead the intensity at some time earlier in the increases should be used. Because of the large rise time differences over the synodic period, the synodic envelope calculated in this way has a much different shape than the envelope calculated with the "equilibrium number density" solution.

Plotted in Figure IV-7 are the synodic envelope using the "equilibrium number density", the curve for $t = \infty$, predicted by Conlon (1978) and by Chenette, et al. (1977c), and the synodic envelope calculated from the electron intensity at t = 9 days. The interval of 9 days after the source starts filling the region was chosen to be sure that the calculated synodic period envelope would include all the maxima of the observed Jovian increases. In fact, the time from an increase start to its maximum varies typically being $\sim$ 5 days with no increase taking longer than $\sim$ 9 days to reach its maximum value. The t = 9 day envelope does not resemble the observed synodic envelope of Figure III-4.

The curves in Figure IV-8 and IV-9 were generated to see what effect varying the value of the diffusion coefficients would have on these predicted synodic envelopes. In Figure IV-8a is the synodic

Figure IV-7

Envelopes of the calculated electron flux at 1 AU over the synodic period for $t = \infty$ and $t = 9$ days. The parameters used to generate these curves are $k_x = 1 \times 10^{21}$ cm^2/sec, $k_y = 5 \times 10^{22}$ cm^2/sec, $V_{SW} = 450$ km/sec, and $\lambda = 0$. The longitudinal angle, ϕ, along the Archimedean spiral from the position of Earth to the intersection of the spiral with the radial line of Jupiter is plotted on the horizontal axis. Angles $\geq 360^\circ$ are for the second intersection along the spiral.

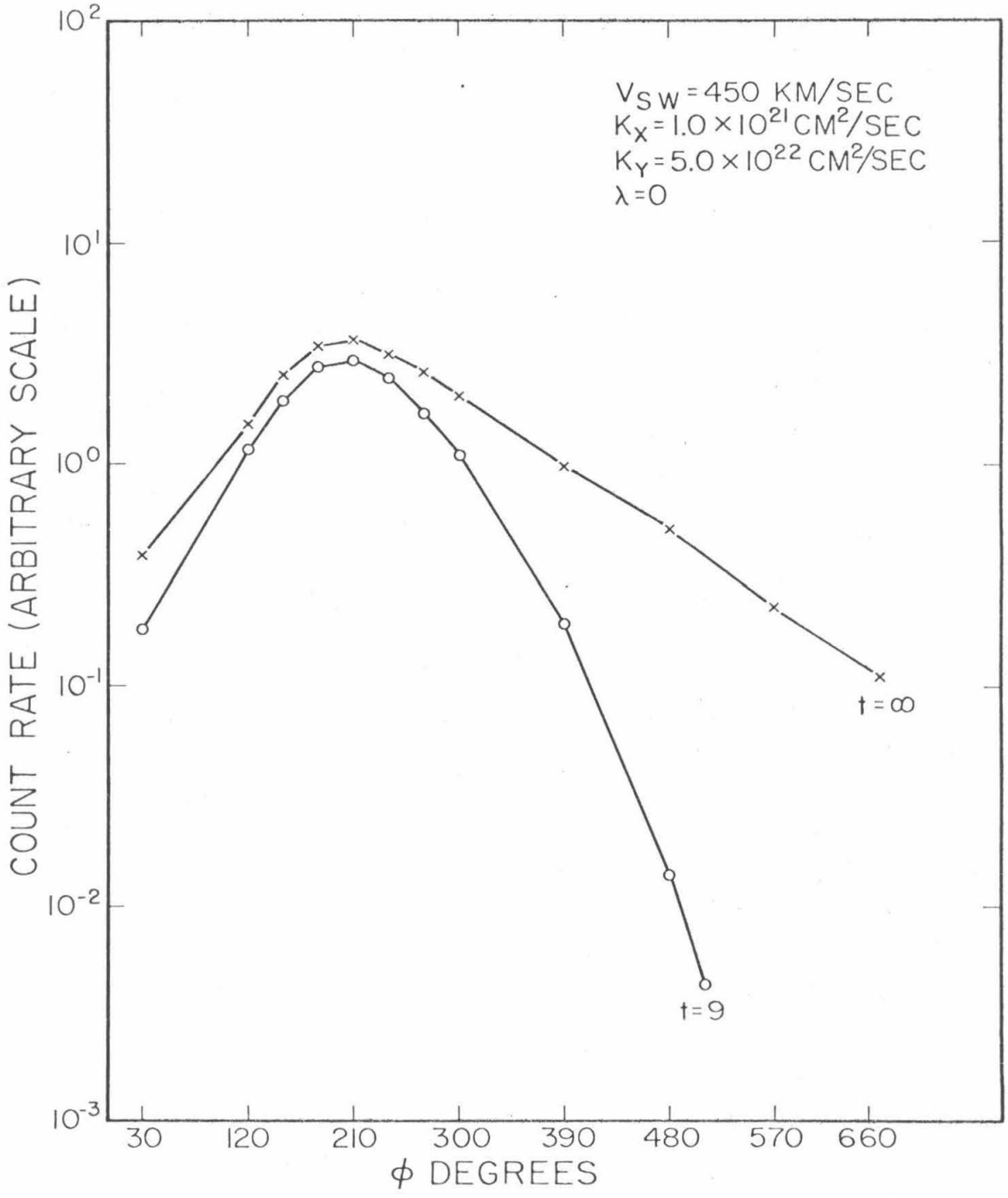
V_{SW} = 450 KM/SEC
$K_X = 1.0 \times 10^{21}$ CM²/SEC
$K_Y = 5.0 \times 10^{22}$ CM²/SEC
λ = 0
t = ∞
t = 9
COUNT RATE (ARBITRARY SCALE)
10²
10¹
10⁰
10⁻¹
10⁻²
10⁻³
30
120
210
300
390
480
570
660
φ DEGREES

Figure IV-8

Envelopes of the calculated electron flux at 1 AU over the synodic period for $t = \infty$. The format is identical to Figure IV-7. In Figure IV-8a the perpendicular diffusion coefficient, k_x, is varied which mainly affects the time period before the nominal connection time. In Figure IV-8b the parallel diffusion coefficient, k_y, is varied which mainly affects the time period after the nominal connection time.

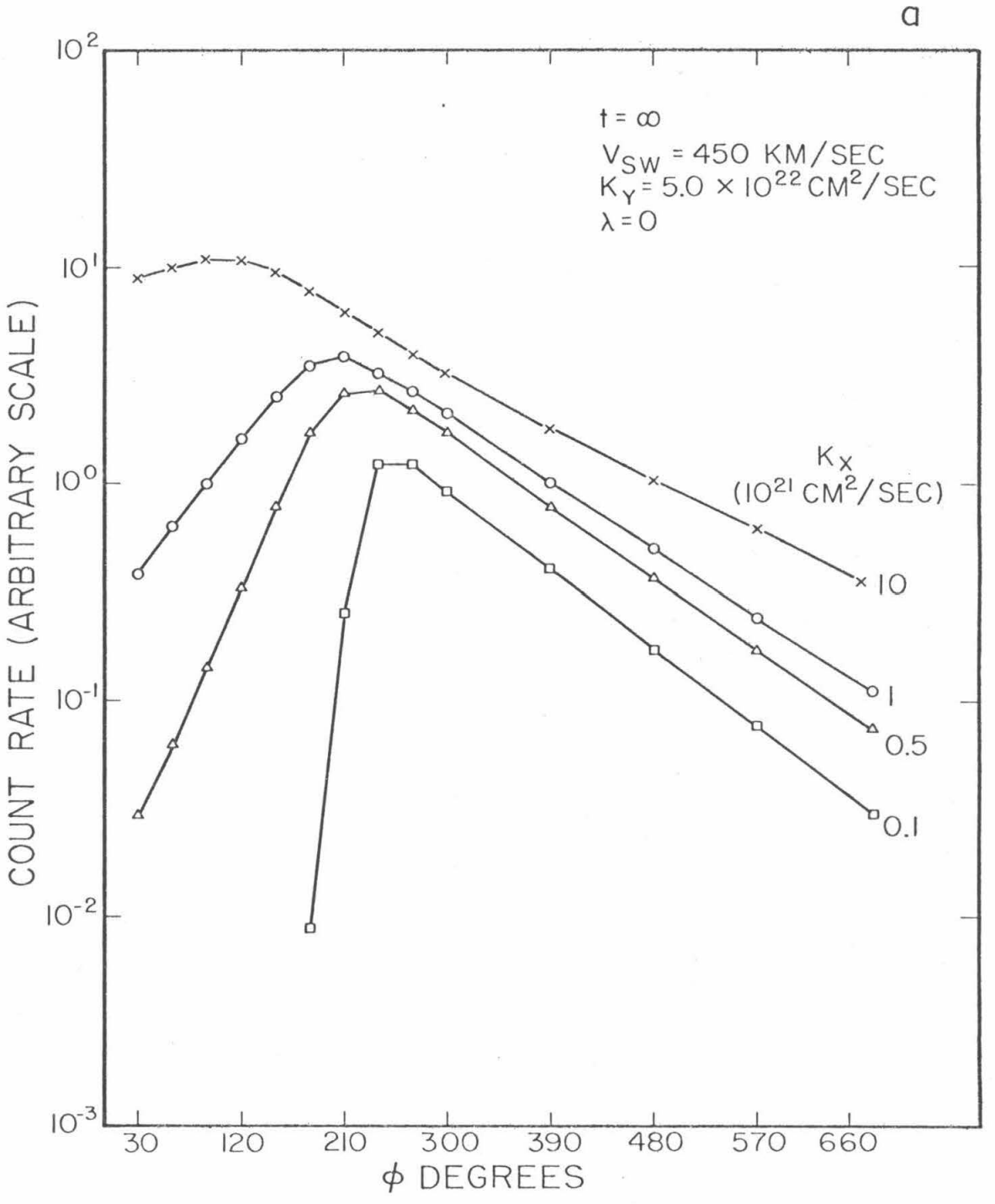
a
t = ∞
V_{SW} = 450 KM/SEC
K_Y = 5.0 × 10^{22} CM^2/SEC
λ = 0
K_X
(10^{21} CM^2/SEC)
10
1
0.5
0.1
COUNT RATE (ARBITRARY SCALE)
10^2
10^1
10^0
10^{-1}
10^{-2}
10^{-3}
30
120
210
300
390
480
570
660
φ DEGREES

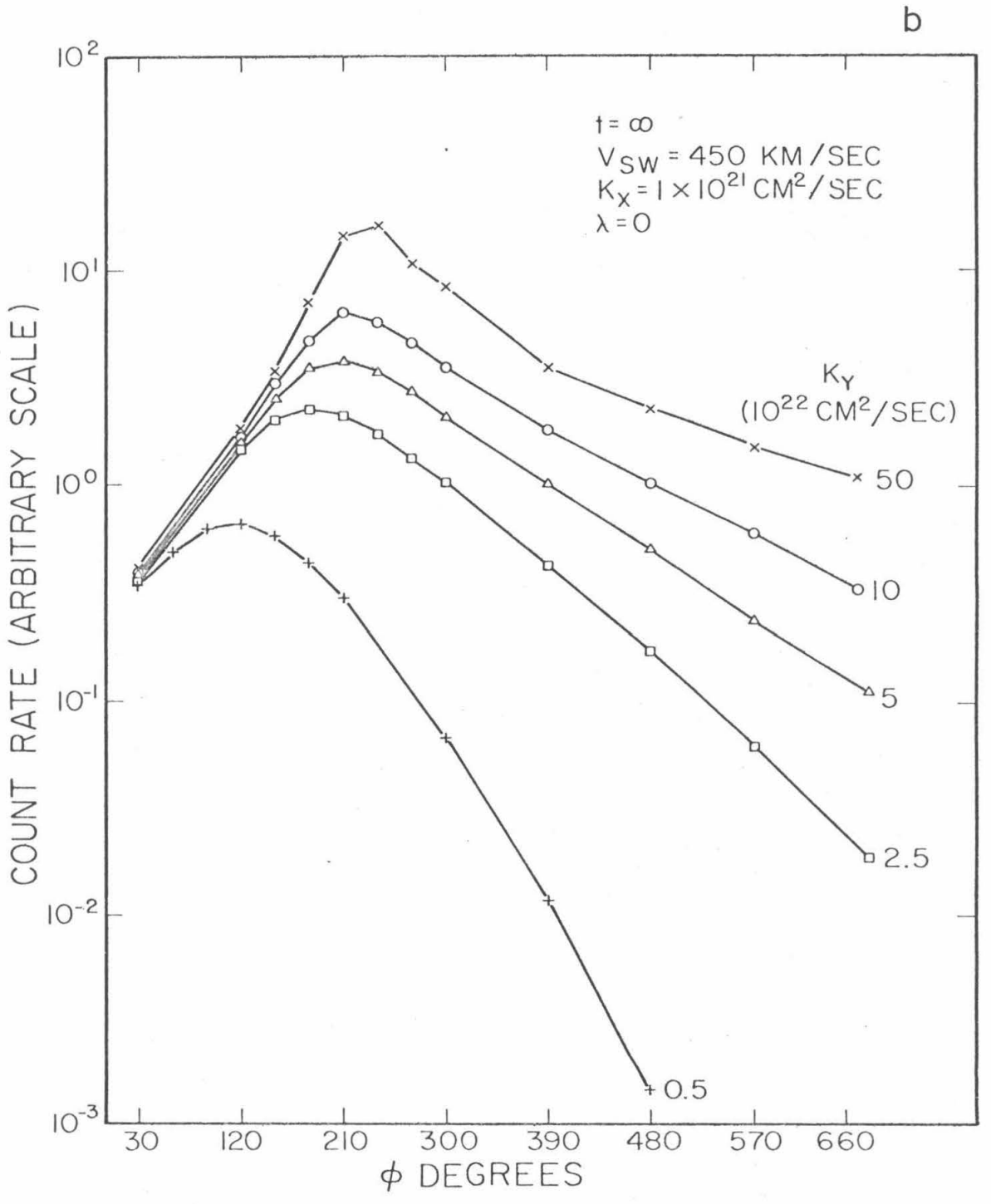
b
$t = \infty$
$V_{SW} = 450$ KM/SEC
$K_X = 1 \times 10^{21}$ CM^2/SEC
$\lambda = 0$
K_Y
(10^{22} CM^2/SEC)
50
10
5
2.5
0.5
COUNT RATE (ARBITRARY SCALE)
10^2
10^1
10^0
10^{-1}
10^{-2}
10^{-3}
30
120
210
300
390
480
570
660
ϕ DEGREES

Figure IV-9

Envelopes of the calculated electron flux at 1 AU over the synodic period for t = 9 days. The format is identical to Figure IV-7. In figure IV-9a the perpendicular diffusion coefficient, k_x, is varied which mainly affects the time period before the nominal connection time. In Figure IV-9b the parallel diffusion coefficient, k_y, is varied which mainly affects the time period after the nominal connection time.

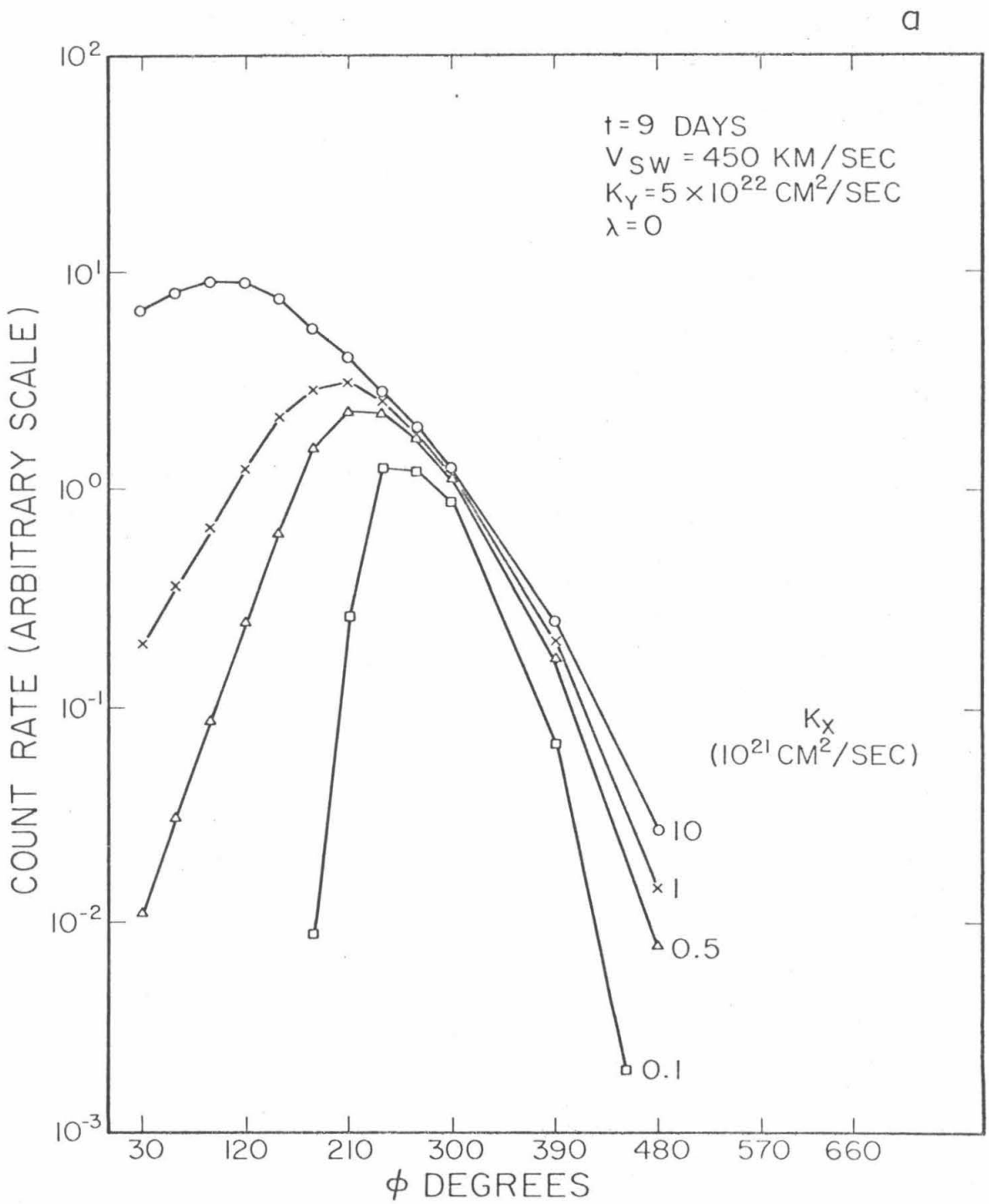
a
t = 9 DAYS
V_{SW} = 450 KM/SEC
$K_Y = 5 \times 10^{22}$ CM^2/SEC
λ = 0
COUNT RATE (ARBITRARY SCALE)
10^2
10^1
10^0
10^{-1}
10^{-2}
10^{-3}
30
120
210
300
390
480
570
660
φ DEGREES
K_X
(10^{21} CM^2/SEC)
10
1
0.5
0.1

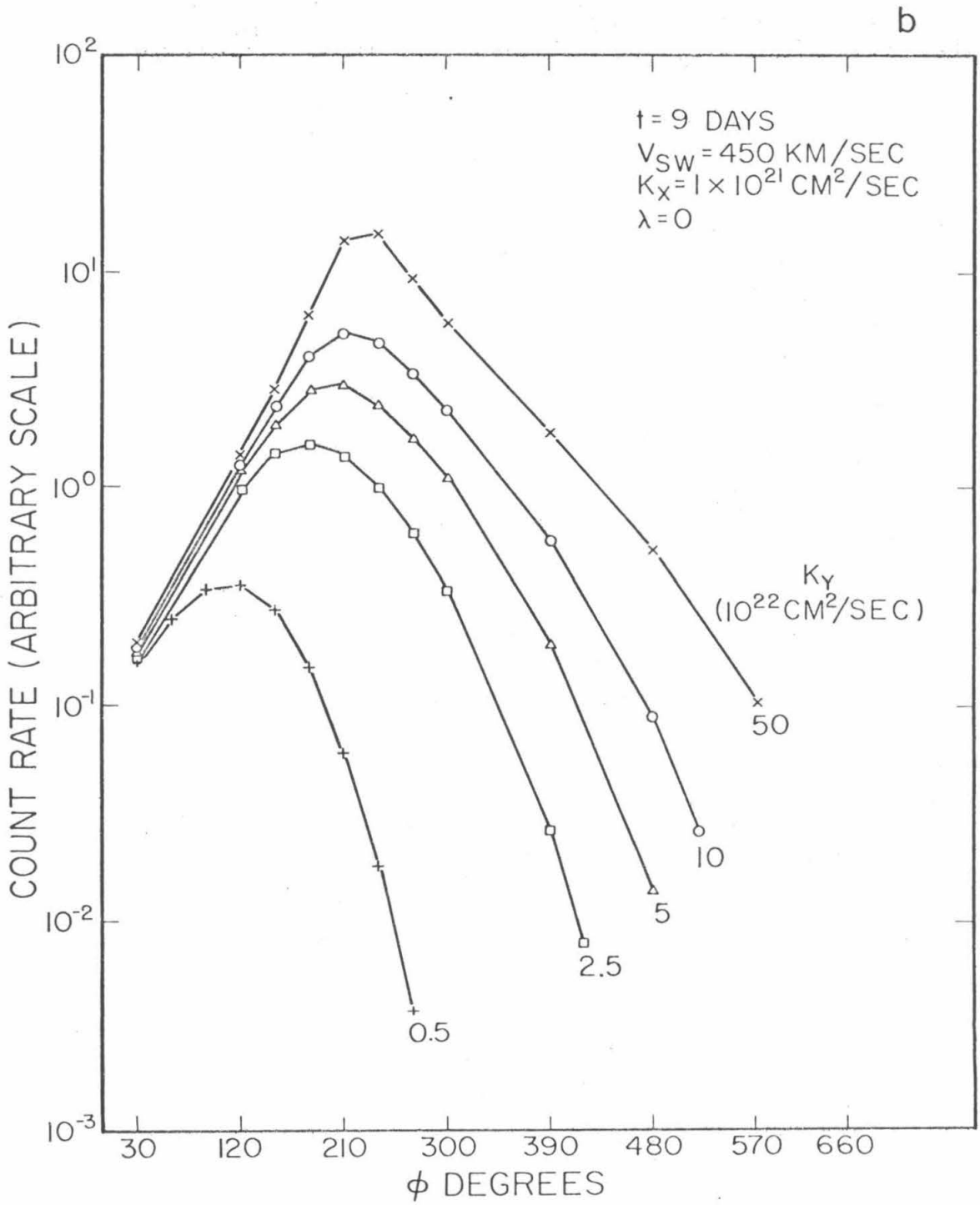
b
t = 9 DAYS
V_{SW} = 450 KM/SEC
$K_X = 1 \times 10^{21}$ CM²/SEC
λ = 0
K_Y
(10^{22} CM²/SEC)
50
10
5
2.5
0.5
COUNT RATE (ARBITRARY SCALE)
10^2
10^1
10^0
10^{-1}
10^{-2}
10^{-3}
30
120
210
300
390
480
570
660
φ DEGREES

envelope for t = ∞ predicted by the convection-diffusion model with k_x as a parameter and in Figure IV-8b with k_y as a parameter. In Figure IV-9a is the predicted synodic envelope for t = 9 days with k_x as a parameter and in Figure IV-9b with k_y as a parameter. Notice that in Figure IV-9 changes in k_x affect the shape of the envelope most for the time period before nominal connection and that changes in k_y affect the envelope shape for the time period after nominal connection. This suggests that we might be able to adjust both k_x and k_y together and produce a shape similar to that predicted by the "equilibrium number density" solution of the convection-diffusion model.

Figure IV-10 shows synodic envelopes for various choices of k_x and k_y. The dotted curve is the "equilibrium number density" envelope calculated from the convection-diffusion model. The synodic envelope at t = 9 days for $k_x = 5 \times 10^{21}$ cm^2/sec and $k_y = 5 \times 10^{23}$ cm^2/sec is similar in shape to the "equilibrium number density" envelope. However, the value of $k_y = 5 \times 10^{23}$ cm^2/sec gives a mean free path of $\lambda \approx \frac{3k_y}{c} \approx$ 3 AU which is too long for diffusion to be appropriate for particles propagating from Jupiter to Earth or Pioneer 11. So, even though it is possible to obtain an envelope shape similar to the observed envelope, the diffusion coefficients needed are not physically reasonable.

Using one time interval, here for example t = 9 days, to calculate a synodic envelope is also not reasonable since the

Figure IV-10

Envelopes of the calculated electron flux at 1 AU over the synodic period. The format is identical to Figure IV-7. The dotted curve shows the "equilibrium number density," or $t = \infty$, envelope. The solid curves show the envelope for t = 9 days for three choices of the diffusion coefficients. The envelope for $k_x = 5 \times 10^{21}$ cm^2/sec and $k_y = 50 \times 10^{22}$ cm^2/sec is similar in shape to the "equilibrium number density" envelope.

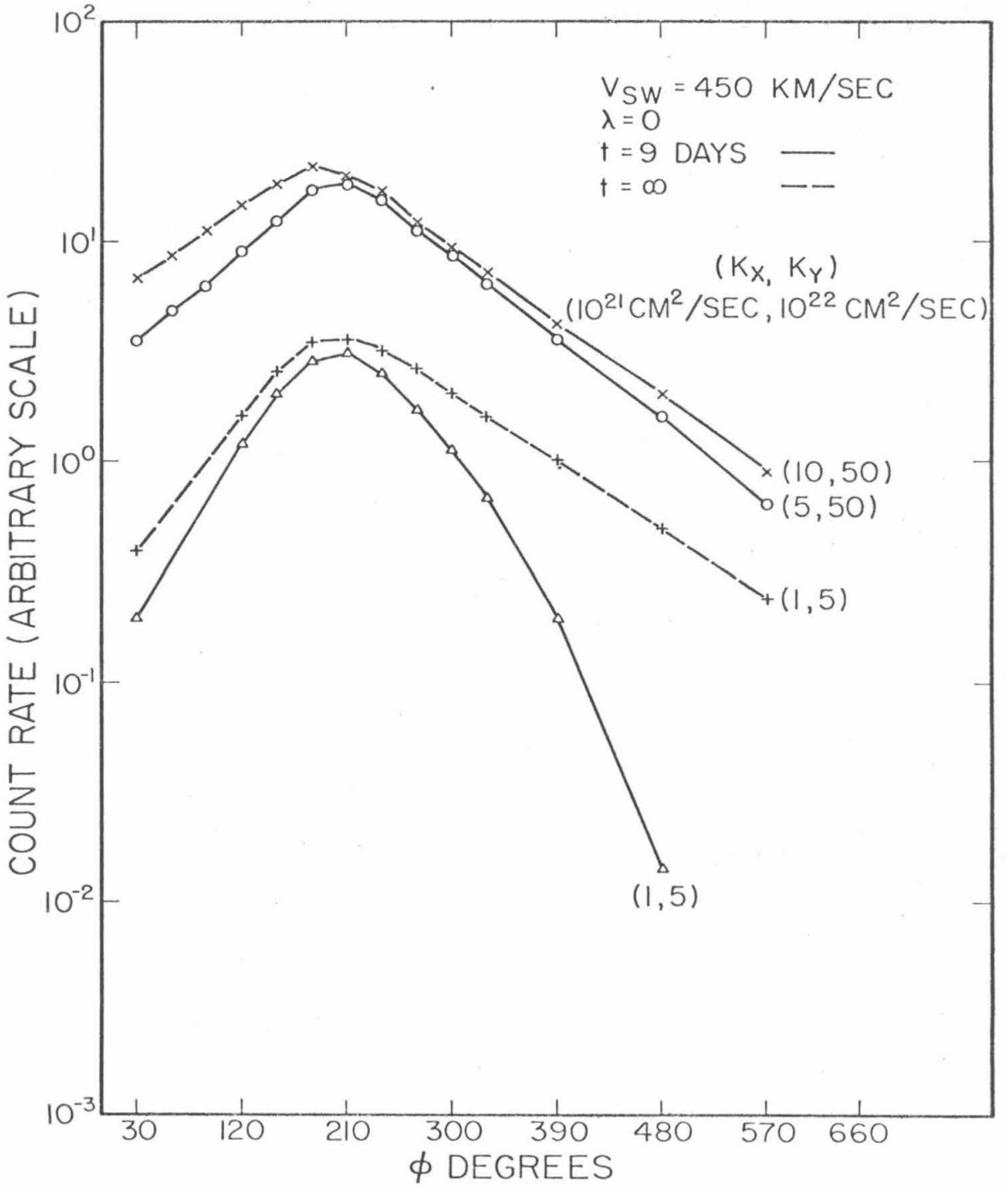
V_{SW} = 450 KM/SEC
λ = 0
t = 9 DAYS
t = ∞
(K_X, K_Y)
(10^{21} CM^2/SEC, 10^{22} CM^2/SEC)
(10,50)
(5,50)
(1,5)
(1,5)
COUNT RATE (ARBITRARY SCALE)
10^2
10^1
10^0
10^{-1}
10^{-2}
10^{-3}
30
120
210
300
390
480
570
660
φ DEGREES

time that the source has been filling the region with electrons varies systematically over the synodic period. Before the nominal connection time Earth will enter the region first and will see the whole rise time profile of an increase while after the nominal connection time Jupiter enters the region first and can spend a long time filling up the region until Earth enters the region when the CIR passes Earth. Also the rise profile of the increase may be cut off by a barrier passing Earth or Jupiter. These two processes give a variation in the maximum flux reached in an increase and must be modeled when calculating a synodic envelope to fit to the observed Jovian increases. Finally, the technique of fitting a calculated envelope to the Jovian increases at 1 AU is biased toward fitting only the large increases or those that have had a long time to reach their maximum values. The envelope fit is therefore very sensitive to a large increase early or late in the synodic period as can be seen in Figures IV-8 and IV-9 which show that the largest variations in the envelopes occur early or late in the synodic period.

As noted earlier the synodic periods for 1973, 1974, and 1977 have relatively fewer Jovian increases in the before nominal connection time period. The occurrence of fewer increases during this time period remains to be explained, perhaps by always having a barrier to electron propagation separating Earth and Jupiter.

IV-D-2. Rise Time Profiles

As discussed in the previous section the characteristics of the interplanetary medium and the relative positions of Earth, Jupiter, and CIR's need to be known or modeled for each individual increase in order to construct a synodic envelope calculated from the convection-diffusion propagation model. It is appropriate then to fit individual Jovian increases at 1 AU to the rise profiles predicted by the convection-diffusion model. In this section three individual increases in the electron flux at 1 AU will be fit with rise profiles calculated from the convection-diffusion model and a range of values for the diffusion coefficients determined from these fits.

Values for the diffusion coefficients have been reported and discussed by Chenette, et al. (1974), Pyle and Simpson (1977), and Conlon (1978). The Pioneer 10 pre-encounter envelope of the Jovian increase maxima was compared to the predicted $|x|^{-1} \exp\left(\frac{xV}{k_x}x\right)$ behavior of the convection-diffusion model to determine a value of k_x. Note that the ratio (V_x/k_x) is determined by this process and in order to determine k_x a value of V_x must be chosen by another means. This determination was done in the region near Jupiter where the y coordinate was close to zero, that is during the time period that the Pioneer 10 spacecraft was approaching Jupiter in a direction perpendicular to the average spiral

magnetic field line.

The numbers determined in this way were reported as V_x = 400 km/sec and $k_x \geq 5 \times 10^{20}$ cm^2/sec. The lower limit was quoted since the data were also consistent with $k_x = \infty$. These values were used by Conlon (1978) "for the purpose of illustration only" in fitting predicted rise time profiles to selected Pioneer 11 pre-encounter Jovian increases. The increases were within ~1.2 AU of Jupiter and the fits were sensitive only to the k_x diffusion coefficient since the y coordinate was close to zero. This pre-encounter period of Pioneer 11 corresponds to the time period before the nominal connection time at 1 AU.

Similar fits of the rise time profiles predicted by the convection-diffusion model to Jovian increases observed at 1 AU are reported here. Since the y coordinate is not close to zero, fits to the observed increases at 1 AU can give information on both the k_x and k_y diffusion coefficients. In the coordinate system used here for the convection-diffusion model k_x is the perpendicular diffusion coefficient and k_y is the parallel diffusion coefficient. Remember that some of the assumptions of the convection-diffusion model, such as the Cartesian coordinate system, are not met when the model is used to predict the inward propagation of electrons to 1 AU. These parametric fits then are only illustrative of the possible variations in the physical parameters

k_x, k_y, and V_{SW} needed to fit three examples of Jovian increases at 1 AU.

Of the three increases fit with predicted rise time profiles, the two starting at 73.344.06 and 73.361.12 were before the nominal connection time. The third increase at 74.072.12 was near the nominal connection time for V_{SW} = 500 km/sec at 74.064. For brevity the hours will be dropped and these increases will be referred to by their year and day-of-year numbers. These three increases were chosen because they did not have data gaps and the CIR passage times at Jupiter were known. Figure IV-11 shows these three increases with an example of a predicted rise time profile. The vertical line is the time that the rear of the CIR passed Jupiter. The fit was done for the time interval indicated by the hatched box which included the rise time profile of the electron increase. The dotted line is an example of a predicted rise time profile fit to each increase in Figure IV-11 with the parameters as shown in each plot. In each case the region of space bounded by CIR's was assumed empty of electrons until the CIR passed Jupiter. After the CIR passed Jupiter the predicted rise time profile was calculated and like the fits of Conlon (1978) the only free parameter was the vertical scale.

The time of the maximum for the |B| enhancement, $|B|_{MAX}$, is also indicated in these plots. The time of $|B|_{MAX}$ for the increase at 73.344 is 18 hours before the predicted profile

Figure IV-11

Examples of the fits of the predicted rise time profiles calculated from the convection-diffusion model of electron propagation for Jovian electron increases at 1 AU. Figure IV-11a is a fit to the Jovian increase at 73.344, Figure IV-11b a fit to the increase at 73.361, and Figure IV-11c to the increase at 74.072. The electron flux is in counts/sec, the data are for six-hour averages and the error bars are the 1σ error estimates. The vertical line at the left in each plot indicates when the rear of the CIR passed Jupiter. The arrow indicates the six-hour interval for the time of $|B|_{MAX}$. The dotted curve is the rise time profile calculated from the convection-diffusion model using the values of ϕ , V_{SW}, k_x, and k_y as shown in each plot. The increases were fit to the six-hour averages for the interval indicated by the hatched box with the goodness of fit, χ^2_ν , as shown calculated for these fitted data points.

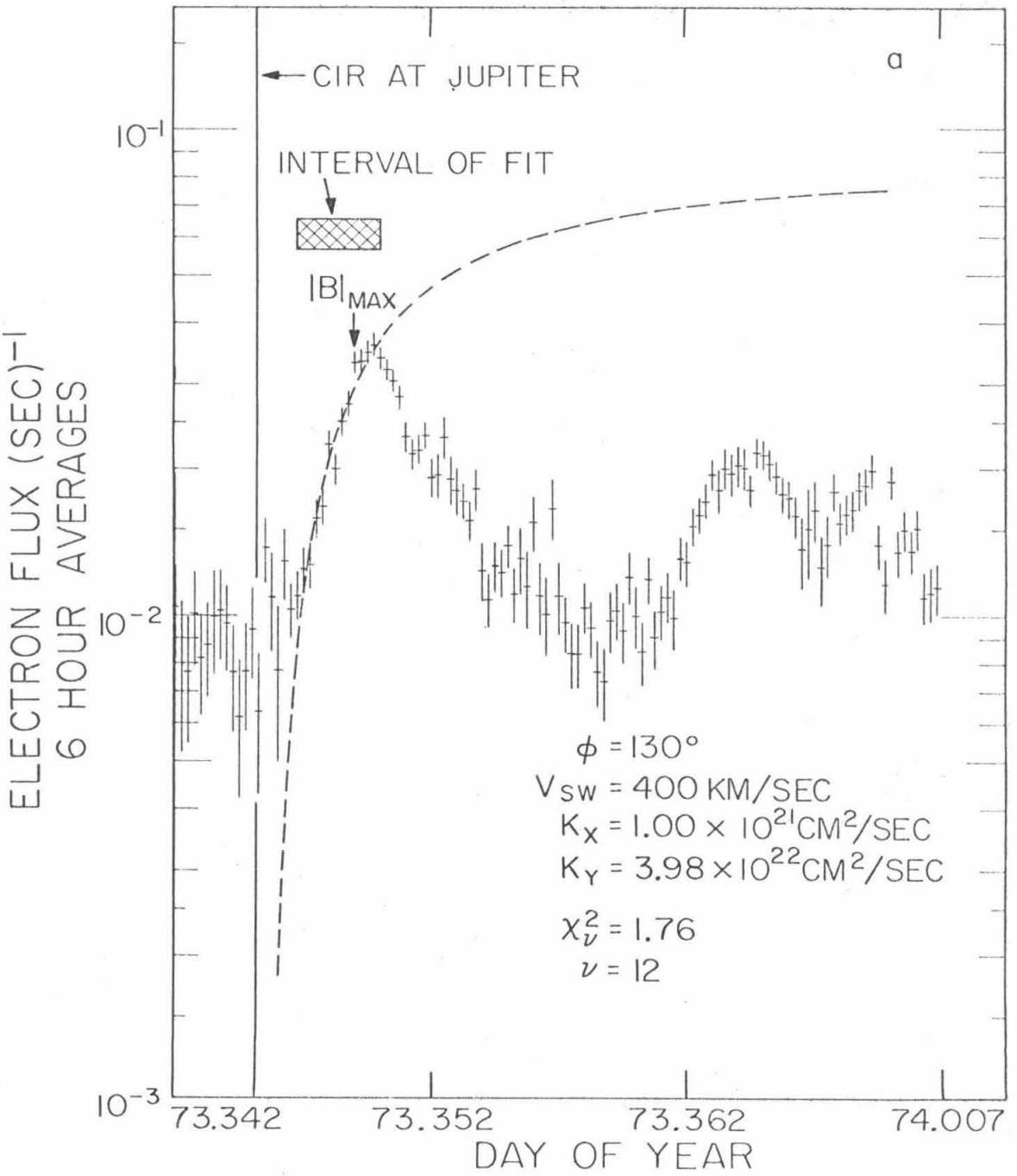
CIR AT JUPITER
a
INTERVAL OF FIT
|B|MAX
10-1
10-2
10-3
ELECTRON FLUX (SEC)-1
6 HOUR AVERAGES
φ = 130°
VSW = 400 KM/SEC
KX = 1.00 × 10^21 CM^2/SEC
KY = 3.98 × 10^22 CM^2/SEC
χ^2_ν = 1.76
ν = 12
73.342
73.352
73.362
74.007
DAY OF YEAR

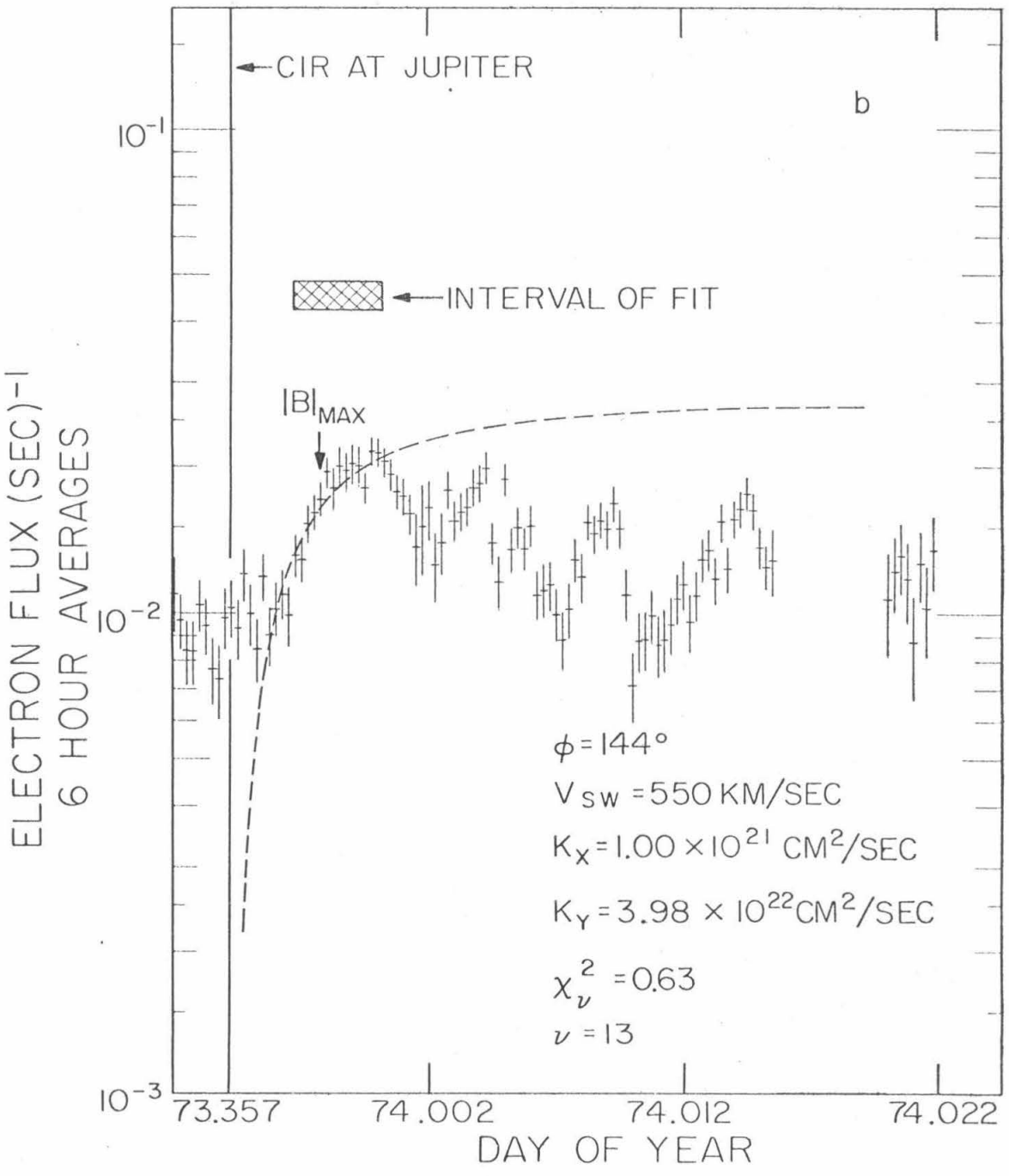
CIR AT JUPITER
b
INTERVAL OF FIT
|B|MAX
ELECTRON FLUX (SEC)-1
6 HOUR AVERAGES
10-1
10-2
10-3
73.357
74.002
74.012
74.022
DAY OF YEAR
φ = 144°
VSW = 550 KM/SEC
KX = 1.00 × 10^21 CM^2/SEC
KY = 3.98 × 10^22 CM^2/SEC
χν^2 = 0.63
ν = 13

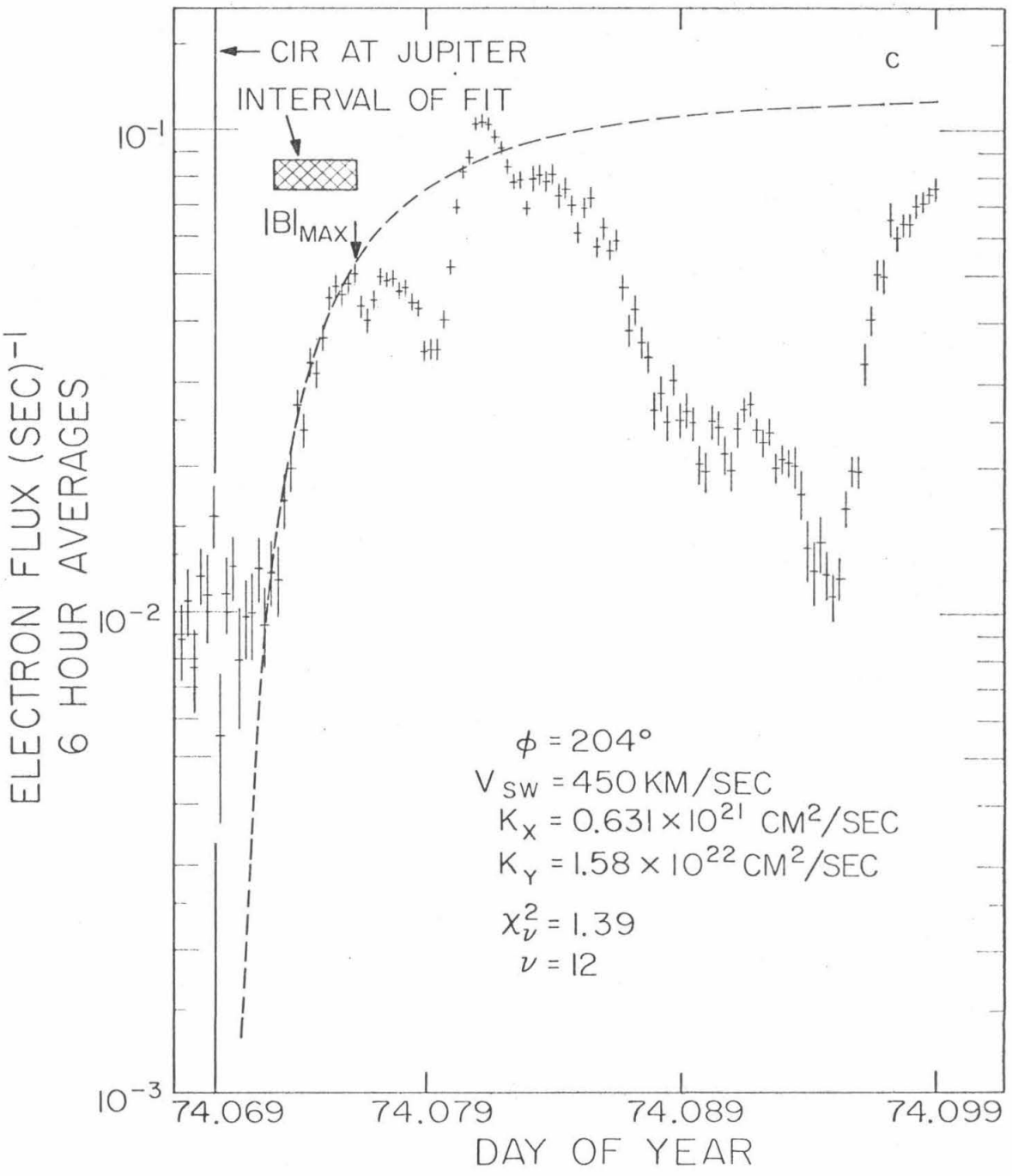
CIR AT JUPITER
INTERVAL OF FIT
|B|MAX
c
ELECTRON FLUX (SEC)⁻¹
6 HOUR AVERAGES
10⁻¹
10⁻²
10⁻³
74.069
74.079
74.089
74.099
DAY OF YEAR
φ = 204°
V SW = 450 KM/SEC
K X = 0.631 × 10²¹ CM²/SEC
K Y = 1.58 × 10²² CM²/SEC
χ²ν = 1.39
ν = 12

deviates from the data. For the increase at 73.361 the time of $|B|_{MAX}$ is ~2 days before the predicted profile deviates from the data. In this particular case a slope change occurred at the time of $|B|_{MAX}$. For the increase at 74.072, the time of the $|B|_{MAX}$ occurred at the time that the predicted profile deviates from the data. This points up the close association found earlier between $|B|_{MAX}$ and the increases at 1 AU.

The two increases at 73.344 and 73.361 are in the before nominal connection time period discussed in Figure IV-5. In this time period Earth is in the region before Jupiter and an increase is seen at Earth after a CIR passes Jupiter. These two increases occurred in the time period corresponding to the times of the three increases fit by Conlon in the pre-encounter period of Pioneer 11. During this period the fit should be sensitive to both k_x and k_y. The two increases should show a difference in only k_x because the y coordinate is essentially the same for the two increases.

The increase at 74.072 occurs around the nominal connection time when a CIR would pass Earth and Jupiter at about the same time. During this period the x coordinate is close to zero so the fit should be sensitive only to k_y.

In Figure IV-12 the goodness of fit, χ^2_ν, is plotted versus the solar wind speed, V_{SW}, for four choices of k_x and k_y. In

Figure IV-12

Plots of the goodness of fit, χ^2_ν, versus the solar wind speed, V_{SW}, for four choices of the diffusion coefficients, k_x and k_y. Figure IV-12a is for the increase at 73.344 which was fit for V_{SW} = 400 km/sec, Figure IV-12b for the increase at 73.361 which was fit for V_{SW} = 550 km/sec, and Figure IV-12c for the increase at 74.072 which was fit for V_{SW} = 450 km/sec.

a

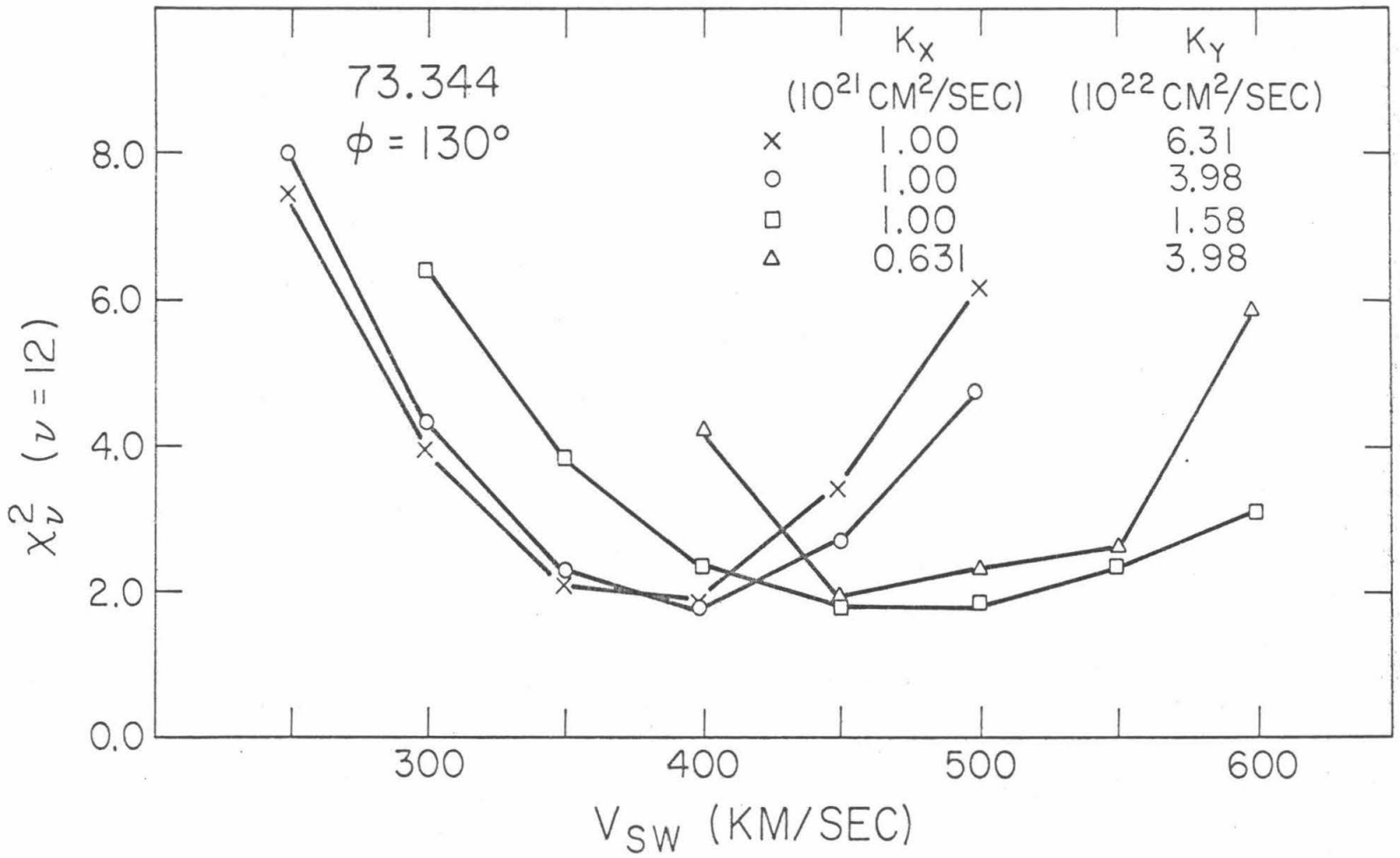
73.344
ϕ = 130°
K_X (10^{21} CM^2/SEC)
K_Y (10^{22} CM^2/SEC)
× 1.00 6.31
○ 1.00 3.98
□ 1.00 1.58
△ 0.631 3.98
χ^2_ν (ν = 12)
8.0
6.0
4.0
2.0
0.0
300
400
500
600
V_{SW} (KM/SEC)

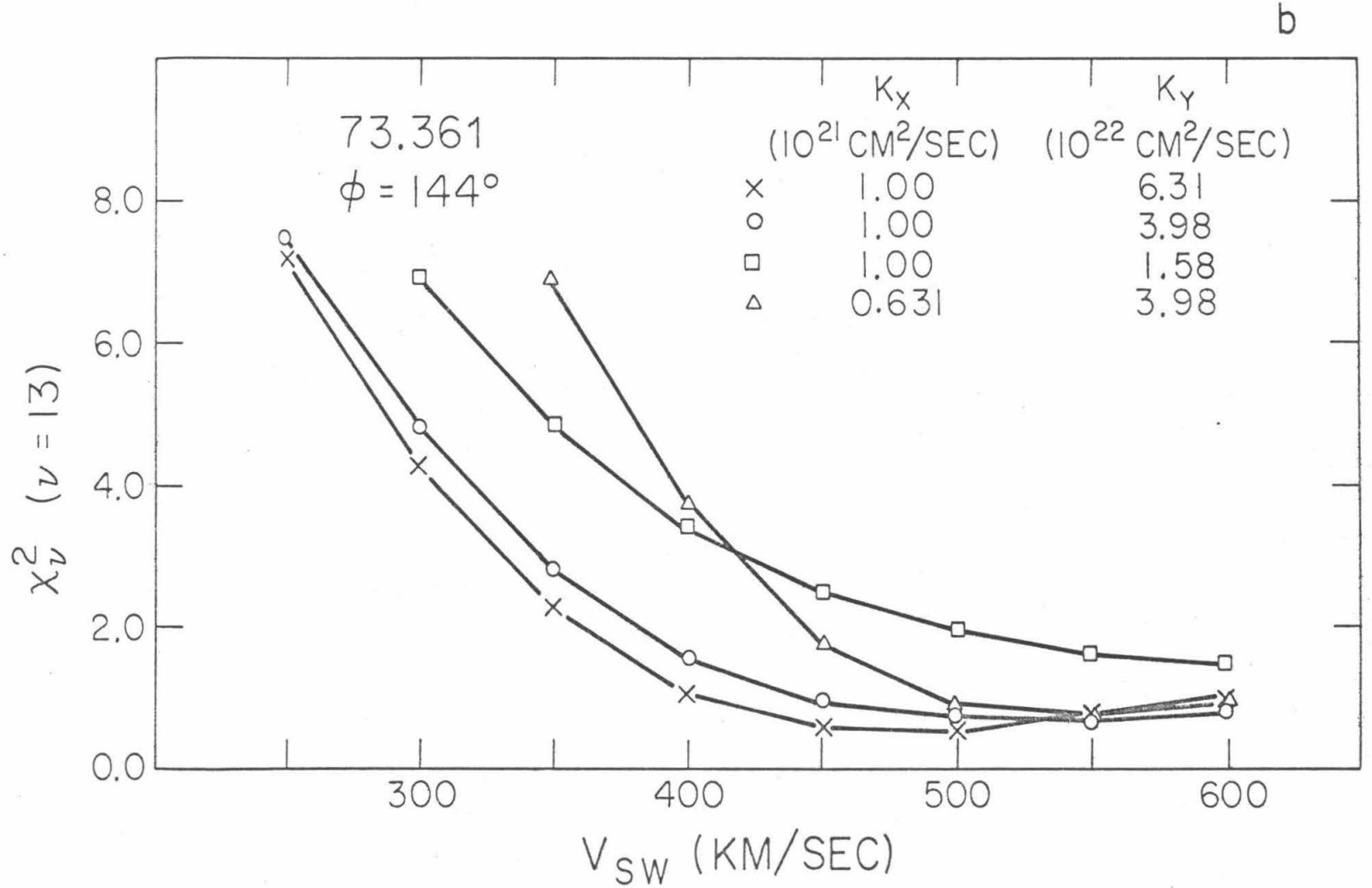
b
73.361
ϕ = 144°
K_X (10^{21} CM^2/SEC)
K_Y (10^{22} CM^2/SEC)
× 1.00 6.31
○ 1.00 3.98
□ 1.00 1.58
△ 0.631 3.98
χ^2_ν (ν = 13)
8.0
6.0
4.0
2.0
0.0
300
400
500
600
V_{SW} (KM/SEC)

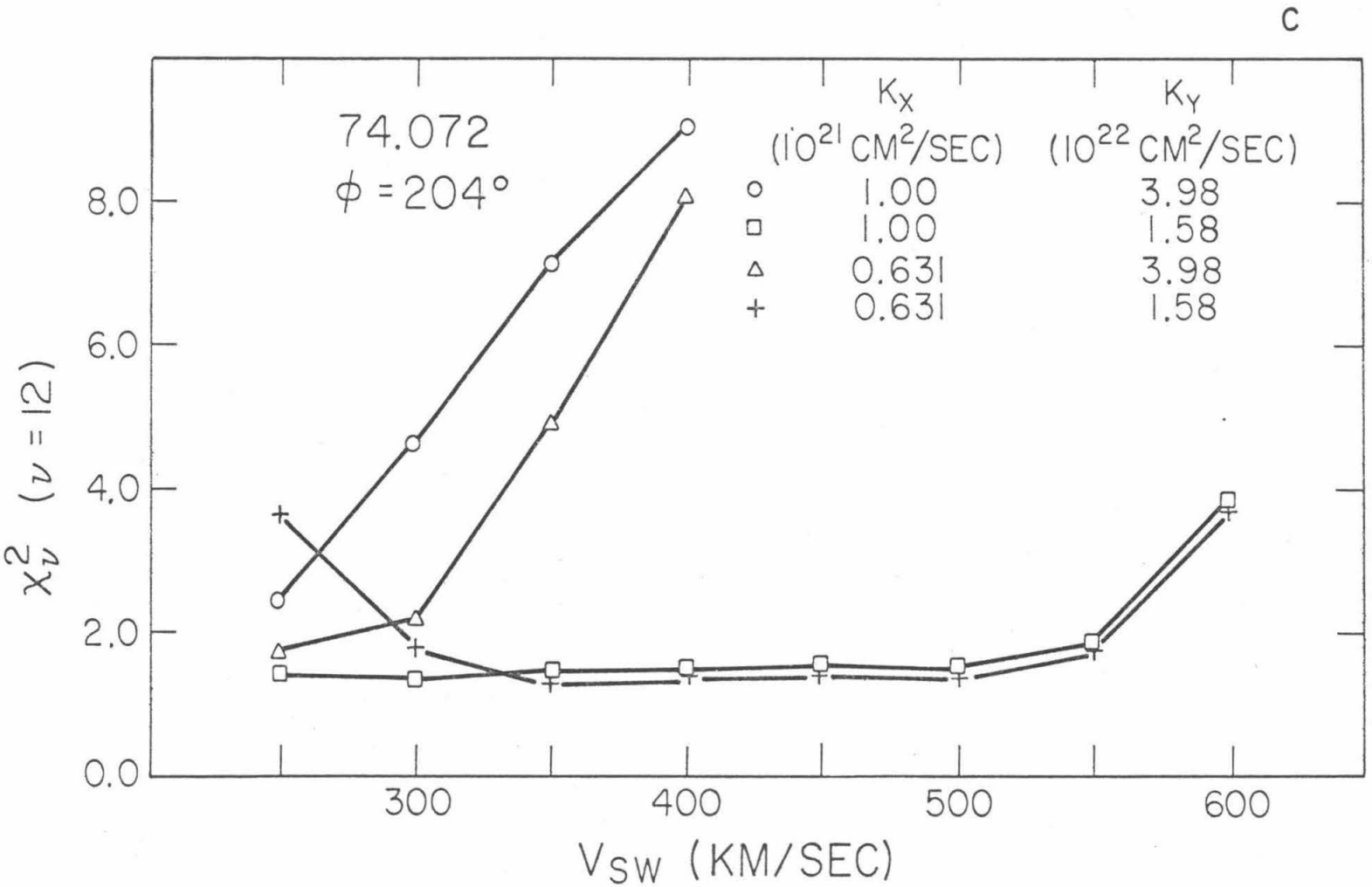
c
74.072
ϕ = 204°
K_X (10^{21} CM^2/SEC)
K_Y (10^{22} CM^2/SEC)
1.00 3.98
1.00 1.58
0.631 3.98
0.631 1.58
χ^2_ν (ν = 12)
0.0
2.0
4.0
6.0
8.0
300
400
500
600
V_{SW} (KM/SEC)

Table IV-5 matrices of χ^2_ν as a function of k_x and k_y are given for each increase for the choice of V_{SW} used in the examples of fits in Figure IV-11. This V_{SW} was chosen to be near a local minimum in the plots of Figure IV-12 and to be representative of the actual V_{SW} for each increase as shown in the solar wind speed plot in Figure IV-4. Even though V_{SW} is not constant during an increase, the variations do not significantly affect the fits.

For the increase at 73.344 the solar wind speed during the interval of fit varies between 360 - 440 km/sec which is at a local minimum in Figure IV-12a for two sets of diffusion coefficients and is near the minimum of ~450 km/sec for the other two sets. The choice of V_{SW} = 400 km/sec is then consistent with the possible range of V_{SW} given by the fit and the actual V_{SW}. The matrix in Table IV-5a shows a band of values for k_x and k_y that have reasonable fits to the data.

Table IV-5

Matrices of the goodness of fit, χ^2_ν , for the three Jovian increases fit in Figure IV-11 as a function of both k_x and k_y. Table IV-5a is for the increase at 73.344 with V_{SW} = 400 km/sec, Table IV-5b for the increase at 73.361 with V_{SW} = 550 km/sec, and Table IV-5c for the increase at 74.072 with V_{SW} = 450 km/sec. The k_x scale is at the left with the values in units of 10^{21} cm^2/sec. The k_y scale is at the top with values in units of 10^{22} cm^2/sec. The diagonal stepped line is the calculated upper limit to the ratio of the diffusion coefficients with $k_x/k_y \leq 0.26$. The possible choices of the diffusion coefficients are restricted by this upper limit and are above the line.

Table IV-5a

Matrix of χ^2_ν For Fit

73.344 $\phi = 130^\circ$ V_{SW} = 400 km/sec

k_x (10^{21}cm^2/sec)	k_y (10^{22}cm^2/sec) 0.5	0.6	0.8	1.0	1.3	1.6	2.0	2.5	3.2	4.
0.10	105.1	102.7	100.7	99.1	97.8	96.8	95.9	95.2	94.8	94.3
0.16	76.5	73.2	70.5	68.3	66.6	65.2	64.0	63.1	62.4	61.8
0.25	52.1	48.0	44.6	41.9	39.7	38.0	36.6	35.5	34.6	33.9
0.4	33.5	28.9	25.3	22.4	20.1	18.3	16.9	15.8	15.0	14.3
0.6	20.7	16.2	12.8	10.2	8.3	6.9	5.9	5.1	4.6	4.1
1.0	12.9	8.8	6.0	4.1	3.0	2.3	2.0	1.8	1.7	1.8
1.6	8.3	5.0	3.0	2.0	1.7	1.9	2.3	2.7	3.3	3.8
2.5	5.8	3.1	2.0	1.7	2.3	3.2	4.3	5.3	6.4	7.4
4.	4.5	2.3	1.7	2.2	3.4	4.8	6.5	8.1	9.6	10.9
6.	3.7	1.9	1.8	2.8	4.4	6.3	8.4	10.3	12.1	13.8
10.	3.3	1.8	2.0	3.3	5.2	7.5	9.8	12.0	14.0	15.9

Table IV-5b

Matrix of χ^2_ν For Fit

73.361 $\quad \phi = 144^\circ \quad V_{SW} = 550$ km/sec

k_x (10^{21}cm^2/sec)	k_y (10^{22}cm^2/sec)									
	0.5	0.6	0.8	1.0	1.3	1.6	2.0	2.5	3.2	4.
0.10	14.0	9.9	7.0	5.0	3.7	2.8	2.1	1.7	1.4	1.2
0.16	15.0	10.4	7.1	4.9	3.4	2.4	1.7	1.3	1.1	0.9
0.25	15.7	10.7	7.1	4.7	3.1	2.1	1.4	1.0	0.8	0.7
0.4	16.2	10.9	7.1	4.5	2.8	1.8	1.2	0.9	0.7	0.6
0.6	16.5	10.9	7.0	4.3	2.6	1.6	1.0	0.7	0.6	0.6
1.0	16.6	11.0	6.9	4.2	2.5	1.5	0.9	0.7	0.6	0.6
1.6	16.7	11.0	6.9	4.1	2.4	1.4	0.9	0.7	0.6	0.7
2.5	16.8	11.0	6.9	4.1	2.4	1.4	0.8	0.6	0.6	0.7
4.	16.9	11.0	6.8	4.0	2.3	1.3	0.8	0.6	0.6	0.8
6.	16.9	11.0	6.8	4.0	2.3	1.3	0.8	0.6	0.7	0.8
10.	16.9	11.0	6.8	4.0	2.3	1.3	0.8	0.6	0.7	0.8

Table IV-5c

Matrix of χ^2_ν For Fit

74.072 $\quad \phi = 204^\circ \quad V_{SW} = 450$ km/sec

k_x (10^{21}cm^2/sec)	k_y (10^{22}cm^2/sec)									
	0.5	0.6	0.8	1.0	1.3	1.6	2.0	2.5	3.2	4.
0.10	22.2	11.1	4.5	1.6	1.5	3.0	5.5	8.2	10.8	13.2
0.16	27.7	15.2	7.0	2.6	1.3	2.0	4.0	6.5	9.2	11.8
0.25	31.6	18.3	9.1	3.7	1.5	1.6	3.2	5.5	8.2	10.8
0.4	34.2	20.5	10.6	4.6	1.8	1.4	2.8	4.9	7.6	10.2
0.6	35.9	21.9	11.7	5.2	2.0	1.4	2.5	4.6	7.2	9.9
1.0	37.0	22.8	12.4	5.6	2.2	1.4	2.4	4.4	6.9	9.7
1.6	37.7	23.4	12.8	5.9	2.3	1.4	2.3	4.2	6.8	9.5
2.5	38.2	23.8	13.1	6.1	2.4	1.4	2.2	4.1	6.7	9.5
4.	38.5	24.0	13.3	6.2	2.5	1.4	2.2	4.1	6.6	9.4
6.	38.6	24.2	13.4	6.3	2.5	1.4	2.2	4.1	6.6	9.4
10.	38.7	24.3	13.5	6.4	2.6	1.4	2.2	4.0	6.6	9.3

From a treatment of cosmic ray diffusion theory by Forman (1977), the ratio of k_x/k_y can be used to further restrict the possible values of k_x and k_y. Forman finds that the upper limit on the ratio of the diffusion coefficients is

$$\frac{k_x}{k_y} < \frac{\langle \Delta B_x^2 \rangle}{B_o^2} \qquad \text{IV-1}$$

where $\langle \Delta B_x^2 \rangle$ is the mean square average of the changes in the perpendicular magnetic field and B_o is the average magnetic field (Forman, 1977). Forman used the velocity correlation function to show that the ratio has this upper limit.

To obtain an estimate of this ratio the data from Tsurutani and Smith (1979) on magnetic field discontinuities was used. They find that the probability of seeing a vector field change of $|\Delta \vec{B}|/B_o$ at 1 AU is given by

$$P\left(\frac{|\Delta \vec{B}|}{B_o}\right) = 2.8 \cdot EXP\left[-\frac{\left(|\Delta \vec{B}|/B_o\right)}{0.36}\right] \qquad \text{IV-2}$$

where $|\Delta \vec{B}| = (\Delta B_x^2 + \Delta B_y^2 + \Delta B_z^2)^{1/2}$ and B_o is the larger of the field magnitudes on either side of the discontinuity. Even though Equation IV-2 applies to discontinuities it should provide an upper limit to the ratio in Equation IV-1 since most of the magnetic field changes are much smaller than the discontinuities

studied by Tsurutani and Smith. Since the upper limit is being calculated $|\Delta \vec{B}|$ can be assumed to be entirely due to ΔB_x so that

$$\frac{\Delta B_x^2}{B_o^2} \leq \frac{|\Delta \vec{B}|^2}{B_o^2} \qquad \text{IV-3}$$

The definition of $\frac{\langle \Delta B_x^2 \rangle}{B_o^2}$ is

$$\frac{\langle \Delta B_x^2 \rangle}{B_o^2} = \int_0^\infty p\left(\frac{\Delta B_x}{B_o}\right) \cdot \left(\frac{\Delta B_x^2}{B_o^2}\right) \cdot d\left(\frac{\Delta B_x}{B_o}\right) \qquad \text{IV-4}$$

which using Equation IV-3 becomes

$$\frac{\langle \Delta B_x^2 \rangle}{B_o^2} \leq \int_0^\infty p\left(\frac{|\Delta \vec{B}|}{B_o}\right) \cdot \left(\frac{|\Delta \vec{B}|^2}{B_o^2}\right) \cdot d\left(\frac{|\Delta \vec{B}|}{B_o}\right) \qquad \text{IV-5}$$

and using Equation IV-2 and integrating yields

$$\frac{k_x}{k_y} < \frac{\langle \Delta B_x^2 \rangle}{B_o^2} \leq 0.26$$

This value is similar to the values published by Rosenberg, et al. (1978) who give the radial dependence of the ratio as

$$\frac{\sigma_c^2}{\langle B \rangle^2} = (0.35 \pm 0.05) \cdot R^{-0.48 \pm 0.10}$$

where σ_c^2 is the composite variance $\sigma_c^2 = \sum (\sigma(B_i))^2$ and R is the radial distance in AU and by Belcher and Davis (1971) where the

amplitude ratio is given as 0.31.

This upper limit for the ratio of the diffusion coefficients is plotted in the matrices of Table IV-5 as the diagonal stepped line. This line is the upper limit with choices of k_x and k_y restricted to the upper part of the matrix. For the fit of the increase at 73.344 the choices of diffusion coefficients are limited to $k_x \approx 1.0 - 2.5 \times 10^{21}$ cm^2/sec and $k_y \gtrsim 0.8 \times 10^{22}$ cm^2/sec. The choice of k_x and k_y for the example of the fit shown in Figure IV-11a is within this range.

The fit of the increase at 73.361 follows a pattern similar to the increase at 73.344. Figure IV-12b shows a minimum in V_{SW} around V_{SW} = 500 - 550 km/sec and Figure IV-4 shows the actual $V_{SW} \approx 400 - 550$ km/sec during the rise time profile. The matrix in Table IV-5b shows, like the increase at 73.344, an indication of a band with $k_x \lesssim 6. \times 10^{21}$ cm^2/sec and $k_y \gtrsim 1.6 \times 10^{22}$ cm^2/sec within the $k_x/k_y < 0.26$ upper limit. The choice of k_x and k_y in Figure IV-11b is within these limits.

For these two increases the fits produce consistent choices of the diffusion coefficients. Looking at Figure IV-11a and Figure IV-11b neither increase reaches the equilibrium value though the increase at 73.361 is within about 80 percent of equilibrium in this example. This supports using a value at a

time earlier than when the equilibrium value is reached to form the synodic period envelopes discussed earlier.

The third increase at 74.072 shows a different characteristic in the fit than the two increases discussed above. In Figure IV-12c there is a minimum near V_{SW} = 300 - 550 km/sec but for a slightly lower value of k_y than for the other two increases. This range in V_{SW} includes the actual variation of $V_{SW} \approx$ 400 - 600 km/sec shown in Figure IV-4. The matrix of χ^2_ν in Table IV-5c has a band with reasonable fits for $k_x \lesssim 4. \times 10^{21}$ cm^2/sec and $k_y \approx 1.0 - 2.0 \times 10^{22}$ cm^2/sec.

This is consistent with the fit being only dependent on the k_y parameter since the x coordinate is close to zero during this time period around nominal connection. The ratio k_x/k_y limits k_x to $\lesssim 4. \times 10^{21}$ cm^2/sec but does not affect k_y. The choice of the diffusion coefficients for the example fit in Figure IV-11c is consistent with these values and as in the other two increases, this increase also does not reach equilibrium.

In the above fits the region between barriers was assumed empty of electrons before Jupiter entered. If a background electron flux is added to the predicted profile, then the values of the diffusion coefficients needed to fit the data are lowered by a factor ~ 2. The background electron flux was estimated by

averaging the observed electron flux in the 1-3 day period immediately preceding the increase.

The fits of predicted rise time profiles at 1 AU using the convection-diffusion propagation model of Conlon (1978) are consistent with the observed range of V_{SW} and show the expected dependence of the fits on k_x and k_y for the increases before the nominal connection time and around the nominal connection time. The values of the diffusion coefficients that are consistent with these three increases are summarized in Table IV-6. The values for the fits of increases at 1 AU are consistent with the lower limit of $k_x \geq 0.5 \times 10^{21}$ cm^2/sec used by Conlon in fitting predicted profiles to increases near Jupiter.

Table IV-6

Range of Diffusion Coefficients for Fits

Increase	Without Background Flux		With Background Flux		Background Electron Flux
	k_x (10^{21} cm^2/sec)	k_y (10^{22} cm^2/sec)	k_x (10^{21} cm^2/sec)	k_y (10^{22} cm^2/sec)	(10^{-3}/sec)
73.344	1.0 - 2.5	$\gtrsim$ 0.8*	0.4 - 1.6	$\gtrsim$ 0.4*	8.4
73.361	$\lesssim$ 6.	$\gtrsim$ 1.6*	$\lesssim$ 4.	$\gtrsim$ 0.6*	9.2
74.072	$\lesssim$ 4.*	1.0 - 2.0	$\lesssim$ 4.*	0.6 - 1.3	10.6
Range[1]	1.0 - 2.5	1.6 - 2.0	0.4 - 1.0	0.8 - 1.3	

* The fit is not sensitive to this parameter for this time period.

[1] Range of diffusion coefficients consistent with all three increases.

V. Summary

The 1-6 MeV electron flux at 1 AU has been measured and the propagation of electrons from Jupiter to Earth studied. The electron flux for the time period October 1972 to December 1977 was measured by the Caltech Electron/Isotope Spectrometers on the Earth orbiting IMP-7 and IMP-8 satellites. Electron bursts from Earth's magnetosphere and solar electron flares were identified and eliminated from the data. The remaining non-solar interplanetary electron flux covered parts of five Jovian synodic periods. A total of 88 Jovian increases were identified in this time period.

The observations of electrons at 1 AU clearly show the ~13 month periodicity characteristic of Jovian electron increases (Teegarden, et al., 1974). Even though the increases may occur at any time within the Jovian synodic period (Chenette, et al., 1977c; Hartman, et al., 1977) variations in the synodic envelope were observed for the five synodic periods reported here. In particular the absence of Jovian increases at 1 AU for the time period before the nominal connection time was noted for the 1973, 1974, and 1977 synodic periods. During the time period late in 1976 the lowest electron fluxes were observed. This time period from 76.322 to 77.070 had no identifiable Jovian electron increases

and the fluxes were ~40 percent lower than fluxes reported earlier (Hurford, et al., 1974).

The 88 Jovian increases identified in these five synodic periods were classified by their time profiles. The peak and fall time profiles showed no systematic variation during the synodic period. The fall time profiles were consistent with an exponential fall with $\tau \approx 4$-9 days. However, the rise time profiles displayed a systematic variation over the synodic period. The exponential rise time profiles with $\tau \approx 1$-3 days tend to occur in the time period before the nominal connection time, the diffusive rise time profiles predicted by the convection-diffusion model in the time period around the nominal connection time, and the abrupt rise time profiles in the time period after the nominal connection time. The abrupt rise time profiles were modeled by the barrier effect of CIR's separating Earth and Jupiter.

The barrier effect of CIR's on electron propagation was examined to see if the times that Jovian increases occur at 1 AU could be explained. The times that CIR's passed Pioneer 11 and Jupiter (Conlon, 1978) were used to calculate the CIR passage times at Earth. These passage times were compared with the increase start times at 1 AU for the 1974 synodic period. It was noted that CIR passage times at Jupiter correlate well with the increase start times at 1 AU while the times that the spiral field lines associated with CIR's passed Earth do not correlate well with

the increase start times especially in the time period after the nominal connection time. The times for other changes in the electron flux at 1 AU were not well correlated with the times that CIR's passed Jupiter or CIR field lines passed Earth.

Since CIR's contain enhanced magnetic fields, the times of enhancements in the magnetic field strength at 1 AU were correlated with the times of increases and changes in the electron flux at 1 AU. For the 1974 synodic period, the enhancements, especially their maxima, showed a better correlation than the CIR's with changes in the electron flux. The correlations were with increase starts, increase peaks, increase falls, and other abrupt changes in the electron flux. However, not all changes in the electron flux were associated with magnetic field enhancements at 1 AU.

The convection-diffusion propagation model of Conlon (1978) was used in predicting the 1 AU synodic envelope of the increase maxima. The Jovian electron increases observed at 1 AU stop rising before they reach the "equilibrium number density" of the convection-diffusion propagation model. Calculations of the synodic envelope of the increase maxima indicated that the envelope is sensitive to the perpendicular diffusion coefficient for times before the nominal connection time and sensitive to the parallel diffusion coefficient for the times after the nominal connection

time. The envelope of the increase maxima was modeled by the envelope formed by the intensities calculated at a time less than the time needed for an increase to reach equilibrium. Even though envelope shapes calculated in this way could be found that were similar to the observed envelope, the diffusion coefficients required were not consistent with a diffusive process.

It was pointed out that the technique of fitting an envelope to the increase maxima is biased toward large increases, especially in the early and late time periods of a synodic period. Also, the solar wind speed for the individual increases needs to be included in the calculation of the envelope. The timing of barrier passages at Earth and Jupiter determines the time of maximum intensity within a calculated increase rise time profile.

Three Jovian electron increases at 1 AU for the 1974 synodic period were fit with rise time profiles calculated from the convection-diffusion model in a manner similar to Conlon (1978). Two of the increases occurred in the time period before the nominal connection time. The fits for these two increases were sensitive to both the perpendicular diffusion coefficient, k_x, and the parallel diffusion coefficient, k_y. The third increase occurred around the nominal connection time. Since the x coordinate was close to zero at this time, the fit was sensitive to only the parallel diffusion coefficient. In all three cases, consistent

fits to the observed rise time profiles were obtained for the range of observed solar wind speeds. For these three increases fit by the convection-diffusion model, the values for the diffusion coefficients that were consistent with the data were $k_x = 1.0 - 2.5 \times 10^{21}$ cm^2/sec and $k_y = 1.6 - 2.0 \times 10^{22}$ cm^2/sec.

The three increases were also fit with predicted profiles formed by adding a background electron flux to the predicted rise time profile. For the fits with an added background electron flux, the values of the diffusion coefficients that were consistent with the data were $k_x = 0.4 - 1.0 \times 10^{21}$ cm^2/sec and $k_y = 0.8 - 1.3 \times 10^{22}$ cm^2/sec.

Appendix A. Calculation of Error in the Flux Measurement

Using the notation of Section II-C-4 the flux is calculated from Equation II-1 which is

$$FLUX = \frac{(EC - CF \cdot NEC)}{\left(\frac{NEC}{NRC} \cdot NAT\right)} \cdot \left(\frac{F}{GF}\right) \qquad A\text{-}1$$

where FLUX is the flux of 1-6 MeV electrons, EC is the raw event count of electron events, NEC is the neutral event count, NRC is the neutral rate count, CF is the background correction factor, GF is the effective geometrical factor, NAT is the neutral accumulation time, and F is the normalization factor.

The variable Q, defined as the fraction of neutral rate counts that are counted as neutral events, is a measure of the probability that a neutral rate count will also be a neutral event count. For the IMP instruments Q is dependent on the total number of events the instrument analyzes and can be considered as being independent of the actual number of neutral rate counts. The value of Q is estimated by Q = (NEC/NRC).

Using the variable Q Equation A-1 can be rearranged to give

$$FLUX = \left(\frac{EC}{Q \cdot NAT} - \frac{CF \cdot NRC}{NAT}\right) \cdot \left(\frac{F}{GF}\right). \qquad A\text{-}2$$

The variables in Equation A-2 are independent and the standard error propagation formula,

$$\sigma_{FLUX}^2 = \sum_{ALL\{x_i\}} \left(\frac{\partial FLUX}{\partial x_i}\right)^2 \cdot \sigma_{x_i}^2 \quad , \qquad A-3$$

applies (Meyer, 1975, Equation 10.3 for independent errors).

The variables EC and NRC are assumed to be Poisson distributed with estimated errors $\sigma_{EC}^2 = EC$ and $\sigma_{NRC}^2 = NRC$. The variable NAT is assumed exact with error $\sigma_{NAT}^2 = 0$. The error in Q is estimated as $\sigma_Q^2 = \frac{Q \cdot (1-Q)}{NRC}$. The values and standard errors for the variables CF, F, and GF used in the calculation of the 1-6 MeV electron flux are listed in Table A-1 and are derived from the calibration data.

By using Equation A-3 with the partial derivatives of Equation A-2 and the error estimates, the estimate of the standard error in the flux measurement is

$$\sigma_{FLUX}^2 = FLUX^2 \cdot \left(\frac{\sigma_F^2}{F^2} + \frac{\sigma_{GF}^2}{GF^2}\right) + \left(\frac{F}{GF} \cdot \frac{NRC}{NEC \cdot NAT}\right)^2 \cdot \qquad A-4$$

$$\left(EC + \frac{EC^2}{NEC} \cdot \left(1 - \frac{NEC}{NRC}\right) + NEC^2 \cdot \left(\frac{CF^2}{NRC} + \sigma_{CF}^2\right)\right) .$$

Table A-1

Variable		Value	Estimated error
GF[1]		1.5 cm^2-sr	$^{+0.11}_{-0.00}$
F[2]		1.095	$\pm$ 0.123
CF[3]	IMP-7	0.20	$\pm$ 0.01
	IMP-8	0.235	$\pm$ 0.010

---

[1] Range of GF for $E_{T_{(eff)}}$ = 1 MeV curve of Figure II-5 over the range of $\mathcal{R}$ = 0.5 - 3.5.

[2] For IMP-8 only. By definition F is unity with σ_F^2 = 0 for IMP-7.

[3] From Garrard, et al. (1977).

The terms for F and GF inside the first set of brackets are constant with the values for their relative error from Table A-1 of $\frac{\sigma_{GF}}{GF} \approx 0.073$ for both IMP-7 and IMP-8 and of $\frac{\sigma_F}{F} = 0.11$ for IMP-8 only since F is by definition unity for IMP-7.

The statistical error varies as the number of measured event counts varies. Distributions of the background corrected flux, the estimated error in this flux, and the relative error are plotted in Figure A-1. Both the error for the flux and the relative error do not include the contribution from $\frac{\sigma_{GF}}{GF}$ and $\frac{\sigma_F}{F}$ which together have a constant relative error of ~ 0.073 for IMP-7 and ~ 0.134 for IMP-8. The distributions clearly show that the relative error for either IMP-7 or IMP-8 is rarely above 30 percent and is generally $\sim$ 5-20 percent. The constant relative error of GF and F increase these limits to $\sim$ 9-21 percent.

The flux and relative error are plotted in Figure A-2 to show how the relative error varies with the flux level. In Figure A-2 the scale at the left is the relative error $\sigma_{FLUX}/FLUX$ while the scale at the right is the inverse of this ratio reflecting the number of standard deviations, σ, the measurement is from a zero counting rate.

The lower edge in these plots is from the fact that there is a maximum number of counts that can be seen in the six-hour averaged interval. The relative error above this lower limit

Figure A-1

Distributions of the corrected flux, FLUX, the estimated error in the flux, σ_{FLUX}, and the relative error in the flux, $\sigma_{FLUX}/FLUX$, for all six-hour averaged intervals with non-zero flux levels. Figure A-1a is for IMP-7 and contains 6562 six-hour intervals while Figure A-1b is for IMP-8 and contains 5373 six-hour intervals. The constant relative error from GF and F is not included in σ_{FLUX} and is ~ 0.073 for IMP-7 and ~ 0.134 for IMP-8.

a

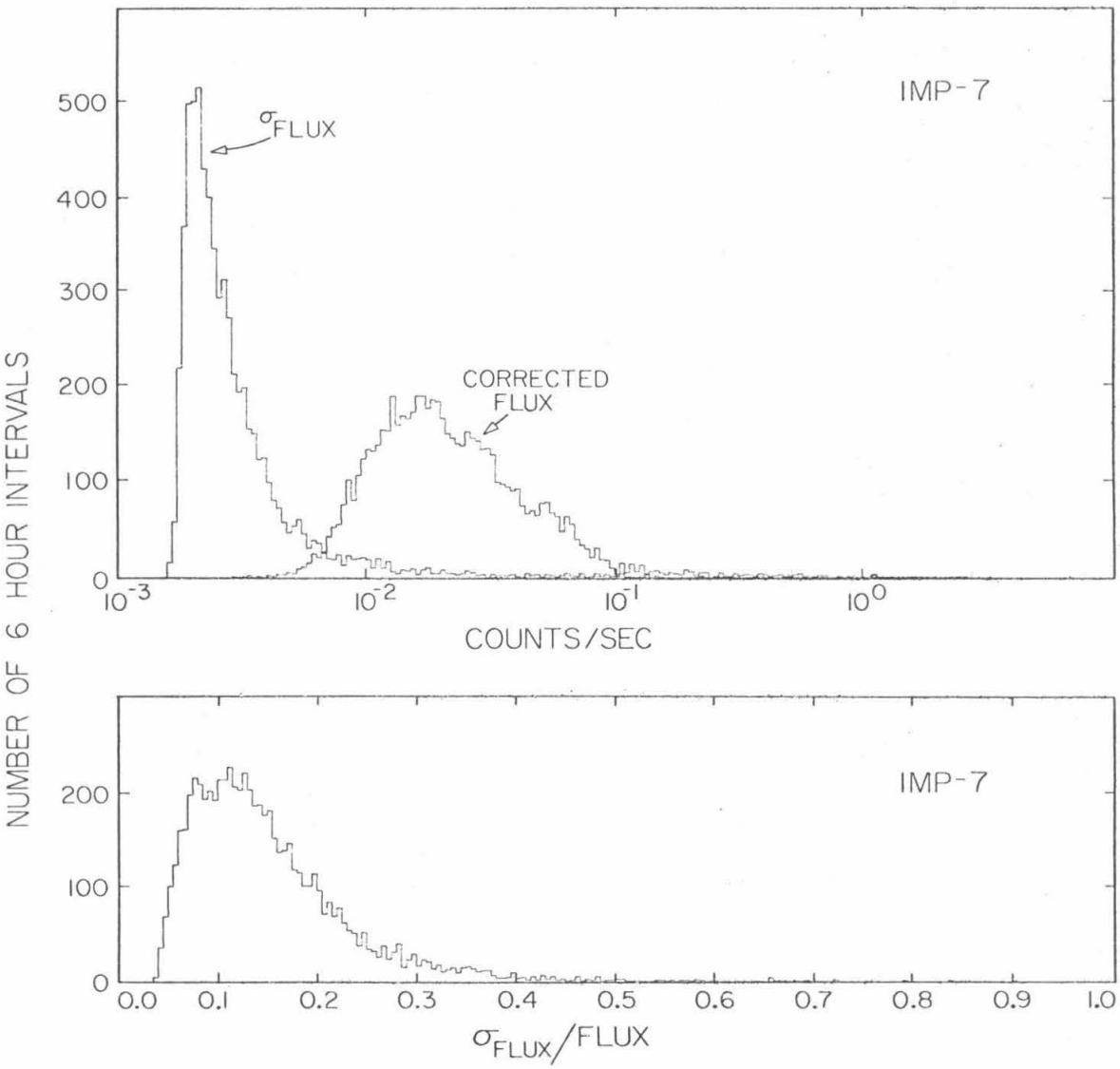
IMP-7
σ_{FLUX}
CORRECTED FLUX
NUMBER OF 6 HOUR INTERVALS
500
400
300
200
100
0
10^{-3}
10^{-2}
10^{-1}
10^{0}
COUNTS/SEC
IMP-7
200
100
0
0.0
0.1
0.2
0.3
0.4
0.5
0.6
0.7
0.8
0.9
1.0
$\sigma_{FLUX}/FLUX$

b

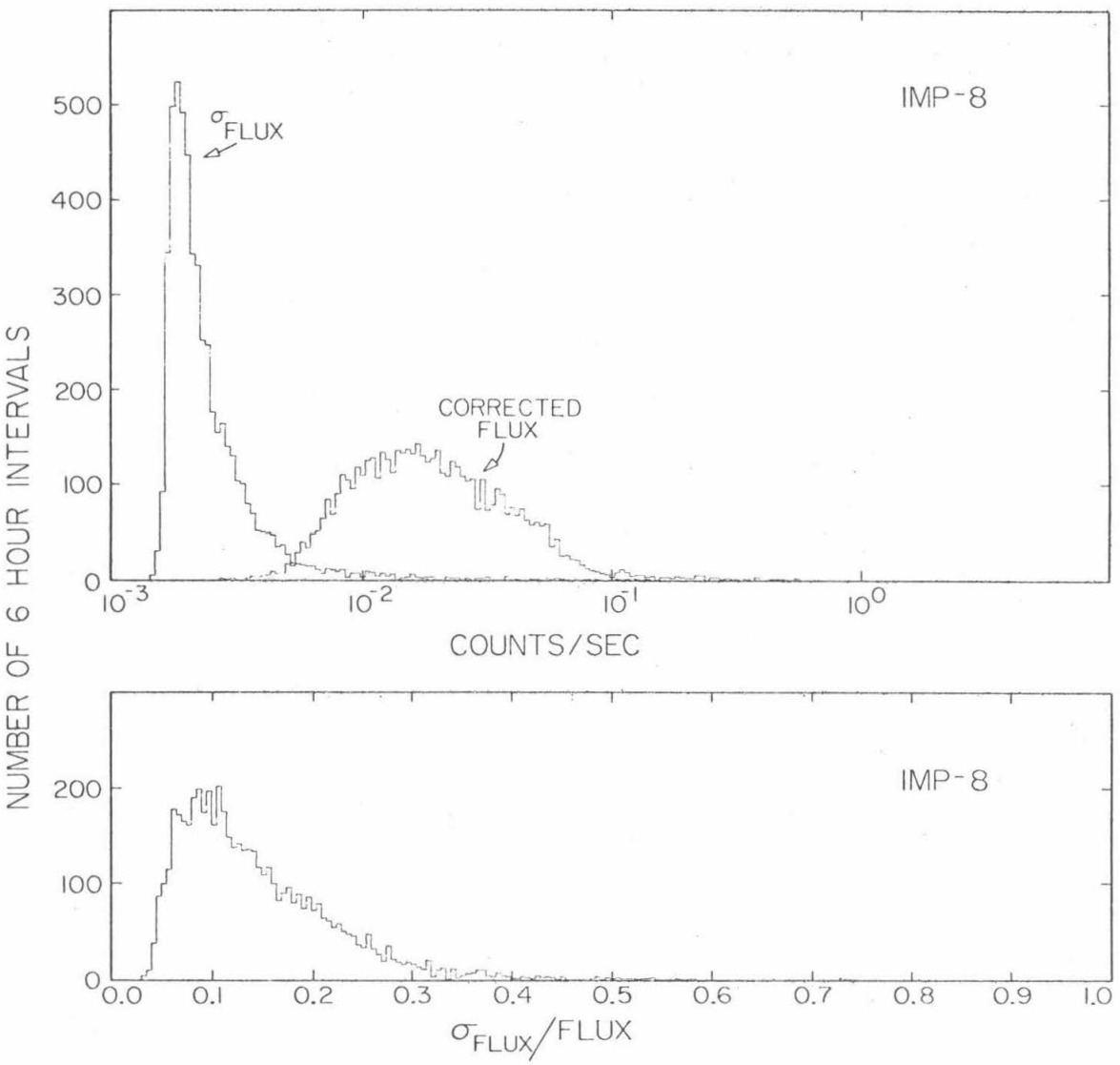
IMP-8
σFLUX
CORRECTED FLUX
NUMBER OF 6 HOUR INTERVALS
500
400
300
200
100
0
10-3
10-2
10-1
100
COUNTS/SEC
IMP-8
200
100
0
0.0
0.1
0.2
0.3
0.4
0.5
0.6
0.7
0.8
0.9
1.0
σFLUX/FLUX

Figure A-2

Distribution of the relative error, $\sigma_{FLUX}/FLUX$, versus the flux level, FLUX. The vertical scale at the left is $\sigma_{FLUX}/FLUX$ and the scale at the right is the number of standard deviations, σ, from a zero flux level. Figure A-2a is for IMP-7 and contains 4332 six-hour intervals with non-zero flux levels and non-zero relative errors while Figure A-2b is for IMP-8 and contains 3770 six-hour intervals.with non-zero flux levels and non-zero relative errors.

a
IMP-7
NUMBER OF σ FROM 0.0 COUNT RATE
2
5
10
20
50
10
1.0
0.1
0.01
(σ_FLUX / FLUX)
10^-1
10^-2
10^-3
FLUX (COUNTS/SEC)

b
IMP-8
NUMBER OF σ FROM 0.0 COUNT RATE
1
2
5
10
20
50
10
1
0.1
0.01
(σFLUX/FLUX)
10⁻³
10⁻²
10⁻¹
FLUX (COUNTS/SEC)

is due to the larger statistical error because of less data coverage in the six-hour interval or a smaller live-time for the interval. For fluxes $\gtrsim 8.5 \times 10^{-3}$/sec essentially all the flux measurements are at a significance $\geq 2\sigma$.

When the neutral rate was "bad" as defined in Section II-C-3, a new neutral rate was calculated from the D8 rate as follows for IMP-7. The new neutral rate, NEUT, was calculated by the equation

$$\text{NEUT} = (0.0104 \pm 0.0001) \cdot \text{D8} .$$

The neutral accumulation time, NAT, was set to 600 seconds if it was less than 600 seconds and a new value for the neutral rate count, NRC, was calculated for this new neutral rate by the equation

$$\text{NRC} = \text{NEUT} \cdot \text{NAT} .$$

The neutral event count, NEC, was then calculated by the equation

$$\text{NEC} = (\text{D01S Events})/(\text{D01S Rate}) \cdot \text{NEUT} .$$

These calculated numbers for this one hour interval in which the neutral rate was originally "bad" were then added into the six-hour sums. For IMP-8 the procedure was the same except that the factor multiplying the D8 rate to derive a new neutral rate was 0.0076 ± 0.0001.

Appendix B. Spiral Geometry of the Interplanetary Magnetic Field

The spiral model of the interplanetary magnetic field was developed by Parker (1958, 1963). This appendix will first give a brief review of the spiral magnetic field lines and the geometry of the Archimedean spiral. Then the hyperbolic spiral which is orthogonal to the Archimedean spiral will be discussed. Finally, the nominal connection times of Earth and Jupiter will be calculated.

B-1. The Archimedean Spiral

At radial distances greater than about ten solar radii from the Sun, the solar wind can be approximated as a radially expanding plasma (Parker, 1958). The solar magnetic field is frozen into the plasma and thus expands with the solar wind. The large scale average structure of this now interplanetary magnetic field is a spiral generated by the outward radial flow and by the rotation of the Sun.

A constant solar wind speed, V_{SW}, generates an Archimedean spiral for the interplanetary magnetic field described by

$$r = \frac{V_{SW}}{\Omega_\odot} \cdot \phi \qquad B\text{-}1$$

where $\Omega_\odot$ is the solar rotation and ϕ is the spiral longitude angle. This report uses the value $\Omega_\odot$ = 25.38 days which is the solar rotation at a solar latitude of 16°. The observed magnetic fields are very turbulent so the spiral structure is apparent only over long term averages. The solar wind speed is also variable in longitudinal position on the Sun and evolves over 2 - 3 solar rotations. This model of an ideal spiral for the field lines is at present only applicable near the solar equatorial plane since little is known of the actual field structure or solar wind at high solar latitudes.

For convenience k is defined by the equation

$$k = \frac{V_{SW}}{\Omega_\odot} \quad . \qquad B\text{-}2$$

Using Equation B-1, Figure B-1 is a plot of an Archimedean spiral. At a radius, r, the tangent to the spiral forms an angle, Ψ, to the radius vector given by

$$\Psi = \text{TAN}^{-1}\left(\frac{r}{k}\right) \quad . \qquad B\text{-}3$$

The length along an Archimedean spiral from the radial position

Figure B-1

Plot of the Archimedean spiral for V_{SW} = 500 km/sec. Note that the longitude angle, ϕ, for the spiral increases in the opposite direction that ϕ_{GSE} increases. The tangent to the spiral at a radius r makes an angle, Ψ, to the radius vector and is given by $\Psi = TAN^{-1}\left(\frac{r}{k}\right)$. The incremental distance, ds, along the spiral is $ds = [dr^2 + r^2 \cdot d\phi^2]^{1/2}$.

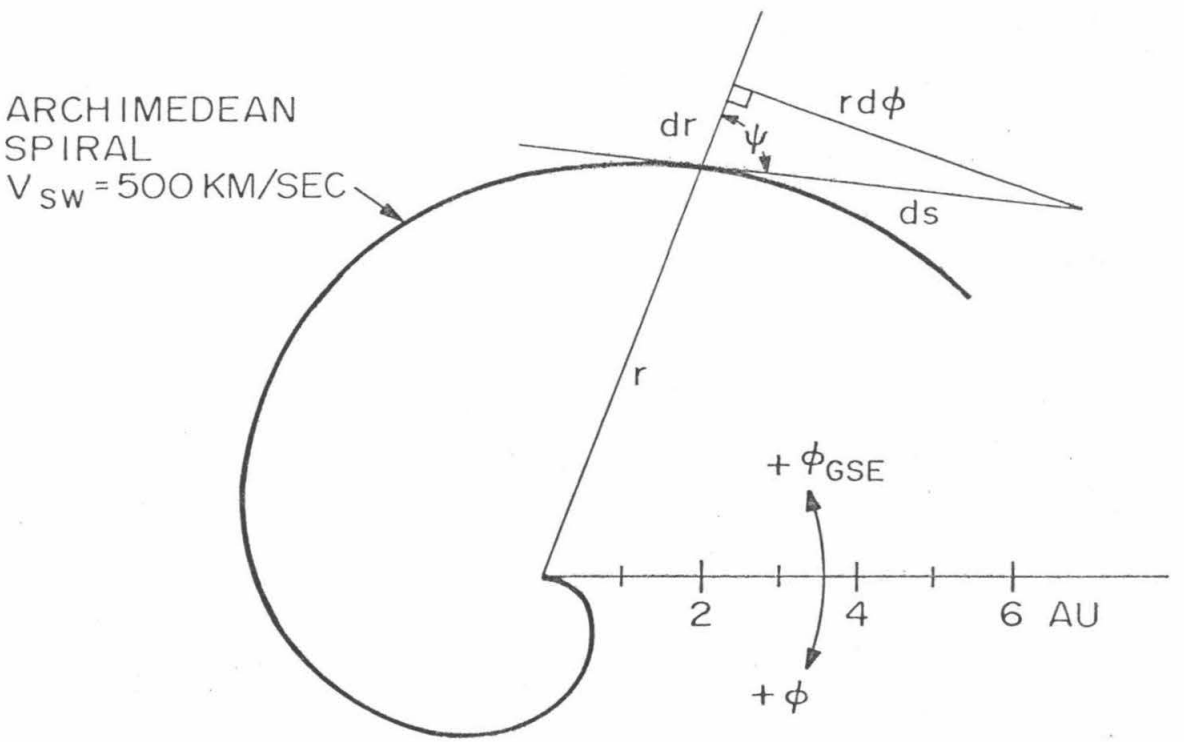
ARCHIMEDEAN
SPIRAL
V_{SW} = 500 KM/SEC
dr
ψ
rdϕ
ds
r
+ ϕ_{GSE}
2
4
6 AU
+ ϕ

r_1 to r_2 can be written as

$$L = \int_{r_1}^{r_2} ds = \int_{r_1}^{r_2} \left[dr^2 + r^2 \cdot d\phi^2 \right]^{\frac{1}{2}} \qquad B-4$$

where ds is defined by the right triangle shown in Figure B-1.

The intergration of Equation B-4 is easily done by noting that from Equation B-1 $\frac{d\phi}{dr} = \frac{1}{k}$, then changing the variable by using Equation B-3, using Dwight (1961, Equation 442.30), and noting that $0 \leq \psi < \frac{\pi}{2}$. The result can be written as

$$\frac{L}{k} = \frac{1}{2} \left[\frac{\sin\psi}{\cos^2\psi} + \ln\left(\frac{1+\tan\left(\frac{\psi}{2}\right)}{1-\tan\left(\frac{\psi}{2}\right)} \right) \right]_{\psi_1}^{\psi_2} \qquad B-5$$

where $\psi_i = \tan^{-1}\left(\frac{r_i}{k}\right)$ for i = 1, 2.

A useful formula to relate the corotation time, $(t_2 - t_1)$, for an ideal spiral to move between two given spatial positions, (r_1, ϕ_1) and (r_2, ϕ_2) both in GSE coordinates is

$$(t_2 - t_1) = \frac{(r_2 - r_1)}{V_{SW}} + \frac{(\phi_2 - \phi_1)}{\Omega_\odot} . \qquad B-6$$

This equation is simply the time for the solar wind to travel from r_1 to r_2 plus the time for the source region on the Sun to rotate from ϕ_1 to ϕ_2 and assumes no change in the solar wind speed or in the source region on the Sun. Equation B-6 can also be used to calculate the solar wind speed given the

times, t_1 and t_2, that the spiral passed the positions (r_1, ϕ_1) and (r_2, ϕ_2).

B-2. The Hyperbolic Spiral

A curve will be orthogonal to the Archimedean spiral if its tangent is always perpendicular to the tangent of the Archimedean spiral. If the orthogonal tangent makes an angle, Ψ_2, to the radius vector as shown in Figure B-2 and if Ψ_1 is the tangent angle for the Archimedean spiral then the angles Ψ_1 and Ψ_2 are related by the equation for a right angle

$$\Psi_1 + \Psi_2 = \frac{\pi}{2} . \qquad B-7$$

The tangent for the sum of two angles is given by Dwight (1961, Equation 405.01) as

$$TAN(\Psi_1 + \Psi_2) = \frac{TAN\,\Psi_1 + TAN\,\Psi_2}{1 - TAN\,\Psi_1 \cdot TAN\,\Psi_2} . \qquad B-8$$

Since $TAN\frac{\pi}{2} = \infty$, Equation B-8 is satisfied by the angles related by Equation B-7 for $r > 0$, i.e. $0 < \Psi_1 < \frac{\pi}{2}$, only if the tangents of the angles are related by

$$1 - TAN\,\Psi_1 \cdot TAN\,\Psi_2 = 0 . \qquad B-9$$

Figure B-2

Plot of an Archimedean spiral for V_{SW} = 500 km/sec. The tangent to this spiral at the radial distance r makes an angle Ψ_1 to the radius vector. The orthogonal tangent makes an angle Ψ_2 to the radius vector. The relationship between the tangent angles is $\Psi_1 + \Psi_2 = \frac{\pi}{2}$.

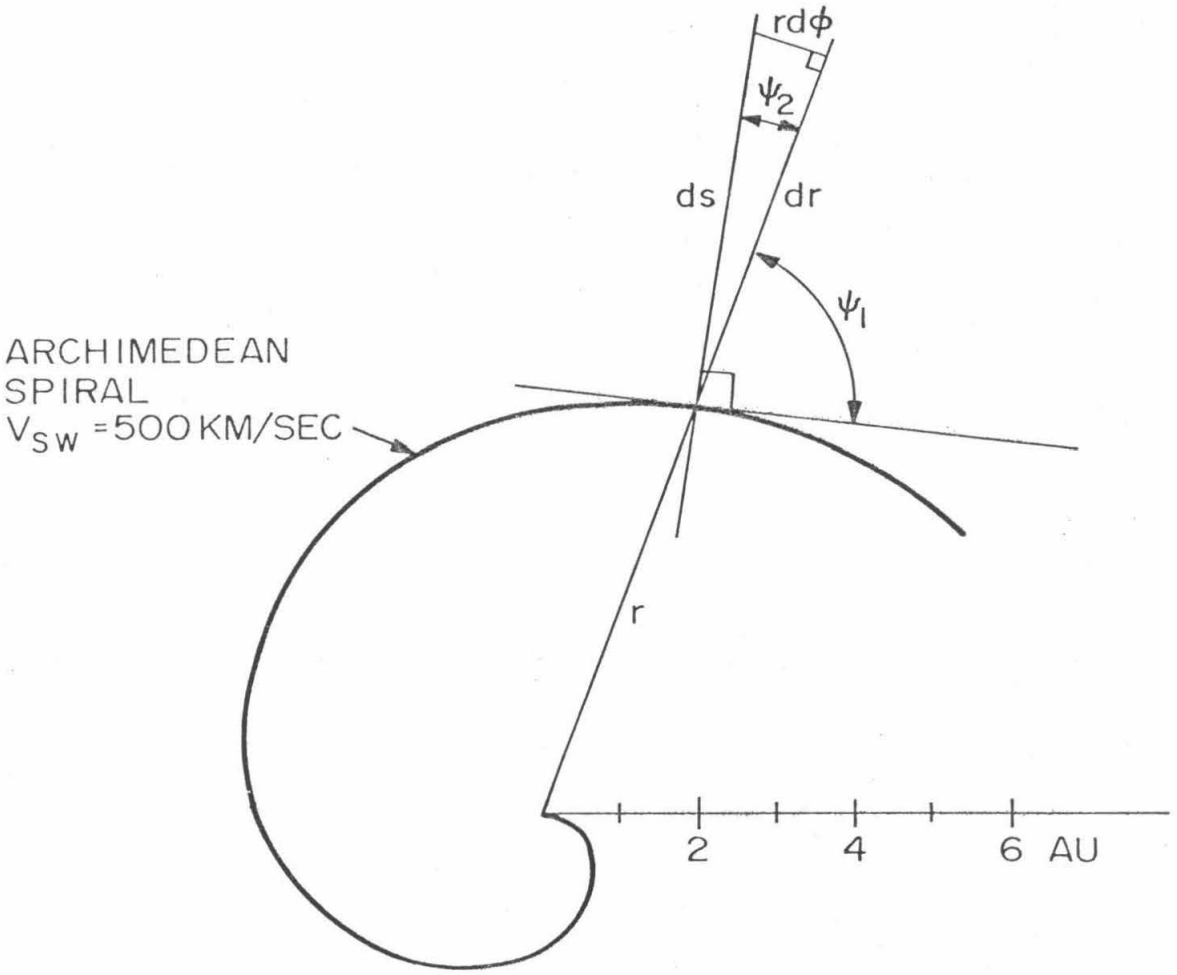
rdϕ
ψ2
ds
dr
ψ1
ARCHIMEDEAN
SPIRAL
VSW =500 KM/SEC
r
2
4
6 AU

The right triangle in Figure B-2 gives

$$\text{TAN } \Psi_2 = \frac{r\, d\phi}{dr} \qquad \text{B-10}$$

and substituting with Equations B-9 and B-3 gives the differential equation

$$r \frac{d\phi}{dr} = \frac{k}{r} \qquad \text{B-11}$$

for the curve orthogonal to the Archimedean spiral.

The solution to Equation B-11 is the hyperbolic spiral given by the equation

$$r = -\frac{k}{\phi} . \qquad \text{B-12}$$

The distance between two points (r_1, ϕ_1) and (r_2, ϕ_2) along the hyperbolic spiral is also given by Equation B-4 but with the incremental distance, ds, defined by the right triangle in Figure B-2. The integration is done by noting that from Equation B-12, $\frac{d\phi}{dr} = \frac{k}{r^2}$, changing the variable by using Equation B-9, using Dwight (1961, Equation 451.12), and noting that for $r>0$, $0<\Psi<\frac{\pi}{2}$. The result can be written as

$$\frac{L}{k} = \left[\frac{1}{\cos\Psi} + \ln\left(\text{TAN}\,\frac{\Psi}{2}\right)\right]_{\Psi_1}^{\Psi_2} \qquad \text{B-13}$$

where $\Psi_i = \text{TAN}^{-1}\left(\frac{r_i}{k}\right)$ for i = 1, 2.

Figure B-3 is a plot of an Archimedean spiral and its orthogonal curve the hyperbolic spiral for a solar wind speed of V_{SW} = 500 km/sec.

B-3. The Nominal Connection Time for Earth and Jupiter

The time of nominal connection for Earth and Jupiter occurs when the two planets are connected by an ideal Archimedean spiral. This relationship occurs when the corotation time in Equation B-6 is zero, that is when

$$\frac{(r_J - r_E)}{V_{SW}} + \frac{(\phi_J - \phi_E)}{\Omega_\odot} = 0. \qquad B-14$$

Table B-1 list the nominal connection times for Earth and Jupiter for the solar wind speed of V_{SW} = 400, 500, and 600 km/sec. The table covers the time period from 1962 to 1978 and uses orbit information furnished by Penzo (1975a). The year in the first column is the year within which the time of nominal connection for V_{SW} = 500 km/sec occurred. This year is also used to label the ~13 month synodic periods of Earth and Jupiter.

Figure B-3

Grid plot of the Achimedean spiral for V_{SW} = 500 km/sec and its orthogonal hyperbolic spiral.

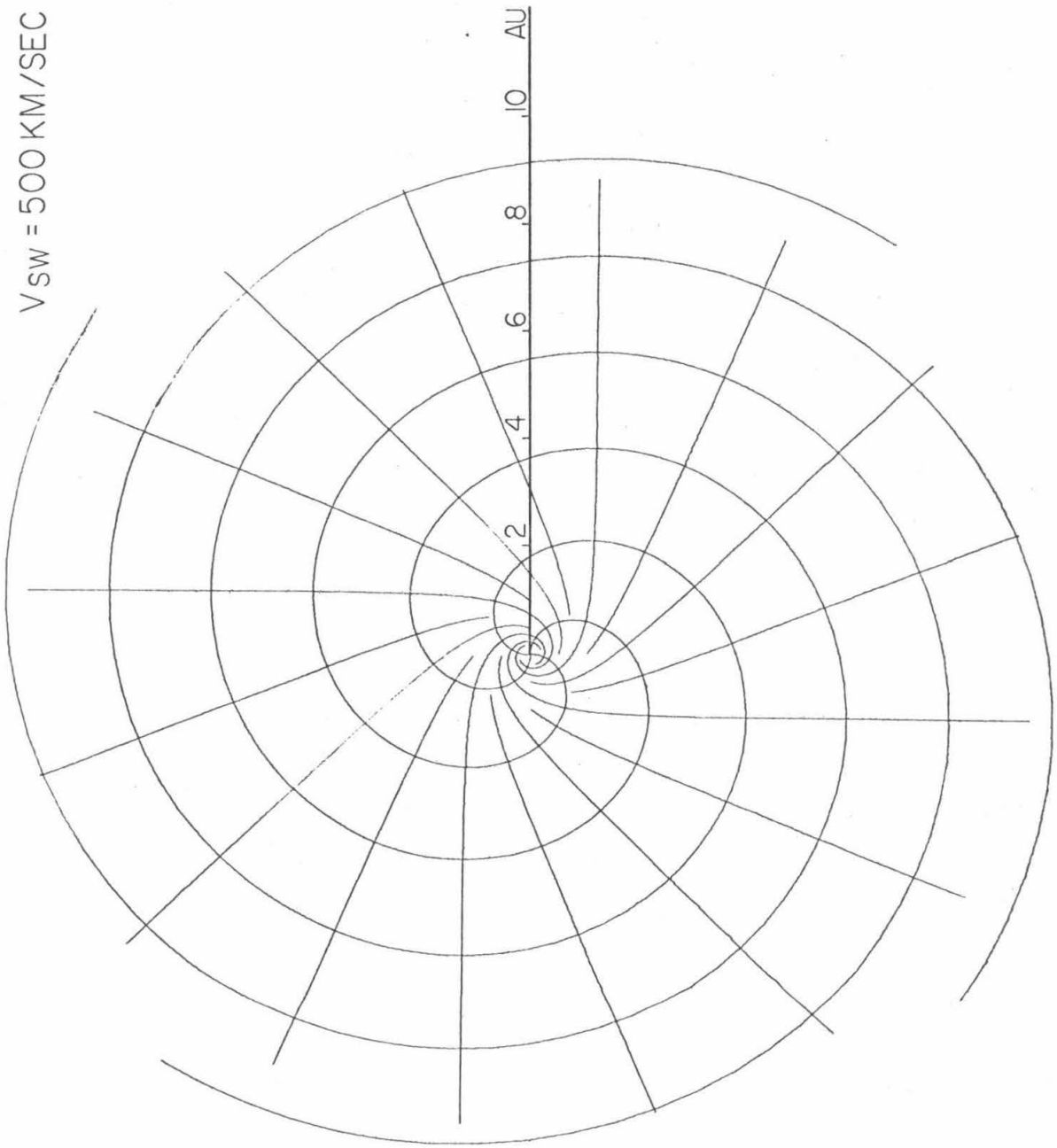
V_{SW} = 500 KM/SEC
,2
,4
,6
,8
,10
AU

Table B-1

Time of Nominal Connection for Earth and Jupiter

Year[1]	Date of Nominal Connection for V_{SW} of			
	400	500	600	km/sec
1962	62.113	62.060	62.025	
1963	63.145	63.091	63.057	
1964	64.185	64.129	64.094	
1965	65.230	65.171	65.133	
1966	66.276	66.216	66.176	
1967	67.318	67.257	67.217	
1968	68.355	68.294	68.254	
1969	70.019	69.325	69.285	
1970	71.045	70.353	70.314	
1971[2]				
1972	72.068	72.013	71.341	
1973	73.090	73.036	73.001	
1974	74.117	74.064	74.030	
1975	75.151	75.096	75.062	
1976	76.191	76.135	76.099	
1977	77.236	77.177	77.139	
1978	78.281	78.222	78.181	

---

[1] Year is the year within which the time of nominal connection for V_{SW} = 500 km/sec occurred.

[2] Since the synodic period is ~13 months long, no nominal connection for V_{SW} = 500 km/sec occurred in 1971.

Appendix C. Convection-Diffusion Propagation Model

This appendix describes the convection-propagation model and the coordinate system used in calculating particle fluxes at 1 AU. The derivation below follows the one Conlon (1978) used to obtain a solution to the equation for energetic particle transport in interplanetary space. From the Fokker-Planck equation (Parker, 1963) the time-dependent equation for the differential number density $U(\vec{x},T,t)$ of particles at $\vec{x}$ with kinetic energy T in Cartesian coordinates is

$$\frac{\partial U}{\partial t} = \frac{\partial}{\partial x_i}\left(k_{ij}\cdot\frac{\partial U}{\partial x_j} - v_i\cdot U\right) + \frac{1}{3}\cdot\left(\frac{\partial v_i}{\partial x_i}\right)\cdot\frac{\partial}{\partial T}(\alpha T U) \qquad C-1$$

where t is the time, v_i is the solar wind velocity, k_{ij} is the diffusion tensor, and $\alpha \approx 1$ for relativistic particles.

To obtain an approximate solution to this equation which describes the interplanetary transport of Jovian electrons, Conlon assumed that k_{ij} is independent of $\{\vec{x},T,t\}$ and is diagonal (i.e. $k_{ij} = k_i$ if $i = j$, and $k_{ij} = 0$ if $i \neq j$), the energy dependence of U is described by a power law (i.e. $U = Q\cdot T^{-\gamma}$), Jupiter is a point source of particles at $\vec{x} = 0$, and the divergence of the solar wind, $\frac{\partial v_i}{\partial x_i}$ is independent of $\vec{x}$. Using these assumptions, Conlon

applied a Green's function technique to obtain the time dependent solution

$$u(\vec{x},T,t)=\left\{\frac{Q\cdot T^{-\gamma}\cdot \exp(2\,\vec{F}\cdot\vec{D})}{(4\pi)^{3/2}\prod_{i=1}^{3}k_i^{1/2}}\right\}\cdot\int_0^t t'^{-3/2}\exp\left[-\frac{D^2}{t'}-(F^2+\lambda)\,t'\right]dt' \qquad C-2$$

where Conlon defined:

$$\lambda=\frac{1}{3}\left(\frac{\partial V_i}{\partial x_i}\right)(\gamma-1)\;,\quad D_i=\frac{x_i}{2k_i^{1/2}}\;,\quad F_i=\frac{v_i}{2k_i^{1/2}}\;. \qquad C-3$$

At this point Conlon argued that $\lambda \ll F^2$ and that therefore deceleration effects can be ignored. The parameter λ will be kept in this derivation.

By using the error function defined by

$$\operatorname{erf}(z)=\frac{2}{\sqrt{\pi}}\int_0^z e^{-x^2}dx$$

and the equation $C-4$

$$\operatorname{erfc}(z)=1-\operatorname{erf}(z)$$

Equation C-2 can be transformed into

$$U(\vec{x},T,t)=\left\{\frac{Q\cdot T^{-\gamma}\ \mathrm{EXP}\left(2\vec{F}\cdot\vec{D}\right)}{16\pi\ D\ \prod_{i=1}^{3} k_i^{1/2}}\right\} \qquad C-5$$

$$\cdot\left\{e^{2DA}\ \mathrm{erfc}\left(D t^{-1/2}+A t^{1/2}\right)-e^{-2DA}\,\mathrm{erfc}\left(D t^{-1/2}-A t^{1/2}\right)\right\}$$

where

$$A^2=F^2+\lambda$$

For large t, the solution for U approaches the asymptotic form

$$U(\vec{x},T)=\frac{Q\cdot T^{-\gamma}\ \mathrm{EXP}\left(2\vec{F}\cdot\vec{D}-2D\cdot A\right)}{8\pi\cdot D\cdot\prod_{i=1}^{3} k_i^{1/2}} \qquad C-6$$

which Conlon referred to as the "equilibrium number density" solution.

Since Conlon was concerned with Jovian increases $\lesssim$ 1.2 AU from Jupiter, a Cartesian coordinate system with the origin at Jupiter was used. Both Conlon and Chenette, et al. (1977c) have noted that a Cartesian coordinate system probably does not accurately represent the propagation of electrons from Jupiter to Earth. Over the distance from Jupiter to Earth the average

spiral magnetic field lines have a large amount of curvature and the coordinates have differing amounts of divergence. During the time period before encounter both Pioneer 11 and Jupiter were within 1° in latitude so Conlon used $z \approx 0$. For the propagation of electrons to 1 AU, Conlon also used $z \approx 0$ even though the latitude difference of Earth and Jupiter varies from $\sim 1^{\circ}$ to $\sim 11^{\circ}$. In this study the z coordinate is set to zero. A more realistic propagation model should include the actual field geometry and the z coordinate.

The coordinate system chosen by Conlon was the y axis along the average spiral field direction with the positive direction inward toward the Sun and the x axis radial with the positive direction outward away from Jupiter. Chenette, et al. modified the x axis so that it was perpendicular to the tangent of the average spiral field line at Jupiter. In this study the x axis was defined to be along the hyperbolic spiral which is orthogonal to the Archimedean spiral as described in Section B-2 of Appendix B. This coordinate system is drawn schematically in Figure C-1.

Both Conlon and Chenette, et al. used the angle, Ψ, between the tangent to the Archimedean spiral and a radial line to calculate the components of the solar wind speed along the coordinates. At Jupiter $\Psi \approx 79^{\circ}$ and at Earth $\Psi \approx 45^{\circ}$ so that the components of the solar wind speed along the coordinates varies. Here the components of the solar wind speed were calculated from averages of $\cos\Psi$ and $\sin\Psi$ given by

$$\langle \cos\Psi \rangle = (R_I - R_E)/\Delta Y \quad , \quad \langle \sin\Psi \rangle = (R_I - R_J)/\Delta X$$

where R_E and R_J are the radial positions of Earth and Jupiter respectively, R_I is the radial value of the intersection of the Archimedean spiral passing through Earth and the hyperbolic spiral passing through Jupiter, ΔX is the distance along the x coordinate from R_J to R_I, and ΔY is the distance along the y coordinate from R_I to R_E.

Plotted in Figure C-2 are examples of the rise time profiles for Jovian increases at 1 AU predicted by this convection-diffusion model. For these plots Jupiter is at 5.2 AU from the Sun and Earth is at 1 AU. Each pair of curves is for a different azimuthal position, ϕ, of Earth relative to Jupiter. The dashed curves are for the convection-diffusion model used by Conlon and Chenette, et al. while the solid curves are for the same model except that the hyperbolic spiral was used as the x axis. The parameters used in the model solution to calculate these rise time profiles were $k_x = 1 \times 10^{21}$ cm^2/sec, $k_y = 5 \times 10^{22}$ cm^2/sec, $V_{SW} = 450$ km/sec, and $\lambda = 0$. The spirals of the curves for $\phi = 360°$, $420°$, and $480°$ in Figure C-2 are the same spirals used for $\phi = 0°$, $60°$, and $120°$ respectively. The curves for these angles are plotted because the intersection of the Archimedean and hyperbolic spirals can be in front of Jupiter or after one rotation along the Archimedean spiral, behind Jupiter.

The only noticeable difference between the two sets of predicted

Figure C-1

Schematic plot of the coordinate system used in the calculations of particle propagation to 1 AU. The orbital radii of Earth and Jupiter are 1 AU and 5.2 AU respectively. The Archimedean spiral passes through the position of Earth and the hyperbolic spiral passes through the position of Jupiter. These spirals intersect at the radial position labeled R_I. The x coordinate, ΔX, is measured from R_J to R_I along the hyperbolic spiral with the positive direction outward away from the Sun. The y coordinate, ΔY, is measured from R_I to R_E along the Archimedean spiral with the positive direction inward toward the Sun. The relative positions of Earth and Jupiter in this figure correspond to the time period shortly after the nominal connection time.

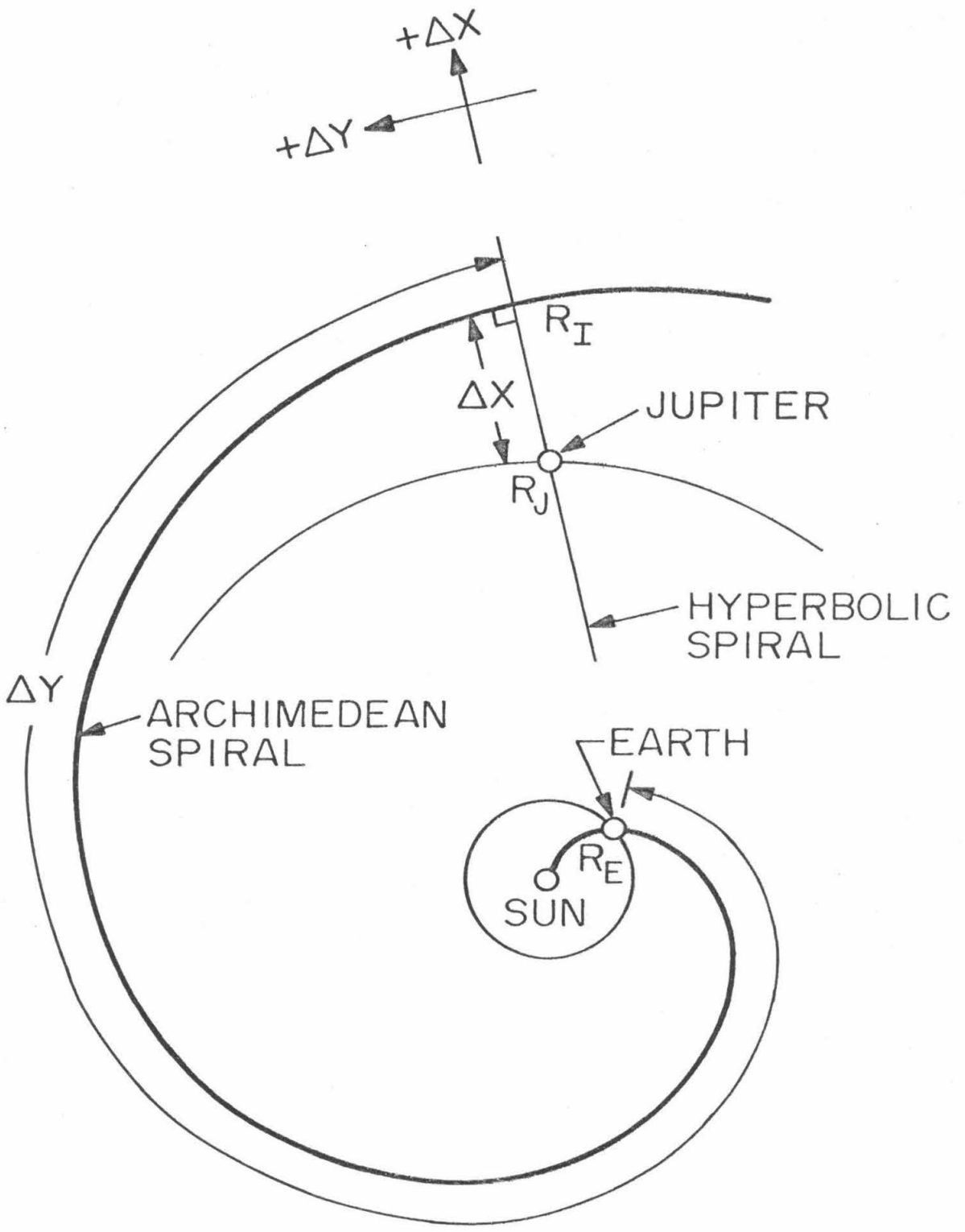
+ΔX
+ΔY
R_I
ΔX
JUPITER
R_J
HYPERBOLIC SPIRAL
ΔY
ARCHIMEDEAN SPIRAL
EARTH
R_E
SUN

Figure C-2

Comparison of the rise time profiles of electron increases predicted at 1 AU by the convection-diffusion model used by Conlon (1978) and Chenette, et al. (1977c), the dashed curves, with the rise time profiles predicted by the same model except that the hyperbolic spiral was used as the x axis. The values of the parameters used in the solution are $k_x = 1 \times 10^{21}$ cm^2/sec, $k_y = 5 \times 10^{22}$ cm^2/sec, $V_{SW} = 450$ km/sec, $\lambda = 0$, $R_J = 5.2$ AU, and $R_E = 1$ AU. Each curve is for the relative azimuthal position of Earth and Jupiter, ϕ, at 60° intervals. The curves for $\phi \geq 360°$ are the same spiral as for $\phi = \phi - 360°$ but with the intersection of the Archimedean and hyperbolic spirals behind Jupiter instead of in front of Jupiter. Note that the vertical scale varies for each curve.

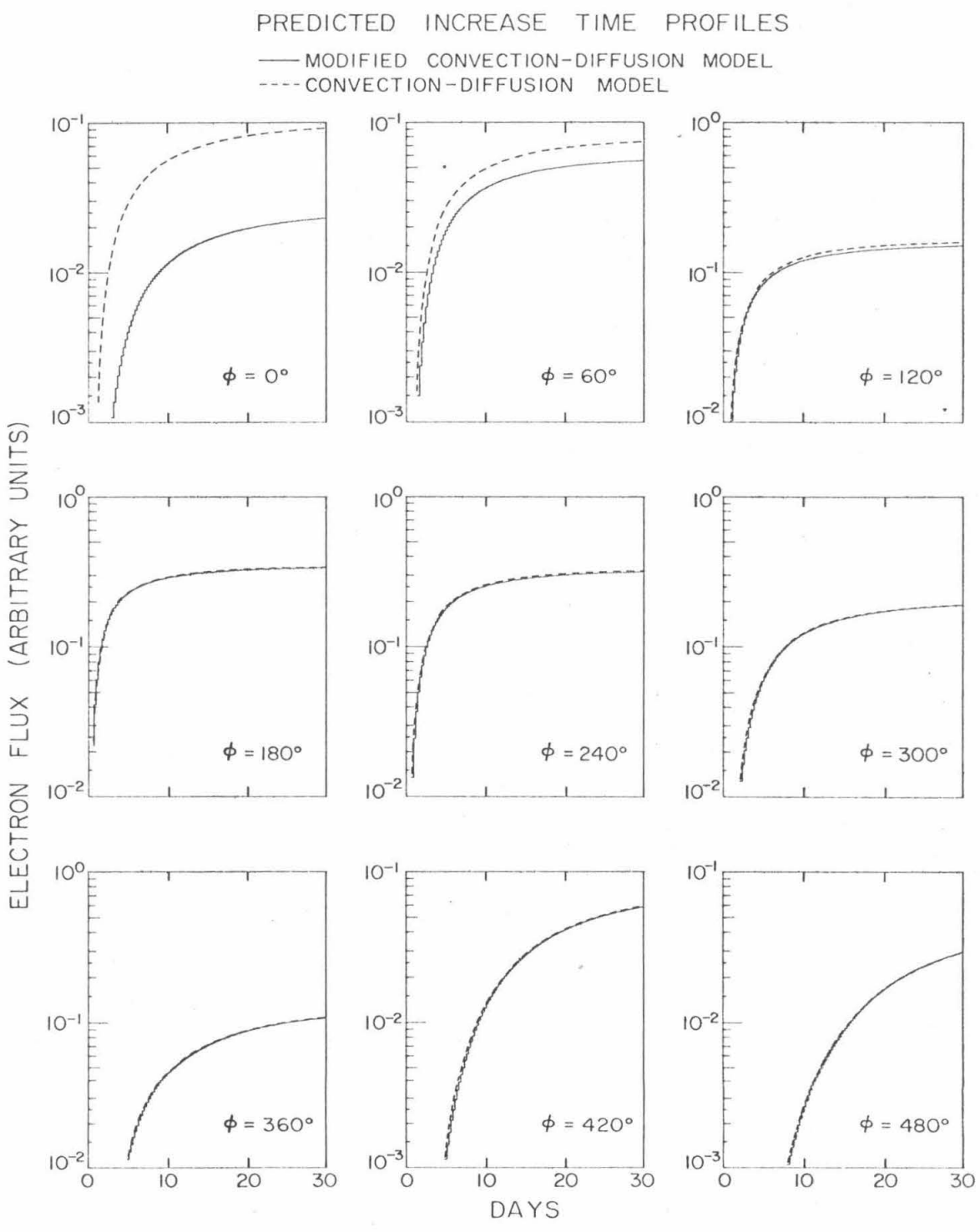
PREDICTED INCREASE TIME PROFILES
MODIFIED CONVECTION-DIFFUSION MODEL
CONVECTION-DIFFUSION MODEL
ELECTRON FLUX (ARBITRARY UNITS)
DAYS
ϕ = 0°
ϕ = 60°
ϕ = 120°
ϕ = 180°
ϕ = 240°
ϕ = 300°
ϕ = 360°
ϕ = 420°
ϕ = 480°

increase time profiles is for the curves with $\phi = 0^{\circ}$ and 60° which have the spiral in front of Jupiter. In this region the effects of the spiral curvature are pronounced and the corresponding profiles for the region behind Jupiter, $\phi = 360^{\circ}$ and 420° respectively, may better represent the expected time profiles at 1 AU. In the region behind Jupiter the x and y coordinates are a closer approximation to the Cartesian assumption of the model than in the region in front of Jupiter. For the other relative positions of Earth and Jupiter there are essentially no differences in the curves for these two variations in the geometry used in the convection-diffusion model.

All of these predicted increase profiles have the diffusive rise time profile. Thus the convection-diffusion model predicts a diffusive rise time profile for the whole synodic period. The time to reach the "equilibrium number density" varies from $\sim$10 days to $\gtrsim$ 30 days.

References

Baker, D.N., and E.C. Stone, "Observations of Energetic Electrons ($E \gtrsim 200$ keV) in the Earth's Magnetotail: Plasma Sheet and Fireball Observations," J. Geophys. Res., 82, 1532, 1977.

Barnes, C.W., and J.A. Simpson, "Evidence for Interplanetary Acceleration of Nucleons in Corotating Interaction Regions," Astrophys. J., 210, L91, 1976.

Beedle, R.E., J.A. Lezniak, J. Rockstroh, and W.R. Webber, "Measurements of the Primary Electron Spectrum in the Energy Range 0.2 MeV to 15 GeV," Acta Phys. Acad. Sci. Hungaricae, 29, Suppl. 1, 131, 1970.

Behannon, K.W., "Mapping the Earth's Bow Shock and Magnetic Tail by Explorer 33," J. Geophys. Res., 73, 907, 1968.

Belcher, J.W., and L. Davis, Jr., "Large-amplitude Alfven Waves in the Interplanetary Medium, 2," J. Geophys. Res., 76, 3534, 1971.

Chenette, D.L., T.F. Conlon, and J.A. Simpson, "Bursts of Relativistic Electrons From Jupiter Observed in Interplanetary Space With a Time Variation of the Planetary Rotation Period," J. Geophys. Res., 79, 3551, 1974.

Chenette, D., T. Conlon, and J.A. Simpson, "Observations at Earth of Jovian Electrons Over the 13 Month Synodic Jovian Year: Implications for Models of Jovian Electron Propagation," Abstract, Topical Conf. on Solar and Interplanetary Physics, Tucson, 1977a.

Chenette, D.L., T.F. Conlon, K.R. Pyle, and J.A. Simpson, "Jupiter's Magnetosphere as a 'Point Source' For Electrons Propagating From 1 to 12 AU," Conf. Papers 15th Int. Cosmic Ray Conf. Plovdiv, 5, 226, 1977b.

Chenette, D.L., T.F. Conlon, K.R. Pyle, and J.A. Simpson, "Observations of Jovian Electrons at 1 AU Throughout the 13 Month Jovian Synodic Year," Astrophys. J., 215, L95, 1977c.

Chenette, D.L., and J.A. Simpson, "Jovian Electron Intensity Correlations With Fast Solar Wind Streams Near Earth," Abstract, Trans. Amer. Geophys. U., 59, 1173, 1978.

Cline, T.L., "Interplanetary 0.1 to 1.5 MeV Electron and Positron Observations From IMP-6 and IMP-7," Conf. Papers 13th Int. Cosmic Ray Conf. Denver, 1, 312, 1973.

Cline, T.L., G.H. Ludwig, and F.B. McDonald, "Detection of Interplanetary 3- to 12-MeV Electrons," Phys. Rev. Lett., 13, 786, 1964.

Cline, T.L., and F.B. McDonald, "Interplanetary and Solar Electrons of Energy 3-12 MeV," Canadian J. Phys., 46, S761, 1968.

Cline, T.L., and G. Porreca, "Cosmic Ray Electrons and Positrons of Energies 2 to 9.5 MeV Observed in Interplanetary Space," Acta Phys. Acad. Sci. Hungaricae, 29, Suppl. 1, 145, 1970.

Conlon, T.F., "The Interplanetary Modulation and Transport of Jovian Electrons," J. Geophys. Res., 83, 541, 1978.

Conlon, T.F., and J.A. Simpson, "Modulation of Jovian Electron Intensity in Interplanetary Space by Corotating Interaction Regions," Astrophys. J., 211, L45, 1977.

Dwight, H.B., Tables of Integrals and Other Mathematical Data, Fourth Edition, The Macmillan Company, New York, 1961.

Forman, M.A., "The Velocity Correlation Function in Cosmic-Ray Diffusion Theory," Astrophys. Space Sci., 49, 83, 1977.

Garrard, T.L., "General Overview of IMP Data Processing," Space Radiation Laboratory Internal Report #59, Calif. Inst. of Technology, 1974.

Garrard, T.L., R.A. Mewaldt, E.C. Stone, and R.E. Vogt, "Data Submission to the NSSDC from the Caltech Electron/Isotope Spectrometer on IMP-7 and IMP-8," Space Radiation Laboratory Technical Report 77-2, Calif. Inst. of Technology, 1977.

Gold, R.E., and E.C. Roelof, "Propagation of Relativistic Jovian Electrons to Pioneers 10 and 11 Via Solar Wind Stream-Stream Interaction Regions," JHU/APL Preprint 76-08, 1976.

Gold, R.E., S.M. Krimigis, E.C. Roelof, and R.W. Fillius, "The Relationship Between Jovian Electrons and Solar Wind Stream Structure," Conf. Papers 15th Int. Cosmic Ray Conf. Plovdiv, 5, 220, 1977.

Gold, R.E., E.C. Roelof, and S.M. Krimigis, "Propagation of Relativistic Jovian Electrons to Earth," JHU/APL Preprint 76-07, 1976.

Gosling, J.T., A.J. Hundhausen, and S.J. Bame, "Solar Wind Stream Evolution at Large Heliocentric Distance: Experimental Demonstration and the Test of a Model," J. Geophys. Res., 81, 2111, 1976.

Hartman, S.R., "Geometrical Factors for IMP-H," Space Radiation Laboratory Internal Report #45, Calif. Inst. of Technology, 1973.

Hartman, S.R., "A Description of the IMP-H/J Caltech Electron Isotope Spectrometer Experiments," Space Radiation Laboratory Report #68, Calif. Inst. of Technology, 1976.

Hartman, S.R., "A Description of the Raw Hourly IMP Data Contained in the RUSTxx Tapes," Space Radiation Laboratory Internal Report #69, Calif. Inst. of Technology, 1978.

Hartman, S.R., R.A. Mewaldt, E.C. Stone, and R.E. Vogt, "Observations of 1 to 6 MeV Jovian Electrons in 1976," Abstract, Topical Conf. on Solar and Interplanetary Physics, Tucson, 1977.

Hurford, G.J., R.A. Mewaldt, E.C. Stone, and R.E. Vogt, "The Energy Spectrum of 0.16 to 2 MeV Electrons During Solar Quiet Times," Astrophys. J., 192, 541, 1974.

Jokipii, J.R., "The Interplanetary Magnetic Field and Energetic Electrons From Jupiter," Geophys. Res. Lett., 3, 281, 1976.

King, J.H., Composite Interplanetary Field and Plasma Tape, 11/02/63 - 1/12/76, National Space Science Data Center, 1978.

Krimigis, S.M., E.T. Sarris, and T.P. Armstrong, "Observations of Quiet-Time Interplanetary Electron Enhancements of Jovian Origin," Conf. Papers 14th Int. Cosmic Ray Conf. Munich, 2, 752, 1975.

L'Heureux, J., and P. Meyer, "On the Quiet-Time Increases of Low Energy Cosmic Ray Electrons," Conf. Papers 14th Int. Cosmic Ray Conf. Munich, 2, 748, 1975.

L'Heureux, J., and P. Meyer, "Quiet-Time Increases of Low-Energy Electrons: The Jovian Origin," Astrophys. J., 209, 955, 1976.

Lin, R.P., K.A. Anderson, and T.L. Cline, "Detection of Interplanetary Electrons from 18 keV to 1.8 MeV During Solar Quiet Times," Phys. Rev. Lett., 29, 1035, 1972.

Lupton, J.E., and E.C. Stone, "Measurement of Electron Detection Efficiencies in Solid State Detectors," Nucl. Instrum. and Methods, 98, 189, 1972a.

Lupton, J.E., and E.C. Stone, "Electron Scattering Effects in Typical Cosmic Ray Telescopes," IEEE Trans. Nucl. Sci., NS-19, No. 1, 562, 1972b.

McDonald, F.B., T.L. Cline, and G.M. Simnett, "Multifarious Temporal Variations of Low-Energy Relativistic Cosmic-Ray Electrons," J. Geophys. Res., 77, 2213, 1972.

Mewaldt, R.A., "Calibrations of the Electron Response of the IMP-H EIS," Space Radiation Laboratory Internal Report #53, Calif. Inst. of Technology, 1975.

Mewaldt, R.A., E.C. Stone, and R.E. Vogt, "Observations of Low Energy Interplanetary Electrons," Conf. Papers 14th Int Cosmic Ray Conf. Munich, 2, 758, 1975.

Mewaldt, R.A., E.C. Stone, and R.E. Vogt, "Observations of Jovian Electrons at 1 AU," J. Geophys. Res., 81, 2397, 1976.

Mewaldt, R.A., E.C. Stone, and R.E. Vogt, "Neutral Paricle Background in Cosmic Ray Telescopes Composed of Silicon Solid State Detectors," Space Sci. Inst., 3, 231, 1977.

Meyer, S.L., Data Analysis for Scientists and Engineers, John Wiley & Sons, New York, 1975.

Parker, E.N., "Dynamics of the Interplanetary Gas and Magnetic Fields," Astrophys. J., 128, 664, 1958.

Parker, E.N., Interplanetary Dynamical Processes, Interscience, New York, 1963.

Penzo, P.A., "Heliographic Coordinates of Earth and Jupiter Encompassing the MJS77 Mission Time Period," Jet Propulsion Laboratory Interoffice Memorandum 392.1-43-PAP, 1975a.

Penzo, P.A., "Heliographic Coordinates of Pioneers 10 and 11 From Launch to September 1979," Jet Propulsion Laboratory Interoffice Memorandum 392-1.44-PAP, 1975b.

Pesses, M.E., and C.K. Goertz, "Jupiter's Magnetotail as the Source of Interplanetary Jovian MeV Electrons Observed at Earth," Geophys. Res. Lett., 3, 228, 1976.

Pyle, K.R., and J.A. Simpson, "The Jovian Relativistic Electron Distribution in Interplanetary Space from 1-11 AU: Evidence for a Continuously Emitting 'Point' Source," Astrophys. J., 215, L89, 1977.

Rosenberg, R.L., M.G. Kivelson, P.J. Coleman, Jr., and E.J. Smith, "The Radial Dependences of the Interplanetary Magnetic Field Between 1 and 5 AU: Pioneer 10," J. Geophys. Res., 83, 4165, 1978.

Simnett, G.M., "Relativistic Electron Events in Interplanetary Space," Space Sci. Rev., 16, 257, 1974.

Simnett, G.M., T.L. Cline, and F.B. McDonald, "Time Variations of the 4 to 12 MeV Interplanetary Electron Intensity Between 1963 and 1968," Acta Phys. Acad. Sci. Hungaricae, 29, Suppl. 1, 151, 1970.

Simnett, G.M., and F.B. McDonald, "Observations of Cosmic-Ray Electrons Between 2.7 and 21.5 MeV," Astrophys. J., 157, 1435, 1969.

Smith, E.J., B.T. Tsurutani, D.L. Chenette, T.F. Conlon, and J.A. Simpson, "Jovian Electron Bursts: Correlation With the Interplanetary Field Direction and Hydromagnetic Waves," J. Geophys. Res., 81, 65, 1976.

Smith, E.J., and J.H. Wolfe, "Observations of Interaction Regions Corotating Shocks Between One and Five AU: Pioneers 10 and 11," Geophys. Res. Lett., 3, 127, 1976.

Teegarden, B.J., F.B. McDonald, and J.H. Trainor, "Interplanetary MeV Electrons of Jovian Origin," J. Geophys. Res., 79, 3615, 1974.

Tsurutani, B.T., and E.J. Smith, "Interplanetary Discontinuities: Temporal Variations and the Radial Gradient from 1 to 8.5 AU," Jet Propulsion Laboratory Preprint Space Physics 78-7, to be published in J. Geophys. Res., 1979.

Vidor, S., "Geometrical Factors for IMP-J," Addendum to Space Radiation Laboratory Internal Report #45, Calif. Inst. of Technology, 1974.

Webber, W.R., J.A. Lezniak, and S.V. Damle, "Cosmic Ray Electrons from 0.2 to 8 MeV: Pioneer 8 and 9 Measurements of their Spectrum, Time Variations, and Interplanetary Gradient," J. Geophys. Res., 78, 1487, 1973.